Kobe University Repository : Kernel

PDF issue: 2025-12-04

Recent Advances in Carbon Dioxide Separation Membranes: A Review

Kamio, Eiji
Yoshioka, Tomohisa
Matsuyama, Hideto

(Citation)
Journal of Chemical Engineering of Japan,56(1):2222000

(Issue Date)
2023-12-31

(Resource Type)
journal article

(Version)
Version of Record

(Rights)
© 2023 The Author(s). Published with license by Taylor & Francis Group, LLC
This is an Open Access article distributed under the terms of the Creative Commons Attribution-NonCommercial License, which permits unrestricted non-commercial use, distribution, and reproduction in any medium, provided the original work is properly…

(URL)
https://hdl.handle.net/20.500.14094/0100483400

Taylor & Francis
Taylor & Francis Group

Journal of Chemical Engineering of Japan

ISSN: (Print) (Online) Journal homepage: https://www.tandfonline.com/loi/tjce20

Recent Advances in Carbon Dioxide Separation Membranes: A Review

Eiji Kamio, Tomohisa Yoshioka & Hideto Matsuyama

To cite this article: Eiji Kamio, Tomohisa Yoshioka & Hideto Matsuyama (2023) Recent Advances in Carbon Dioxide Separation Membranes: A Review, Journal of Chemical Engineering of Japan, 56:1, 2222000, DOI: 10.1080/00219592.2023.2222000

To link to this article: https://doi.org/10.1080/00219592.2023.2222000

© 2023 The Author(s). Published with license by Taylor & Francis Group, LLC

Published online: 26 Jun 2023.

Submit your article to this journal

Article views: 1055

View related articles

View Crossmark data

Full Terms & Conditions of access and use can be found at
https://www.tandfonline.com/action/journalInformation?journalCode=tjce20

JOURNAL OF CHEMICAL ENGINEERING OF JAPAN
2023, VOL. 56, NO. 1, 2222000
https://doi.org/10.1080/00219592.2023.2222000

Taylor & Francis
Taylor & Francis Group

REVIEW ARTICLE

OPEN ACCESS Check for updates

Recent Advances in Carbon Dioxide Separation Membranes: A Review

Eiji Kamio[a,b,c], Tomohisa Yoshioka[a,b,d], and Hideto Matsuyama[a,b]

[a]Research Center for Membrane and Film Technology, Kobe University, 1-1 Rokkodai-cho, Nada-ku, Kobe, 657-8501, Japan; [b]Department of Chemical Science and Engineering, Kobe University, 1-1 Rokkodai-cho, Nada-ku, Kobe, 657-8501, Japan; [c]Center for Environmental Management, Kobe University, 1-1 Rokkodai-cho, Nada-ku, Kobe, 657-8501, Japan; [d]Graduate School of Science, Technology and Innovation, Kobe University, 1-1 Rokkodai-cho, Nada-ku, Kobe, 657-8501, Japan

ABSTRACT

Separation membranes, which have the possibility to develop energy-saving and compact processes, are expected to be applied in the field of CO_2 separation and capture and are attracting considerable interest from both industries and academia. The purpose of this review is to provide an overview of recent advances in both organic and inorganic materials for high-performance CO_2 separation membranes from the viewpoint of molecular design to an engineering perspective. The overview includes gas permeation theory for CO_2 capture and separation, controlled intrinsic micropores and their size-sieving property, CO_2 diffusivity in the membrane matrix, selective CO_2 solubility and selective permeability, functionalization using chemical reactions, etc. CO_2 separation mechanisms and the effects of properties of membrane materials on both the CO_2 permeability and permselectivity over other light gases are discussed, and the recent developments regarding inorganic and glassy polymer membranes with intrinsic microporous structures, rubbery polymer membranes, ionic liquid-based gel membranes, and facilitated-transport membranes are reviewed. Taking into consideration the industrial applications, the characteristics of each membrane with respect to process design, such as membrane thickness, and physical aging, and dependence of CO_2 permeability on gas properties, are also discussed. Finally, future research challenges and perspectives for the commercialization of CO_2 capture and separation process using high-performance materials are proposed.

ARTICLE HISTORY
Received 22 October 2022
Accepted 31 May 2023

KEYWORDS
CO_2 separation; Membranes; Material design; Permeation mechanism; Permeability and selectivity

1. Introduction

The release of large amounts of CO_2 into the atmosphere has been recognized as a global problem for over 20 years. The rapid increase in atmospheric CO_2 concentration since the industrial revolution is undoubtedly one of the main causes of the recent drastic climate change and severe global warming. The increase in the average temperature on Earth causes not only abnormal weather patterns and climate change but also environmental destruction on a global scale; this can be observed through phenomena such as rising sea levels and impacts on the different ecosystems. Furthermore, environmental destruction may cause problems directly related to human life, such as adverse effects on agricultural products and the depletion of water resources. For the sustainable development of human beings and the conservation of ecosystems, we must urgently stop the destruction of the global environment caused by an increase in atmospheric CO_2 concentration. The increase in the atmospheric CO_2 concentration is primarily caused by the release of CO_2 during industrial activities that use fossil fuels. However, owing to the strong dependence of humans on the use of fossil fuels for their comfort, immediately stopping their usage is difficult. To reduce CO_2 emissions, various efforts have been made, and energy-saving technologies have been developed. The reduction of energy used in our daily life and the development of energy-saving devices and systems have contributed to the reduction of CO_2. However, currently, the CO_2 concentration in the atmosphere continues to increase. To stop this increase, technologies to reduce the emission of CO_2 derived from fossil fuels must be developed and installed. Thus, the development of technologies to separate and capture CO_2 from exhaust gases that are emitted from various CO_2 sources is vital.

Carbon dioxide Capture and Storage (CCS), which is one of the large-scale CO_2 reduction technologies, Carbon dioxide Capture, Utilization and Storage (CCUS), which is the technology to reduce CO_2 emission by using the recovered CO_2 as raw material, and Direct Air Capture (DAC), which separates and captures CO_2 directly from the atmosphere, are expected to be direct and effective methods for CO_2 reduction. However, these CO_2 reduction technologies still experience problems. The bottleneck in the effective operation of these technologies is the CO_2 separation process. CO_2 separation technologies, such as chemical and physical

CONTACT Hideto Matsuyama matuyama@kobe-u.ac.jp

© 2023 The Author(s). Published with license by Taylor & Francis Group, LLC
This is an Open Access article distributed under the terms of the Creative Commons Attribution-NonCommercial License (http://creativecommons.org/licenses/by-nc/4.0/), which permits unrestricted non-commercial use, distribution, and reproduction in any medium, provided the original work is properly cited. The terms on which this article has been published allow the posting of the Accepted Manuscript in a repository by the author(s) or with their consent.

absorption, temperature and pressure swing adsorption, and cryogenic distillation, are well-established and effective but are high-energy consumption processes. Among these CO_2 separation technologies, amine absorption is a proven technology to treat industrial gas streams. However, it is estimated that the cost for CO_2 capture would be \$40–100/ton-CO_2 when an amine absorption system is used to capture 90% of CO_2 in flue gas (Figueroa et al. 2008). Moreover, these processes require significantly large equipment size and hence incur large costs. The high CO_2 separation costs, including energy, operation, and equipment costs, make it difficult to achieve energy-effective CO_2 separation by conventional CO_2 separation technologies. Furthermore, because of the huge process size, conventional CO_2 separation processes have limited applicability to small-scale processes such as chemical processes and biogas purification. Therefore, a low-cost, energy-saving, and compact CO_2 separation process is highly desired.

In recent years, the membrane separation method has attracted considerable attention as a next-generation CO_2 separation method to achieve a highly efficient and compact CO_2 separation process. It is predicted that the cost of capturing 90% of CO_2 in flue gas using a high-performance CO_2 separation membrane could be lower than \$40/ton-CO_2 (Merkel et al. 2010). Furthermore, because membranes can be used as a size-effective membrane module with high-density membrane integration, the membrane separation method can allow the establishment of a compact, onsite, and on-demand process. To achieve a highly effective CO_2 separation process using the membrane separation technology, high-performance CO_2 separation membranes, which have a much higher CO_2 permeation rate than other light gases such as N_2, O_2, H_2, and CH_4, must be used. However, the performance of conventional CO_2 separation membranes is still insufficient and does not meet practical requirements. Therefore, several researchers are continuously expending efforts to develop high-performance CO_2 separation membranes and have achieved remarkable progress in recent years.

Various types of CO_2 separation membranes have been developed, including organic membranes such as polymer membranes, ionic liquid (IL)-based membranes, facilitated transport membranes, and inorganic membranes with crystalline and amorphous structures composed of inorganic oxides, such as silica, alumina, and titania. In recent years, several new concepts have been proposed to design the structure and properties of membranes to improve CO_2 separation performance. For example, glassy polymer membranes with intrinsic microporous structures have been developed. To improve the CO_2 selective permeability, subnanoscale control of the microporous structure is being attempted by precise control of the free volume based on molecular design. Conversely, ultrathin membranes with a significantly high CO_2 permeation rate have been developed for rubbery polymer membranes. IL-based membranes have entered a new stage of development using gel technology. For facilitated transport membranes, using an IL-type CO_2 carrier was proposed to overcome the serious drawback. In inorganic membranes, improvement in perm selectivity has been achieved by designing the crystal structure of zeolite membranes and by controlling the pore size of silica membranes by incorporating coordinative chemical compounds. While these types of CO_2 separation membranes are still under development, some of them with high CO_2 separation performance, which overcomes the tradeoff that exists between CO_2/light gas selectivity and CO_2 permeability, according to the Robeson upper bound (Robeson 1991, 2008), have been successively reported. For organic-inorganic composite membranes, only inorganic-based membranes will be presented in this paper. Readers can consult previous reviews for the Metal-organic framework (MOF) membranes (Chakrabarty et al. 2022; Demir et al. 2022; Kamble et al. 2021; Kang et al. 2022; Wong and Jawad 2019).

In this review, the performances and properties, theoretical considerations for selective CO_2 permeation, and recent noteworthy developments of each membrane are provided. The remaining challenges for each membrane are also discussed.

2. Organic CO_2 Separation Membranes

2.1 CO_2 separation mechanism

In general, gas permeation through polymer membranes proceeds in the following three steps: (I) a gas molecule is dissolved in a membrane at the surface in contact with a feed gas; (II) the dissolved gas molecules diffuse within the polymer matrix of the membrane; and (III) the dissolved gas molecules reach the membrane surface at the permeate side and are desorbed and removed from the membrane. This permeation mechanism is called the solution-diffusion mechanism. The gas permeation potential of the membrane material is evaluated by the gas permeability, P, which is a parameter expressing the number of gas molecules permeating through a unit area of the membrane at the unit time under the condition that a unit partial pressure difference is applied between the feed and permeate gases. Thus, the permeability coefficient is a scale expressing "how fast the developed membrane material can permeate a gas molecule" and is useful in material development. Gas permeability can be expressed by the following equation based on Fick's diffusion law:

$$P = D \times \frac{\Delta C}{\Delta p} \tag{1}$$

where D (m^2/s) is the effective diffusion coefficient of a dissolved gas molecule in a membrane, ΔC (mol/m^3) is the concentration gradient of the dissolved gas between the feed- and permeate-side surfaces of the membrane, and Δp (Pa) is the transmembrane partial pressure difference between the feed and permeate gases. The unit of P is $mol{\cdot}m/(m^2{\cdot}s{\cdot}Pa)$ in the SI system of measurement. In the research field of gas separation membranes, "barrer" is often used as the unit of gas permeability (1 barrer = 3.35×10^{-16} $mol{\cdot}m/(m^2{\cdot}s{\cdot}Pa)$). The parameter $\Delta C/\Delta p$ in Eq. (1) is the solubility coefficient, which is expressed as

S (mol/(m^3 Pa)). Using S, Eq. (1) can be rewritten as $P = D \cdot S$. This equation indicates that gas permeability can be determined from the diffusivity of the dissolved gas in the membrane matrix and solubility of gas molecules in the membrane matrix.

Conversely, the gas separation properties of membrane materials are expressed by the perm selectivity, $\alpha_{i/j}$, which is a ratio of permeabilities of gas species i and j ($\alpha_{i/j} = P_i/P_j$). Thus, $\alpha_{i/j}$ is a scale to evaluate "how fast the gas species i permeates through the developed membrane compared to j."

$$\alpha_{i/j} = \frac{P_i}{P_j} = \frac{D_i}{D_j} \cdot \frac{S_i}{S_j} \tag{2}$$

Equation (2) is a formula that is rewritten using Eq. (1). In Eq. (2), D_i/D_j and S_i/S_j denote the diffusion and solubility selectivities, respectively. Thus, the gas separation properties of a membrane can be improved in two ways: by increasing the diffusivity and solubility differences. Therefore, the ability of membrane materials is evaluated using both $\alpha_{CO2/j}$ and P_{CO2}. Materials that can permeate CO_2 faster and with greater selectivity are suitable as high-performance CO_2 separation membranes. However, as is well known, there is a tradeoff between $\alpha_{CO2/j}$ and P_{CO2}. This tradeoff relationship was recognized worldwide as the upper bound line by Robeson (1991). The upper bound line is used as a reference index for evaluating the performance of CO_2 separation membrane materials and is updated with the creation of high-performance CO_2 separation membranes.

2.2 Recently developed high-performance organic membranes for CO_2 separation

2.2.1 Glassy polymer membranes

2.2.1.1 Novel glassy polymer membranes. Before the 1990s, studies had empirically confirmed that glassy polymers with a rigid main chain skeleton had high CO_2 separation performance (Koros et al. 1988; Robeson 1991; Stern 1994). Moreover, polymer membranes with a large free volume fraction, such as polydimethylsiloxane (PDMS) and poly[1-(trimethylsilyl)-1-propyne] (PTMSP), were confirmed to have high gas permeability. In particular, it is well known that PTMSP, which is a glassy polymer with a significantly large free volume fraction, has a very high gas permeability. PTMSP was first described by Masuda et al. (1983). The Brunauer–Emmett–Teller surface area was reported to be 550 m^2/g (Nagai et al. 2001). The free volume in freshly prepared PTMSP (~30%) is interconnected, thus allowing rapid diffusion and significantly high permeations of gases. Since the discovery of the highest gas permeability of PTMSP, various polyacetylene-based polymer membranes have been developed and evaluated for gas separation performance, including CO_2/N_2 and CO_2/CH_4 systems (Hu et al. 2008; Masuda et al. 1988). However, because of the low solubility selectivity of the polyacetylene-based polymer membranes, the gas separation performance of PTMSP is severely limited and below the upper bound. Besides, glassy polymer membranes such as polyimide membranes (Al-Masri et al. 1999, 2000; Cho and Park 2011; de Abajo et al. 2003; Hiarayama et al. 1995; Kazama et al. 2002; Nagel et al. 2002; Sen and Banerjee 2010), polyamide membranes (de Abajo et al. 2003), cellulose acetate membranes (Jami'an et al. 2016; Liu et al. 2021b; Puleo et al. 1989; Raza et al. 2021), polysulfone membranes (Aitken et al. 1992; Ghosal et al. 1996; Kim et al. 2001; McHattie et al. 1991b, 1991a, 1992), and polyethersulfone membranes (Chiou et al. 1987; Naderi et al. 2018) have been studied; however, the CO_2 permeability of these glassy polymer membranes is small and the CO_2 separation performance is below the upper bound line.

Besides the above, based on the platform of conventional polymers, many attempts have been made to develop polymers with high selectivity and high permeability. Although developing polymers with not only high permeability but also high selectivity that have a CO_2 separation performance beyond the Robeson upper bound was difficult, from the early 2000s, new polymer materials suitable for CO_2 separation were discovered. One is a microporous polymer with rigid ladder-like backbone, termed polymer of intrinsic microporosity (PIM), and the other is a microporous polymer obtained by the thermal rearrangement of specified polyimides, termed thermally rearranged (TR) polymer. In the following sections, the properties, CO_2 permeation performance, and challenges of these polymer membranes are discussed.

2.2.1.2 Polymers of intrinsic microporosity (PIMs) membrane. PIMs are glassy polymers with intrinsic micropores. The main chain of the PIMs has a rigid ladder-like structure. PIM-1, a representative PIM developed by Budd et al. (2004a), was synthesized via condensation polymerization of an aromatic monomer with four hydroxyl groups and an aromatic monomer with four halogen groups (Figure 1(a)). PIM-1 has no rotational single bonds in the backbone. Thus, the backbone of PIM-1 is rigid. The rigid ladder-like backbone limits intra-segmental mobility and prevents efficient chain packing. The other feature of the main chain of PIM-1 is the sharply bent spiro-center (i.e., a single tetrahedral C atom shared by two rings), which provides a contorted backbone structure. The rigid and contorted structure allows the formation of interconnected molecular-level micro-void spaces in the PIM-1 matrix. Therefore, interconnected micropores (less than 2 nm) and ultra-micropores (less than 0.7 nm) are formed in the polymer membrane of PIM-1 (Staiger et al. 2008). Owing to its highly developed microporous structure, a separation membrane composed of PIM-1 has a large surface area (>600 m^2/g)(Budd et al. 2004a) and a relatively large fractional free volume (FFV; 0.15) (Staiger et al. 2008). Therefore, the CO_2 diffusivity and solubility of PIM-1 are greater than those of conventional polymers (Budd et al. 2005). The outstanding CO_2 permeability of the PIM-1 membrane (2300 barrer) was first demonstrated by Budd et al. (2005). The CO_2/CH_4 separation performance of the PIM-1 membrane was found to be beyond the Robeson upper bound that was reported in 1991 (Robeson 1991). Considering the high CO_2 separation performance of the PIM-1 membrane, Robeson revised the upper bound in 2008 (Robeson 2008). The CO_2/N_2

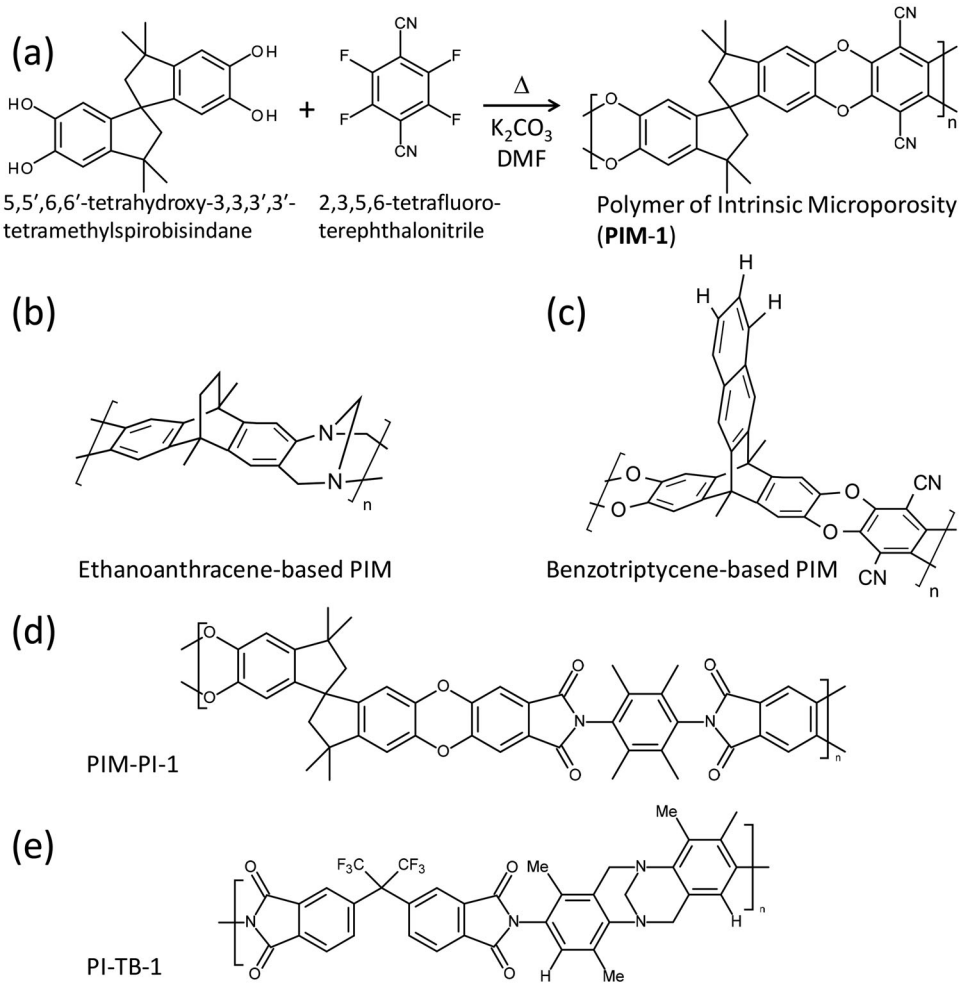

Figure 1. Examples of PIMs: (a) Synthesis route and chemical structure of PIM-1; chemical structures of (b) ehanoanthracene-based PIM, (c) benzotriptycene-based PIM, (d) PIM-PI with spirobisindane structure (PIM-PI-1), and (e) PIM-PI with Tröger's base structure.

separation performance was also good, which was located on the upper bound in 2008 (Robeson 2008). Another significant advantage of this material over other conventional microporous materials is their solution processability. PIM-1 can be dissolved in several polar organic solvents. Therefore, it has superior processability and can be shaped into a membrane.

After demonstrating the superior CO_2 separation performance of PIM-1, various studies have been performed on PIM membranes. PIMs can be synthesized via a double aromatic nucleophilic substitution polycondensation reaction. To improve the CO_2 separation performance, many PIMs have been derived either by using various monomers with different chemical structures or by post-functionalization of the synthesized PIMs. For example, using PIM monomers with different unit lengths, various PIMs with spiro-centers, such as PIMs-2, 3, 7–9, were synthesized (Bezzu et al. 2018; Budd et al. 2004b, Ghanem et al. 2008a). Post-functionalization of PIM-1 has also been achieved by the conversion of the nitrile group in PIM-1 to amine (Mason et al. 2014, Satilmis et al. 2018), amide (Yanaranop et al. 2016), tetrazole (Du et al. 2011), thioamide (Mason et al. 2011), methyl tetrazole (Du et al. 2012), amidoxime (Patel and Yavuz 2012; Swaidan et al. 2014), hydroxyalkylaminoalkylamide (Satilmis et al. 2015), and carboxylic acid (Du et al. 2009; Jeon et al. 2017; Mizrahi Rodriguez et al. 2020; Weng et al. 2015; Wu et al. 2018) groups. Some of these functionalizations lead to the tightening of the microstructure owing to the enhancement of intermolecular interactions such as hydrogen bonding. The tightening microstructure allows for an increase in the size-sieving effect, resulting in the diffusion selectivity of CO_2 over CH_4 and N_2. Recently, to make PIM-1 more rigid, the formation of an intramolecular eight-membered ring structure that connects the carbon atoms of the spirobisindane structure and the nitrile group of PIM-1 has been proposed (Zhang et al. 2016). The formation of an intermolecular crosslinked structure of PIM-1 by thermal crosslinking has also been studied (Li et al. 2012a). On the other hand, to synthesize PIMs with a more rigid main skeleton, various types of precursor monomers with cardo (Ghanem et al. 2008a), iptycene (Carta et al. 2014; Comesaña-Gándara et al. 2019; Ghanem et al. 2014a, 2014b; Rose et al. 2015, 2017), ethanoanthracene (Carta et al. 2013; Ma and Pinnau 2018; Tocci et al. 2014), and Tröger's base (Carta et al. 2013, 2014; Rose et al. 2015; Tocci et al. 2014; Williams et al. 2018) were used instead of monomers with spiro-centers. Figure 1(b,c) show examples of PIMs with ethanoanthracene and benzotriptycene structures,

respectively. In addition, studies have shown that polyimides incorporating spirobisindane structures also have intrinsic microporosity (Ghanem et al. 2008b, 2009; Weber et al. 2007; Zhang et al. 2007). Such polyimides are a type of PIM and are called polyimides of intrinsic microporosity (PIM-PIs). PIM-PIs with iptycene structures (Alghunaimi et al. 2015; Ghanem et al. 2014a), ethanoanthracene structures (Rogan et al. 2014), and Tröger's base (Lee et al. 2016) can also be synthesized by selecting monomers. Some examples of PIM-PIs are shown in Figure 1(d,e). The synthetic methods and properties of PIMs and PIM-PIs with various structures have been summarized in detail in recent reviews (Bandehali et al. 2021; Lee et al. 2020; Low et al. 2018; McKeown and Budd 2006; Wang et al. 2016).

One of the problems of PIM membranes is the change in the gas permeation performance over time, which is recognized as physical aging. Owing to physical aging, the CO_2 permeability drastically decreases and the CO_2/N_2 and CO_2/CH_4 permselectivities increase. A previous study reported that the CO_2 permeability of the as-prepared PIM membranes decreased to 25–40% within one year. For example, the CO_2 permeability of the PIM-1 membrane declined by approximately 40% (from ca. 2500 barrer to ca. 1550 barrer) after 140 h (Staiger et al. 2008). As another example, benzotriptycene-based PIM (PIM-Btrip) membrane, which is a state-of-the-art PIM membrane, showed a 63% reduction in CO_2 permeability from 21,500 to 8020 barrer after one year (Comesaña-Gándara et al. 2019). The CO_2 permeability continuously decreased and eventually became 3770 barrer after 718 d. This reduction in CO_2 permeability is due to the reduction in the free volume of PIMs (Staiger et al. 2008), which is similar to the physical aging trend for other polymers such as PTMSP (Nagai et al. 2000; Tiwari et al. 2014), amorphous fluoropolymers, *i.e.*, Teflon AF1600 and AF2400 (Tiwari et al. 2014), and poly(4-methyl-2-pentyne) with a high free volume (Merkel et al. 2003). In contrast to the CO_2 permeability, the CO_2/N_2 and CO_2/CH_4 permselectivities of the PIM-Btrip membrane increased from 18.1 and 12.7–33.7 and 33.4 after 718 d, respectively (Comesaña-Gándara et al. 2019). A similar trend in physical aging, *i.e.*, a decrease in gas permeability and an increase in the permselectivity of faster permeating gases, was confirmed for all PIM membranes. For PIM-1 and PIM-Btrip membranes, the decrease in the CO_2 permeability and the increase in the CO_2/N_2 and CO_2/CH_4 permselectivities were due to the decrease in the diffusion coefficients of each gas species over time (Bernardo et al. 2017; Longo et al. 2020). Interestingly, the solubility of the gases did not change significantly over time. Therefore, it was considered that the increase in permselectivity improved the size-sieving character during physical aging. Although the decrease in CO_2 permeability has a negative effect, the increase in permselectivity is positive because the not-so-significantly high permselectivity is one of the drawbacks of the PIM membranes. As shown in the example above, the CO_2 permeability of the membranes composed of PIM-Btrip was still sufficiently high after physical aging. Moreover, the CO_2/N_2 and CO_2/CH_4 permselectivities significantly improved. After physical aging, the CO_2 separation performance, *i.e.*, the relationships between CO_2/N_2 and CO_2/CH_4 permselectivities and CO_2 permeability, was still beyond the upper bound lines that were reported in 2008. Thus, it cannot be unconditionally stated that physical aging causes a reduction in the CO_2 separation performance of PIM membranes.

However, in practical applications, the performance change that occurs in the CO_2 permeation properties during a separation process is not desirable. The use of membranes with a constant permeation property, *i.e.*, equilibrated gas permeation performance, is preferable for simplifying the process design. To achieve a fast equilibration, the use of a thin film is favorable because it was reported that the performance change due to physical aging became faster when the thickness of the PIM membrane was reduced (Tiwari et al. 2017). Moreover, from the perspective of operation cost, the use of thin membranes with sufficient CO_2 permeance is vital. Here, CO_2 permeance is defined as the gas permeation rate through a membrane with a given thickness and unit area per unit time. The unit of permeance is $mol/(m^2 \cdot s \cdot Pa)$ in the SI system of measurement. In the research field of gas separation membranes, "GPU" is often used as the unit of gas permeance (1 GPU = $3.35 \times 10^{-10}\,mol/(m^2 \cdot s \cdot Pa)$). A thinner membrane has higher CO_2 permeance. Therefore, in practical applications, the use of significantly thin PIM membranes with equilibrated gas permeation performances is favorable. However, the formation of thin and defect-free rigid-polymer-based films is often difficult, *i.e.*, the fabrication of thin PIM membranes with sufficient CO_2 separation performance that meets the requirements of practical applications is a big challenge. There have been only a few reports on the fabrication of thin PIM membranes. Jue et al. (2017) developed an asymmetric PIM-1 hollow-fiber membrane. The thickness of the dense layer formed at the outer surface of the hollow-fiber membrane was ~2.8 μm. After two months of physical aging, the CO_2 permeance and CO_2/CH_4, CO_2/N_2 permselectivities were measured as 360 GPU and 23, 28, respectively. As another thin PIM membrane, Liang et al. (2018) prepared a thin-film composite (TFC) membrane with a PIM layer on the outer surface of a hollow-fiber-type support membrane composed of a porous polyacrylonitrile membrane coated with a thin PDMS gutter layer. They prepared a TFC membrane using the dip-coating method. In their research, PIM-1 and PIM incorporated with beta-cyclodextrin (PIM-CD) were used. The thickness of the dense PIM layer formed on the PDMS gutter layer was approximately 5 μm. The CO_2 permeability and CO_2/N_2 selectivity of the TFC membrane with the PIM-1 layer were 402.6 GPU and 21.3, respectively, and those of the TFC membrane with the PIM-CD layer were 483.4 GPU and 22.5, respectively. Because these performances are still insufficient for practical applications, such as CO_2 capture from exhaust gases that are released from coal-fired power plants (the required membrane performance was reported by Merkel et al. (2010)), the thickness of the PIM layer must be further decreased. Some other TFC membranes were prepared by Benito et al. (2019). They prepared TFC membranes with

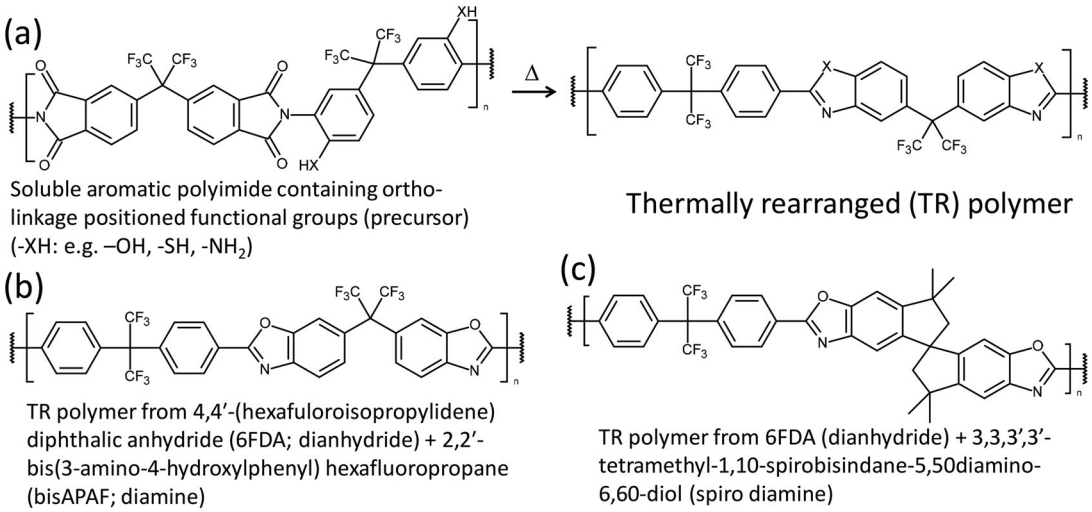

Figure 2. Examples of TR polymers: (a) chemical structures of the precursor and TR polymers; (b,c) chemical structures of representative TR polymers.

ultrathin PIM-1, PIM based on tetramethyltetrahydronaphthalene unit coupled with bicyclic triptycene, and PIM consisting of Tröger's base and ethanoanthracene layers using Langmuir–Blodgett technique and Langmuir–Schaefer horizontal deposition method. The prepared TFC membranes had a dense PIM multilayer with a thickness of several tens of nanometers. Unfortunately, the CO_2 permeance and CO_2/N_2 permselectivity of the prepared TFC membranes were lower than those expected from thick-membrane samples. From these results, it can be said that the fabrication method for thin PIM membranes has not yet been well established. Thus, the development of a thin-film formation technique should be established for the practical application of PIM membranes.

2.2.1.3 Thermally rearranged (TR) polymers. Another polymer with an intrinsic microporous structure is the TR polymer. TR polymers are completely aromatic, insoluble, and rigid polymers prepared via post-fabrication polymer-modifying reactions. The TR polymer membrane was first developed by Park et al. (2007). They prepared a membrane called TR-1 from polyimides with ortho-positioned functional groups (PIOFG-1) (aromatic polyimide) synthesized via thermal imidization of 4,4′-(hexafluoroisopropylidene)-diphthalic anhydride and 2,2′-bis(3-amino-4-hydroxylphenyl) hexafluoropropane. In addition to aromatic polyimides, aromatic polyetherimide (Calle and Lee 2011; Do et al. 2013) and aromatic polyamide (Do et al. 2013; Han et al. 2012; Kim et al. 2015b; Ye et al. 2019, 2020) can also be used as thermally rearrangeable (TR-able) polymers. TR-able polymers must have ortho-positioned functional groups, such as hydroxyl, amine, and thiol groups. Thus, an aromatic diamine monomer, which is a precursor monomer of TR-able polymers, must also contain ortho-positioned functional groups such as hydroxyl, amine, and thiol groups. As the other monomer, either aromatic carboxylic acid dianhydride or aromatic dicarboxylic acid chloride can be used. Several precursor monomers are commercially available, which is advantageous for achieving the chemical structural diversity of TR polymers. The synthesis routes, precursor materials, and properties of various TR polymers have been detailed in recent reviews (Bandehali et al. 2021; Lee et al. 2020; Low et al. 2018; McKeown and Budd 2006; Wang et al. 2016).

Because precursor TR-able polymers are highly soluble in several organic solvents, the solution can be spread into a film and dried to form a precursor membrane. Subsequently, to prepare the TR polymer membrane, irreversible molecular rearrangement is conducted at the temperature range of approximately 350–450 °C (Figure 2(a)). The thermal treatment converts the relatively flexible, twisting pairs of short, flat planes in the precursor polymer to single, long, flat planes. The TR moieties of the polymer chain become much more rigid than those of the parent polymer via the formation of meta- and para-linked chains. Consequently, random chain conformations with interconnected microcavities (free volume elements) are formed in the amorphous polymer matrix (Park et al. 2007). Figure 2(b,c) show examples of representative TR polymers.

The outstanding CO_2 permeability and CO_2/CH_4 permselectivity of the TR-1 membrane were first demonstrated by Park et al. (2010). The CO_2/CH_4 separation performance of the TR-1 membrane was found to be beyond the revised Robeson upper bound, which was proposed in 2008 (Robeson 2008). The size of the microcavity could be increased via thermal treatment. Moreover, the size distribution of the microcavities was sharpened by the thermal treatment. For example, TR-1 prepared at 450 °C, which is named TR-1-450, exhibited a sharp microcavity with an average radius of approximately 0.38 nm, whereas PIOFG-1, which is the precursor polymer of TR-1-450, had a broadly distributed microcavity with an average radius of approximately 0.28 nm. Because of its highly developed microcavities, TR-1-450 has a large surface area (>500 m^2/g) and large FFV (26.3%) (Park et al. 2007, 2010). The size of the microcavities can be controlled by controlling the degree of thermal conversion by changing the temperature and time of the thermal treatment. The CO_2 permeability and CO_2/CH_4 permselectivity of the TR-1-450 membrane were > 2000 barrer and > 45, respectively (Han et al. 2010; Kim

et al. 2013a; Park et al. 2010). However, the size of the microcavity and FFV are strongly affected by the imidization routes of the TR-able precursor polymers. For example, the TR-1 polymers prepared from hydroxyl-containing polyimide (HPI) and acetate-containing polyimide (AcPI), which are the precursor polymers of TR-1, had different FFVs and cavity sizes. HPI could be synthesized via thermal imidization (tHPI) and azeotropic imidization (aHPI), while AcPI could be synthesized via chemical imidization (cAcPI) and chemical imidization with silylation treatment (sAcPI) (Han et al. 2010). The order of the d-spacing of the TR-1 polymers prepared from these precursor polymers were sAcPI > cAcPI > tHPI $\gg$ aHPI. The small d-spacing and FFV of the TR-1 polymer from aHPI can lead to a significant decrease in the diffusion coefficient and permeability of gases in the membrane (Kim et al. 2013a). Thus, to fabricate a high-performance TR membrane for CO_2 separation, the suitable synthesis route of the TR-able precursor polymer should be selected.

After the superior CO_2 separation performance of TR-1 was reported, various studies on TR membranes have been conducted. As mentioned above, TR polymers can be prepared from TR-able polymers synthesized using various precursor monomers. Many types of TR polymer membranes have been developed by combining various precursor monomers (Calle and Lee 2011; Jiang et al. 2011; Park et al. 2010). TR-able copolymers can also be synthesized using multiple precursor monomers. TR copolymers can be prepared from TR-able copolymers (Choi et al. 2010; Gan et al. 2019, 2020; Soo et al. 2013). Furthermore, similar to PIMs, the micropore structure of TR polymers can be controlled by introducing rigid and bulky iptycene structures (Huang et al. 2022), spiro-ring structures (Li et al. 2013b), cardo structures (Yeong et al. 2012), and Tröger's bases (Hu et al. 2020; Meckler et al. 2018).

Similar to PIM membranes, physical aging is a problem in practical applications. Only a few studies have investigated the physical aging of TR polymer membranes. However, some reports indicated that the gas permeation performance of TR polymer membranes changed over time, *i.e.*, the gas permeability decreased and the permselectivity of faster permeating gases increased (Brunetti et al. 2016; Comesaña-Gándara et al. 2017; Wang et al. 2014a). For example, the CO_2 permeability of the mTR-PBO membrane, which was prepared by a thermally rearrangement of the TR-able precursor polymer synthesized from 2,2′-bis(3,4-dicarboxyphenyl)hexafluoropropane dianhydride (6FDA) and 3,3′-diamino-4,4′-dihydroxybiphenyl (mHAB), decreased from 720 to 488 barrer after six months of aging, CO_2/CH_4 permselectivity increased marginally from 23 to 28, and CO_2 permeation performance showed a shift parallel to the Robeson upper bound line (Comesaña-Gándara et al. 2017). Thus, similar to PIM membranes, it cannot be unconditionally said that physical aging causes a reduction in the CO_2 separation performance of TR polymer membranes. To overcome the decline in CO_2 permeance by physical aging, an interesting investigation on the recovery of the gas permeation performances of TR hollow-fiber membrane modules was conducted by Brunetti et al. (2016). They developed an *in situ* recovery process without disassembling the membrane module by exposing the membrane to methanol at 80 °C. The CO_2 permeance and CO_2/N_2 permselectivity of the module were completely recovered by the recovery process. The recovery of the gas permeation performance is an effective way to extend the life of the membrane and is useful for practical applications. However, a continuous change in gas permeation performance during the separation process complicates the process design. Thus, the development of TR membranes with aging resistance or sufficient performance after aging is highly desired.

The other challenge of TR polymer membranes is the development of a thin-film formation process. Because of the high solubility of the TR-able precursor polymers in commonly used organic solvents, a hollow-fiber membrane of the precursor polymers with a dense and thin skin layer on the surface can be prepared by a nonsolvent-induced phase separation (NIPS) method. However, unlike PIMs, TR polymers are prepared by post-thermal treatment of the precursor polymer. From the perspective of preparation cost, thermal treatments that are performed at high temperatures for a long time may not be economically or industrially feasible. Moreover, it has been reported that the thickness of the skin layer is increased by thermal rearrangement at high temperatures. The increase in the skin layer thickness was caused at elevated temperatures by the densification of a portion of the porous transition or support layer and their conversion into the skin layer (Woo et al. 2016). Therefore, a preparation method for TR polymer membranes must be developed at low temperatures. Fortunately, a study reported that the thermal rearrangement of a thin TR membrane was more rapid and extensive than that of a thick one (Wang et al. 2014b). Moreover, the conversion of the ortho-functional polyimide to polybenzoxazole can be started at a lower temperature for thinner films than that for thicker films (Wang et al. 2014b). Thus, the preparation of thin TR polymer membranes would not only be preferable to increase the CO_2 permeability but to also achieve a cost-effective process. By conducting thermal rearrangement under preferable conditions, an asymmetric TR polymer hollow-fiber membrane with high CO_2 permeability and good CO_2 selectivity over CH_4 and N_2 can be fabricated. Kim et al. (2012) prepared a TR-polybenzoxazole (TR-PBO) hollow-fiber membrane from hydroxyl polyimide hollow fibers fabricated by the NIPS method. The thickness of the skin layer formed on the outer surface of the hollow-fiber membrane was approximately 1.5 µm. When the rearrangement was performed at 450 °C for 1 h, the CO_2 permeance and CO_2/CH_4 and CO_2/N_2 permselectivities were 1938 GPU and 14 and 13, respectively. A hollow-fiber membrane composed of TR copolymer from the precursor copolymer with TR-able and non-TR-able segments was also prepared via the NIPS method followed by thermal rearrangement at different temperatures for 1 h (Woo et al. 2016). When the thermal rearrangement was performed at 375 °C, the prepared membrane had 0.2 µm of the skin layer with 36.6% thermal rearrangement. The CO_2 permeance and CO_2/N_2

permselectivity values were 560 GPU and 17, respectively. Recently, Lee et al. (2019) fabricated densification-induced hollow-fiber membranes composed of crosslinked-TR-PBO. The crosslinked TR hollow-fiber membranes prepared at a thermal rearrangement temperature of 425 °C exhibited a skin layer thickness of approximately 100 nm and a superior CO_2 permeance of ~2300 GPU and CO_2/N_2 selectivity of 17.4. These reports show that the CO_2 permeance of some of the TR polymer hollow-fiber membranes is significantly high and sufficient for practical applications such as CO_2 capture from exhausted gases from coal-fired power plant (the required membrane performance is reported by Merkel et al. (2010)). However, the permselectivities of CO_2 over N_2 and CH_4 were insufficient. Thus, the CO_2 separation performance of the TR polymer hollow-fiber membranes are still lower than that of thick TR polymer membranes. Clarifying the reason for the insufficient performance and developing a thin TR polymer membrane with the same performance as the thick membrane are highly desirable.

2.2.2 CO_2 separation membranes with soft and flexible diffusion field

2.2.2.1 Robbery polymer membranes. Although the 1991 Robeson plot shows that glassy polymer membranes have high CO_2 separation performance closer to the upper bound line than rubbery polymer membranes, rubbery polymer membranes with superior CO_2 separation performance are also being developed. One of the rubbery polymer membranes is a PDMS membrane. It is well known that PDMS has high gas permeability attributed to the highly dynamic nature of the polymer chain and the large free volume. In addition, PDMS can be shaped as a thin film so that it has extremely high CO_2 permeance. Combining the unique material property of PDMS with a thin-film formation technology, a superior PDMS membrane was developed by Fujikawa et al. (2019). They prepared a self-standing and ultrathin PDMS membrane via spin coating of PDMS solution on a water-soluble sacrificial layer followed by a detachment of the PDMS thin film by dissolving the sacrificial layer. The thinnest sample had a thickness of only 34 nm and CO_2 permeance of more than 40,000 GPU. Moreover, the authors overcame the mechanical strength issue of the ultrathin PDMS membrane by adding cellulose nanofibers (CNFs) (Ariyoshi et al. 2021). The fabricated PDMS/CNF composite membrane with a thickness of 150 nm was robust and had a CO_2 permeance of 10,000 GPU. They proposed the use of a thin PDMS membrane for not only a gutter layer of TFC membranes but also a highly permeable CO_2 separation membrane for direct air capture applications (Fujikawa et al. 2021; Selyanchyn et al. 2020). However, PDMS has a low solubility selectivity of CO_2 over other light gases, and the PDMS membrane has a CO_2 permselectivity over N_2 of approximately 10. Owing to this low CO_2 permselectivity, a multi-stage process must be designed for practical use.

Another rubbery polymer membrane with high CO_2 separation performance is a poly(ethylene oxide) (PEO)-based membrane. It is well known that PEO and polyethylene glycol (PEG) are CO_2-philic because of the polar ether oxygen atoms in the ethylene oxide group having strong interactions with CO_2 (Lin and Freeman 2005; Lin et al. 2006). Commercially available CO_2 separation membranes, such as Pebax (Brinkmann et al. 2017; Embaye et al. 2021) and Polyactive (Brinkmann et al. 2017; Rahman et al. 2018), are PEO-based block copolymers with high CO_2 permselectivity. Because of the high affinity of the ether oxygen for CO_2, PEO-based membranes have a high CO_2/N_2 permselectivity of more than 40; however, the CO_2 permeability of the membranes is moderately low (in most cases, less than 200 barrer) at around 30 °C. Owing to the relatively low CO_2 permeability, when a PEO-based membrane is used for CO_2 capture from exhaust gases released from a coal-fired power plant, the thickness should be decreased to less than 200 nm to achieve more than 1000 GPU, which is the required CO_2 permeance reported by Merkel et al. (2010).

2.2.2.2 Ionic liquid-based CO_2 separation membranes. ILs are molten salts composed only of ions. The "first" IL, ethylammonium nitrate, was synthesized and reported by Walden (1914). The greatest feature of ILs is their significantly low vapor pressure, that is, they are nonvolatile liquids. Moreover, because ILs are organic salts, their molecular structures can be designed relatively freely, and their physical properties can also be controlled by tuning the molecular structure. Research on ILs as CO_2 separation media began with a report by Blanchard et al. (1999). They synthesized 1-butyl-3-methylimidazolium hexafluorophosphate and used the IL as a CO_2 absorbent in a wide range of CO_2 pressures, up to 8 MPa. They reported that (1) CO_2 is highly soluble in the IL, (2) no IL was distributed in the CO_2 phase, and (3) the dissolution of CO_2 in the IL was completely reversible.

After the report by Blanchard et al. (1999), many experimental and theoretical studies have been performed to utilize ILs as high-performance CO_2 separation media, including the synthesis and tailoring of the chemical structures of novel ILs, fundamental investigations on the physical and physicochemical properties of ILs, and the development of IL-based CO_2 separation processes such as absorption and membrane separation. Owing to the multiple studies that have been conducted so far, some ILs have been identified as suitable materials for CO_2 separation membranes. For example, ILs composed of imidazolium cation have high CO_2 solubility. In particular, imidazolium-based ILs with bis(trifluoromethanesulfonyl)imide ($[Tf_2N^-]$), tricyanomethanide ($[C(CN)_3^-]$), and tetracyanoborate ($[B(CN)_4^-]$) have high CO_2 solubility because of the relatively weak interaction between the imidazolium cation and each of these anions. The CO_2 solubility in imidazolium-based ILs is primarily dominated by the anion. The dominant effect of the anion on the CO_2 solubility was experimentally confirmed and evidenced via attenuated total reflection infrared analysis (Cadena et al. 2004; Kazarian et al. 2000). Moreover, a molecular dynamics simulation clarified that the weaker cation-anion interaction enables the easy expansion of the free volume and the insertion of more CO_2 into

the free volume (Babarao et al. 2011; Cadena et al. 2004). For instance, when comparing 1-ethyl-3-methylimidazolium [Tf_2N] ([Emim][Tf_2N]) and [Emim][$B(CN)_4$], [Emim][$B(CN)_4$] can dissolve a larger amount of CO_2 than [Emim][Tf_2N] because the interaction between [Emim] and [$B(CN)_4$] is weaker than that between [Emim] and [Tf_2N] (Babarao et al. 2011). The importance of the formation of free volume in the ILs, which is attributed to the cation-anion interaction, is revealed in other reports (Anthony et al. 2005; Klahn and Seduraman 2015; Liu et al. 2014a; Shannon et al. 2012; Zhang et al. 2009). Thus, flexible ionic structure is an important factor for the formation of cavities to dissolve gas molecules (Hu et al. 2011; Kanakubo et al. 2016). Other gases such as N_2 also occupy the free volume of ILs similar to CO_2 (Liu et al. 2014b). However, all the aforementioned ILs dissolve a significantly larger amount of CO_2 when compared to N_2. This is because of the difference in the interactions between the gas molecules and the ILs. Research has demonstrated that the C atom of CO_2 acts as a Lewis acid, while the negatively charged parts of the anion in ILs act as Lewis bases. The acid-base interaction between CO_2 and the anions in ILs enhances the amount of CO_2 that can be dissolved in the ILs (Aki et al. 2004; Kazarian et al. 2000; Makino et al. 2014). Thus, the interaction between CO_2 and the anion is an important factor affecting selective CO_2 solubility in ILs. Conversely, unlike N_2, hydrocarbons such as CH_4 can be easily dissolved in an IL because of the stronger interaction with ILs caused by the alkyl chain in the cation of ILs (Carvalho and Coutinho 2011). Therefore, the solubility selectivity of CO_2 over CH_4 is significantly lower than that of CO_2 over N_2. Thus, ILs are more suitable as CO_2 separation membranes for CO_2/N_2 separation than for CO_2/CH_4 separation. When considering ILs as a material for CO_2 separation membranes, it is worth mentioning that permselectivity is mainly dominated by solubility selectivity, as shown in Figure 3. It was reported that supported IL membranes (SILMs) containing CO_2-philic ILs have a high CO_2 permselectivity over N_2 of over 20, *i.e.*, 23 for [Emim][Tf_2N] (Scovazzo 2009), 57 for [Emim] [dicyanamide] (Scovazzo 2009), 57 for [Emim][$C(CN)_3$] (Tome et al. 2014), and 53 for [Emim] [$B(CN)_4$] (Mahurin et al. 2010, 2012).

As for the diffusion coefficient, the CO_2 diffusivity in ILs depends on the viscosity of the ILs. The IL viscosity depends on the cation-anion interactions, and ILs with stronger cation-anion interactions have higher viscosities. For example, the order of cation-anion interactions is [Emim][BF_4] > [Emim][Tf_2N] > [Emim][$B(CN)_4$] (Babarao et al. 2011), which is identical to the order of the viscosity of these ILs (Liu et al. 2014a). Thus, there is no tradeoff relationship between CO_2 solubility and CO_2 diffusivity in ILs, and ILs with small cation-anion interactions have both high CO_2 solubility and high CO_2 diffusivity. To the best of our knowledge, [Emim][$B(CN)_4$] has both high CO_2 solubility and high CO_2 diffusivity among currently reported ILs and is the best IL that can be used as a CO_2 separation medium. The theoretical maximum CO_2 permeability of this IL calculated from the solubility and diffusion coefficients of CO_2 determined by molecular dynamics simulation was more

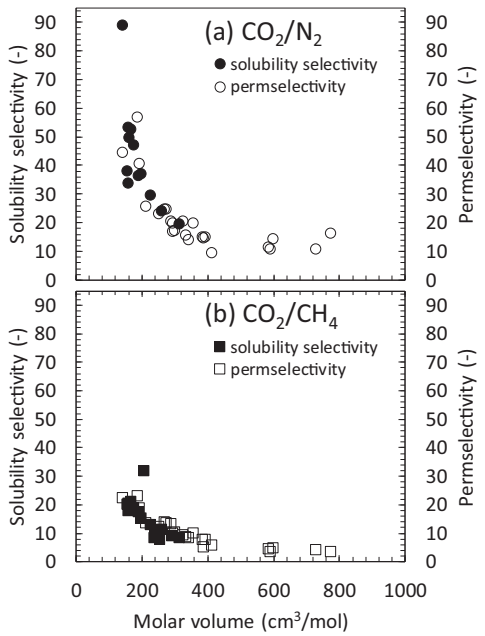

Figure 3. Relationship between solubility selectivity of ionic liquids with different molar volumes and permselectivities of a supported ionic liquid membrane in: (a) CO_2/N_2 system and (b) CO_2/CH_4 system.

than 4000 barrer (Liu et al. 2014a). In the calculation of the theoretical maximum value, it should be noted that a virtual IL membrane composed of only an IL without a porous support and gel network was considered.

To use the "liquid" ILs as a material for a "solid" membrane, the ILs should be solidified. In the early stages of the research on IL-based CO_2 separation membranes, SILMs were well investigated. SILMs are composite membranes composed of an IL and a porous support membrane. The ILs were impregnated into the porous support membrane by a weak capillary force. Therefore, in practical applications, the low-pressure resistance of SILMs is sometimes a serious problem. Moreover, decreasing the membrane thickness of SILMs is a challenge. The membrane thickness of SILMs is determined by the thickness of the porous support; however, the preparation of a significantly thin, porous membrane with a thickness of less than 1 μm is difficult. Additionally, the pressure resistance should be decreased by decreasing the thickness of the support membrane. Furthermore, because gases are hardly dissolved in the dense polymer matrix of a porous support membrane, the porosity of the support membrane should be increased to increase the CO_2 permeability. However, if the porosity increases, the pressure resistance decreases. Therefore, because of the limitations of the support membranes, increasing the CO_2 permeance of SILMs is considerably challenging.

To overcome the abovementioned problems of SILMs, polymerized IL membranes have been developed. Polymerized IL membranes can be prepared using an IL monomer with polymerizable functionalized groups, such as vinyl groups. Polymerized IL membranes are dense polymer electrolyte membranes retaining IL moiety with selective CO_2 solubility (Li et al. 2011). However, because polymerized IL membranes are dense polymer membranes without interconnected intrinsic micropores, their CO_2 diffusivity is

low (Li et al. 2011). Thus, most polymerized IL membranes have a low CO_2 permeability of less than 100 barrer. To increase the low diffusivity and permeability, Bara et al. (2008) developed a composite membrane by incorporating a liquid IL in a polymerized IL membrane. They reported that only 20 mol% of IL loading improved the CO_2 permeability to four times that of a polymerized IL membrane with no free IL. Further investigations on the effect of IL loading were performed by Carlisle et al. (2012). They prepared composite membranes with IL loading of up to 75 wt% and reported that the CO_2 permeability of the composite membrane increased with the increase in the IL loading. These studies on polymerized IL/IL composite membranes were then shifted to the development of membranes composed of a gel containing a large amount of IL as the solvent.

A gel containing an IL as its main component is named ion gel, ionogel, ionic gel, and so on. In this article, we call it an ion gel. The gel network strongly holds the IL under the osmotic pressure of the gel to prevent IL leakage. By selecting a suitable combination of the gel network polymer and IL, ion gels with IL contents of 80 wt% or more can be prepared. Ion gels with high IL content have superior CO_2 diffusivities. Therefore, ion-gel-based membranes can overcome both the low-pressure resistance of SILMs and the low CO_2 diffusivity of polymerized IL membranes. Using an ion gel, Zhou et al. (2014a) developed a composite membrane composed of a thin ion gel layer, PDMS gutter layer, and porous support membrane. Although the IL content of their ion gel layer was still not very high (approximately 60 wt%), the composite membrane exhibited a superior CO_2 permeance of approximately 6000 GPU because of the significantly thin ion gel layer with a thickness of approximately 100 nm. CO_2 permeance can be further increased by increasing the IL content of the ion gel layer. However, conventional ion gels have the serious problem of low mechanical strength, which limits the increase in the IL content in the ion gel membrane.

To overcome the issue of low mechanical strength, tough ion gels with high IL content have been developed in recent years. Examples of tough ion gels that have been reported to date are listed in Table 1. An image of a characteristic gel network formed in some examples of toughening of ion gels is illustrated in Figure 4. The toughening mechanism can be

Table 1. CO_2 permeability, N_2 permeability, and CO_2/N_2 permselectivity of ion gel membranes containing [Emim][Tf_2N].

	IL content	Permeability (barrer)		CO_2/N_2 permselectivity	Ref
		CO_2	N_2		
Poly(RTIL)-based gel film[a]	75 mol%	490	15.3	32	Carlisle et al. (2012)
PVDF-HFP-based gel film[b]	80 wt%	500	21	23.8	Jansen et al. (2011)
Triblock copolymer-based gel film[c]	85 wt%	840	35	24	Gu et al. (2012)
	85 wt%	710	17	42	Gu et al. (2012)
	85 wt%	980	25	39	Gu et al. (2012)
	90 wt%	870	40	22	Gu et al. (2012)
Tetra-PEG-based gel film[b]	94 wt%	877	81	21	Fujii et al. (2015)
Ion gel with interpenetrating polymer network[b]	80 wt%	670	30	29	Zhang et al. (2022b)
	84 wt%	761	28	27	Zhang et al. (2022b)
	86 wt%	917	31	30	Zhang et al. (2022b)
	90 wt%	1116	40	28	Zhang et al. (2022b)
	91 wt%	1412	52	27	Zhang et al. (2022b)

[a]298 K
[b]303 K
[c]Room temperature

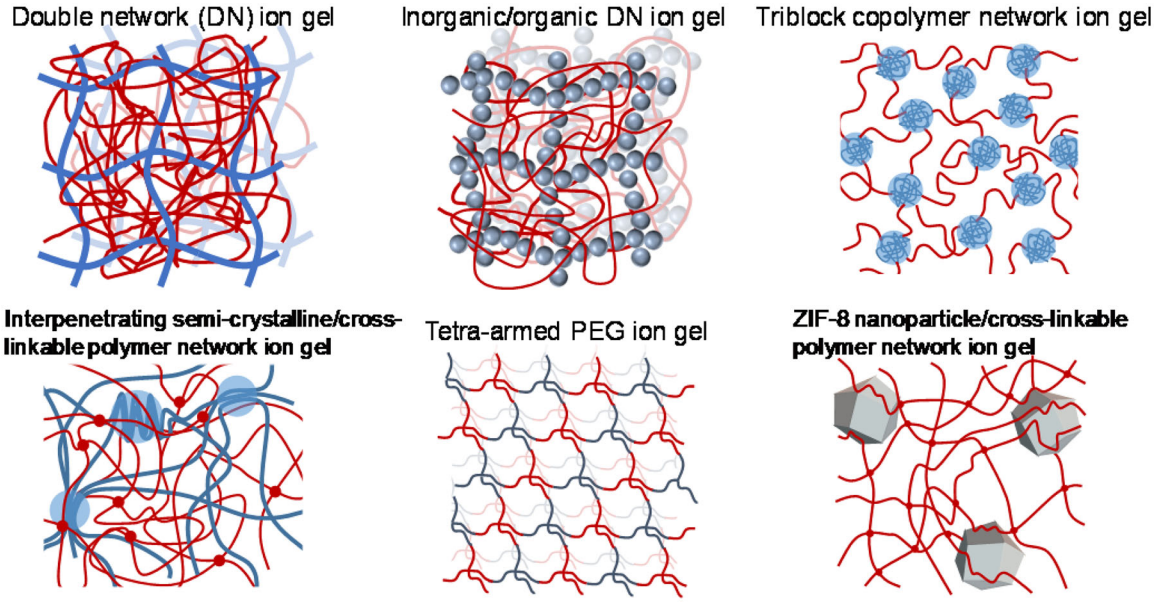

Figure 4. Schematic representations of tough ion gel network structures; Double network (DN) ion gel (Moghadam et al. 2015), Inorganic/organic DN ion gel (Kamio et al. 2017c), Triblock copolymer network ion gel (Lodge and Ueki 2016), Interpenetrating semi-crystalline/cross-linkable polymer network ion gel (Zhang et al. 2022b), Tetra-armed PEG ion gel (Fujii et al. 2012), ZIF-8 nanoparticle/cross-linkable polymer network ion gel (Kamio et al. 2022).

roughly categorized into (1) energy dissipation and (2) energy dispersion mechanisms. The toughening mechanisms of the double network (DN) ion gels, inorganic/organic DN ion gels, interpenetrating semicrystalline/crosslinkable polymer network ion gels, and zeolitic imidazolate framework-8 nanoparticle/polymer composite ion gels are considered as energy dissipation mechanisms. Conversely, ion gels composed of a triblock copolymer network and tetra-arm PEG ion gel would disperse the applied force by multiple polymer chains with well-aligned lengths between crosslinking points.

Table 1 shows the possibility of increasing the IL content in tough ion gels by more than 90 wt%. Based on theoretical models, *e.g.*, the Ogston model (Ogston 1958), the diffusion coefficient of a solute in the gel exponentially increases with increasing solvent content. Consequently, as indicated in Figure 5, the CO_2 permeability of the tough ion gel membrane increases exponentially with increasing IL content (Kamio et al. 2021; Ranjbaran et al. 2017). An ion gel membrane with an IL content of 90 wt% had a CO_2 permeability of approximately 45% of the theoretical maximum CO_2 permeability. When the IL content reached 95 wt%, the CO_2 permeability increased significantly to approximately 67% of the theoretical maximum value.

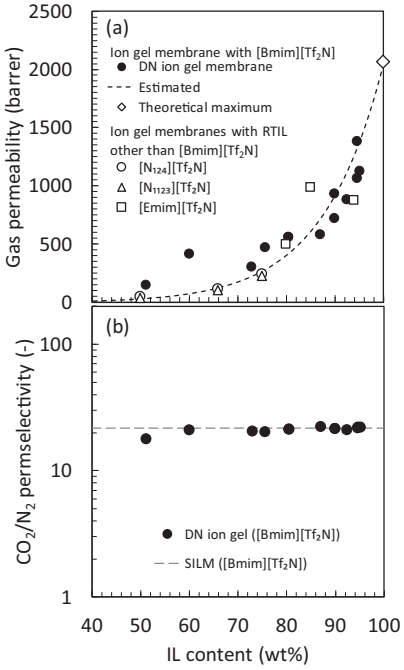

Figure 5. Relationship between (a) CO_2 permeability and (b) CO_2/N_2 permselectivity and ionic liquid content of ion gel membranes. Black circle: inorganic/organic double network (DN) ion gel membranes containing 1-butyl-3-methylimidazolium bis(trifluoromethanesulfonyl)imide ([Bmim][Tf_2N]) (Kamio et al. 2021), white diamond: theoretical maximum CO_2 permeability calculated from the diffusion coefficient (8.5×10^{-10} m^2/s) and Henry's law constant (42 bar) of CO_2 in [Bmim][Tf_2N] (Hou and Baltus 2007), white circle and triangle: sulfonated polyimide-derived ion gel membrane containing *N,N,N*-butylethylmethylammonium bis(trifluoromethylsulfonyl)amide ([N_{124}][Tf_2N]) and *N,N,N,N*-ethyldimethylpropylammonium bis(trifluoromethylsulfonyl)amide ([N_{1123}][Tf_2N]) (Hayashi et al. 2019), white square: ion gels containing [Emim][Tf_2N] with polymerized ionic liquid network (Cowan et al. 2016), triblock copolymer network (Gu and Lodge 2011), and tetra-arm polyethylene oxide network (Fujii et al. 2015). Broken line in (a) is the theoretically calculated result for the ionic liquid-based membrane with [Bmim][Tf_2N]. Dashed line in (b) is the CO_2/N_2 permselectivity of an SILM containing [Bmim][Tf_2N] (Kamio et al. 2021).

The highly tough ion gels with high IL content can be regarded as quasi-liquid materials that maintain the solute diffusivity in an IL at high extent. ILs with small cation-anion interactions are soft and flexible diffusion fields for solutes, and their CO_2 diffusion coefficients are as large as those of PDMS. Therefore, a tough ion gel membrane with a large amount of ILs with small cation-anion interactions can achieve extremely high CO_2 diffusivity. Although the solubility coefficient of CO_2 in ILs is small because CO_2 is dissolved in ILs according to Henry's law, some CO_2-philic ILs have high solubility selectivity for CO_2 when compared to other light gases. Tough ion gels maintain high solubility selectivity, and therefore, tough ion gel membranes have high permselectivity for CO_2 over other light gases. For example, a tough inorganic/organic DN ion gel membrane containing 80 wt% of [Emim][$B(CN)_4$] has a CO_2 permeability of approximately 2600 barrer and a $\alpha_{CO2/N2}$ of 43 (Ranjbaran et al. 2017).

To the best of our knowledge, there are no reports on the effects of aging on the CO_2 separation performance of ion gel membranes. However, the IL may leak from the ion gel membrane, resulting in performance degradation. Therefore, investigations on the effect of aging on the performance of ion gel membranes must be considered in the future.

With respect to the development of thin ion gel membranes, as mentioned above, Zhou et al. reported a composite membrane having a thin ion gel layer of 100 nm. However, to the best of our knowledge, there are only a few reports on tough ion gel thin membranes after their report. For example, Zhang and colleagues recently reported a composite membrane composed of a tough inorganic/organic μ-DN ion gel containing 80 wt% [Bmim][Tf_2N] (Zhang et al. 2021b). The gel layer was formed on a PDMS gutter layer by spin coating. To utilize the spin coating method, which is performed in an open system, they developed the preparation method of the μ-DN ion gel using nonvolatile network precursors such as "solid" silica nanoparticles and "presynthesized" crosslinkable copolymers (Kamio et al. 2020b; Yasui et al. 2018, 2019, 2020a, 2020b; Zhang et al. 2021c). Their fabricated composite membrane had an ion gel layer with approximately 5 μm thickness, CO_2 permeance of approximately 120 GPU, and CO_2/N_2 permselectivity of approximately 20 (Zhang et al. 2021b). In their report, they raised the following three issues that must be solved to increase the CO_2 permeance: (1) to further decrease the gel layer thickness, the aggregation of the silica nanoparticles that are used for the first network precursor during the spin coating process must be prevented, (2) to increase the CO_2 permeability and CO_2/N_2 permselectivity of the ion gel layer, a CO_2-philic IL suitable for CO_2 separation should be used, and (3) to prevent diffusion through the gutter layer from becoming the rate-limiting step for CO_2 permeation, a high-performance ultrathin gutter layer should be used. Recently, the authors reported another composite membrane with a tough ion gel layer containing 90 wt% of [Emim][Tf_2N] with 600 nm of thickness. In the ion gel layer, they used a semicrystalline polymer as the precursor of the first network to solve the aforementioned issue (1) of the aggregation of the network precursor; moreover,

[Emim][Tf_2N] having a higher CO_2 absorbability than [Bmim][Tf_2N] was used to overcome the aforementioned issue (2) (Zhang et al. 2022a, 2022b). As the CO_2 permeance of the PDMS gutter layer that was used in their research (Zhang et al. 2022a) was 60 times lower than that used by Zhou et al. (2014a), the CO_2 permeance of their developed composite membrane was insufficient (778 GPU); however, the CO_2 permeability of the gel layer of the developed composite membrane was significantly high and was estimated to be 1860 barrer (Zhang et al. 2022a). To develop ion gel-based high-performance CO_2 separation membranes, the development of a preparation technology for a thin ion gel layer and a high-performance gutter layer capable of coating a thin ion gel layer is vital. For instance, the abovementioned ultrathin PDMS with significantly high CO_2 permeance (Ariyoshi et al. 2021; Fujikawa et al. 2019; Selyanchyn et al. 2020) can be used as the gutter layer for ion-gel-based TFC membranes.

2.3 Theoretical consideration of the upper bound and design criteria of high-performance CO_2 separation membranes

2.3.1 Theoretical consideration of the upper bound

As mentioned above, in 1991, Robeson demonstrated the upper bound line which is the tradeoff between $\alpha_{CO2/j}$ and P_{CO2}. The upper bound line is described by the following equation:

$$\alpha_{i/j} = \beta_{i/j}/P_i^{\lambda_{i/j}}, \tag{3}$$

where $\lambda_{i/j}$ and ln $\beta_{i/j}$ are the slope and intercept of the upper bound line, respectively.

In Figure 6, four upper-bound lines are shown. The black broken line is the upper bound for conventional polymer membranes, such as polyimide, polysulfone, cellulose acetate. The black solid line is the upper bounds for polyethylene oxide (PEO) containing polymer membranes. The red and blue lines represent the upper bounds for recently developed high-performance CO_2 separation membrane materials, polymers of intrinsic microporosity (PIMs), and thermally rearranged (TR) polymers, respectively. The characteristics of each high-performance CO_2 separation membrane material are described in the previous sections. Importantly, the membranes of these new polymer materials have structures that follow the design criteria expected from the upper bounds. The design criteria for the membrane structure were proposed by Freeman (1999) based on the theoretical consideration of the upper bound. His theory is based on the following four assumptions:

I. Solution-diffusion model (Eq. (1)) is applicable.
II. The diffusion of small molecules through the polymer is an activated process, for which the Arrhenius equation is obtained:

$$D_i = D_{0,i} \cdot \exp\left(-\frac{E_{D,i}}{RT}\right), \tag{4}$$

where $D_{0,i}$ is the front factor, $E_{D,i}$ is the activation energy for diffusion, R is the gas constant, and T is the absolute temperature.

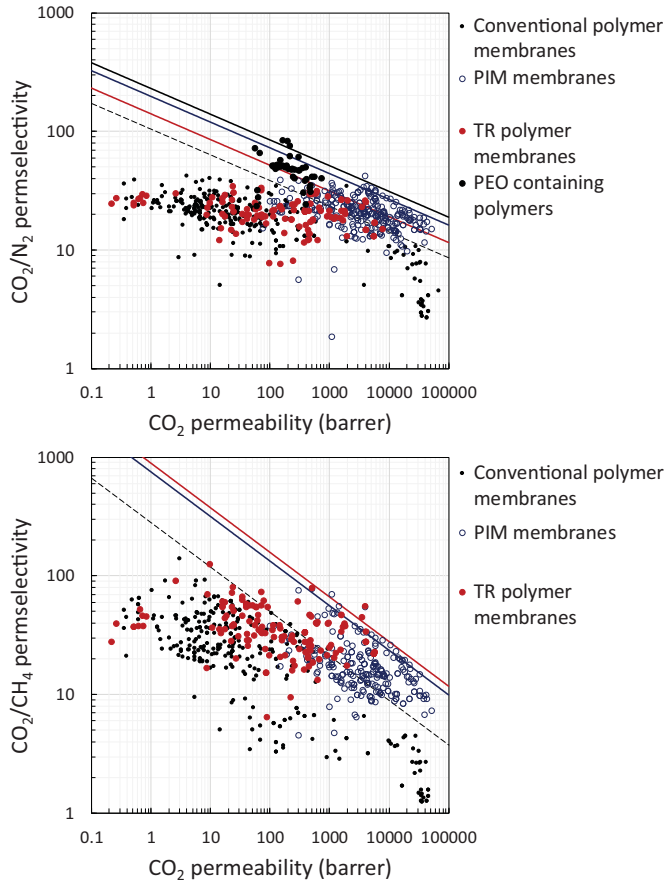

Figure 6. Relationship between P_{CO2} and (a) $\alpha_{CO2/N2}$ and (b) $\alpha_{CO2/CH4}$. Straight lines indicate the upper bounds for classic polymer membranes (broken black), membranes comprising polyethylene oxide (PEO) (solid black), polymers of intrinsic microporosity (PIMs) (blue), and thermally rearranged (TR) polymer membranes (red) with the highest class performances. The straight lines were determined using Eq. (12).

A so-called "linear free energy" relation exists, which is a correlation between the pre-exponential term of the Arrhenius equation and the activation energy:

$$\ln D_{0,i} = a\frac{E_{D,i}}{RT} - b \tag{5}$$

where a is a constant ($a = 0.64$) that is independent of the gas and polymer. Conversely, b is independent of the gas type but dependent on the polymer type, *i.e.*, b is 9.2 and 11.5 for rubbery and glassy polymers, respectively.

The activation energy is related to the kinetic diameter of the gas molecules.

$$E_{D,i} = c \cdot d_i^2 - f \tag{6}$$

where d_i is the kinetic diameter of the gas i. c is a constant related to the rigidity and flexibility of the diffusion medium, *i.e.*, a large c indicates that the diffusion medium is rigid. f is a parameter related to the frozen void space

formed between polymer chains in the diffusion matrix, *i.e.*, 0 for rubbery and significantly dense glassy polymers and more than 10,000 for highly permeable glassy polymers.

Based on these assumptions, the effective diffusion coefficients of CO_2, D_{CO2}, CO_2 permeability, P_{CO2}, and the permselectivity of CO_2 over gas j, $\alpha_{CO2/j}$, can be described by the following equations.

$$\ln D_{CO2} = -\left(\frac{1-a}{RT}\right)\cdot c\cdot d_{CO2}^2 + f\cdot\left(\frac{1-a}{RT}\right) - b \tag{7}$$

$$\ln\frac{D_{CO2}}{D_j} = \left(\frac{1-a}{RT}\right)\cdot c\cdot\left(d_j^2 - d_{CO2}^2\right) \tag{8}$$

$$\ln P_{CO2} = -\left(\frac{1-a}{RT}\right)\cdot c\cdot d_{CO2}^2 + f\cdot\left(\frac{1-a}{RT}\right) - b + \ln S_{CO_2} \tag{9}$$

$$\ln\alpha_{CO2/j} = \ln\left(\frac{S_{CO2}}{S_j}\right) + \left(\frac{1-a}{RT}\right)\cdot c\cdot\left(d_j^2 - d_{CO2}^2\right) \tag{10}$$

As indicated in Eq. (7), the use of significantly soft rubbery polymers (with smaller b and c values) is preferred to increase the diffusion coefficient. Conversely, for glassy polymers, increasing the frozen void space between the polymer chains, f, is effective. For the diffusion coefficient, the following relationship based on the free volume theory (Alentiev and Yampolskii 2000) is widely accepted.

$$\ln D_{CO2} = -\frac{B}{\mathrm{FFV}} + A \tag{11}$$

where A and B are constants and FFV is the fractional free volume of the polymer. Based on this equation, the material of the membrane matrix with a large FFV has a large diffusion coefficient. On the other hand, according to Eq. (8), a membrane matrix with high rigidity (large c) is preferable for increasing diffusion selectivity.

Furthermore, from Eqs. (7) (9) and (10), the following equation is derived.

$$\ln\alpha_{CO2/j} = -\left[\left(\frac{d_j}{d_{CO2}}\right)^2 - 1\right]\cdot\ln P_{CO2} + \left\{\ln\left(\frac{S_{CO2}}{S_j}\right) - \left[\left(\frac{d_j}{d_{CO2}}\right)^2 - 1\right]\cdot\left(b - f\left(\frac{1-a}{RT}\right)\right) - \ln S_{CO2}\right\} \tag{12}$$

This equation expresses the upper bound line as a function of the size of the penetrant gases, permeability of the more permeable gas, solubility of the penetrant gases in the polymers, and some characteristic parameters related to the polymers. Based on Eq. (12), the slope of the upper bound line is determined to be independent of the membrane material and depends only on the size ratio of the penetrant gases. The straight lines in Figure 6 are drawn according to Eq. (12), using the data for each class of membranes with around the highest CO_2 separation performances. The straight lines were observed to be well-fitted to the experimentally reported upper-bound data for each class of membranes. This result indicates that the theoretical considerations introduced above are reasonable. Equation (12) shows that a higher $\alpha_{i/j}$ can be obtained for membrane materials with larger solubility selectivity (S_{CO2}/S_j), larger solubility coefficient of CO_2 (S_{CO2}), and larger frozen void space between polymer chains (f). When considering the solubility coefficient, glassy polymers have a higher solubility coefficient than rubbery polymers because of the additional gas absorption in micropores that are formed in glassy polymers, *i.e.*, for rubbery polymers, the gas sorption can be described by Henry's law, and for glassy polymers, it can be described by the dual-sorption model, which includes both Henry-type sorption in the free volume of the membrane matrix and Langmuir-type sorption in micropores. Therefore, from the perspective of permselectivity, a glassy polymer membrane with a large CO_2 solubility coefficient and large f value is superior.

As expected from Eq. (12), the improvement in the solubility and solubility selectivity of a more permeable gas in a rigid membrane is also meaningful. For glassy polymers, an increase in gas solubility can be achieved by the sorption of gas molecules in micropores, which are the voids formed between the polymer chains under a nonequilibrium frozen state via rapid cooling of the polymer from an elevated temperature to below the glass transition temperature. Conversely, if a large diffusion selectivity cannot be expected, *e.g.*, in the case of rubbery polymers, the permselectivity of the membrane can be increased by increasing the solubility selectivity of the more permeable gas.

In accordance with the consideration based on the above-derived equations, there are two ways in which polymer membranes that can perform beyond the upper bound might be achieved for gas separation:

i. one method is to increase the stiffness of the polymer chain while simultaneously increasing the interchain spacing and
ii. another way is to increase the softness of the polymeric material while simultaneously improving the solubility selectivity by tuning the interaction with a more permeable penetrant.

2.3.2 Glassy polymer membranes developed in accordance with the design criterion (i)

In the separation of light gases, the polymer membranes with a separation performance close to the upper bound are generally glassy polymers. Thus, the abovementioned criterion (i) is widely recognized as a straightforward way for developing membrane materials that can exceed the upper bound for gas separation performance. The polymers with the microporous structure relative to criterion (i) are PIMs and TR polymers.

PIMs are rigid glassy polymers with interconnected micropores that follow the abovementioned design criterion (i) for the development of high-performance CO_2 separation membranes. In accordance with the design criterion, PIM-1 has high permeability for light gases. Owing to the highly developed interconnected micropores, PIM membranes have higher CO_2 diffusivity and solubility than conventional

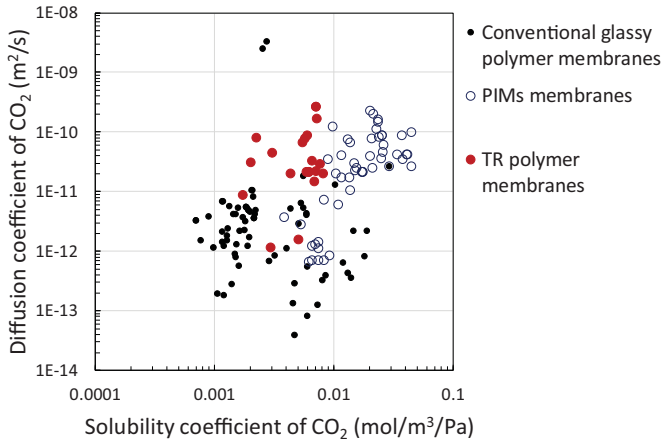

Figure 7. Relationship between diffusion and solubility coefficients of CO_2 in conventional polymer, PIM, and TR polymer membranes.

polymer membranes (Figure 7). Consequently, the CO_2 permeability of PIM membranes is significantly higher than that of conventional polymer membranes. In fact, PIM-based membranes have updated the upper bounds of conventional polymer membranes for CO_2/N_2 and CO_2/CH_4 separation (blue lines in Figure 6). Despite their high CO_2 permeabilities, PIM membranes have relatively high CO_2/N_2 and CO_2/CH_4 permselectivities. A possible reason for the high permselectivity of the PIM membranes is shown in Figure 8. By comparing the data shown in Figure 8(a,b), for both CO_2/N_2 and CO_2/CH_4 systems, the CO_2 solubility selectivities of many PIMs is confirmed to be significantly larger than those of conventional glassy polymers. To the best of our knowledge, there is no report that clearly explains the high CO_2 solubility selectivity of PIMs. However, as shown in Figure 7, PIMs have a higher solubility coefficient than conventional glassy polymers. High solubility coefficients can be attributed to a combination of microporous character, which enhances uptake, and the presence within the molecular structure of polar groups that strengthen intermolecular interactions (Ghanem et al. 2008b). The high solubility coefficient for CO_2 could contribute to enhancing both the CO_2 permeability and CO_2/N_2 and CO_2/CH_4 permselectivities (refer to Eqs. (9) and (12)).

The other glassy polymer membrane relative to the abovementioned design criterion (i) is the TR polymer membrane. Owing to the highly developed microcavity formed in the rigid TR polymer matrix and the large FFV, the TR polymer membrane follows design criterion (i) of high-performance CO_2 separation membranes. As expected, the TR polymer membranes had high permeability for light gases. Because of the highly developed interconnected micropores, both CO_2 diffusivity and solubility in TR polymers are greater than those of conventional glassy polymers (Figure 7). The formed micropores in TR polymers are smaller than PIMs and conventional glassy polymers (Gan et al. 2019, Han et al. 2010; Staiger et al. 2008). The sizes of micropores formed in PIM-1, TR-1-450, and conventional glassy polymers with high CO_2 permeability, which were measured via positron annihilation lifetime spectroscopy (PALS), are summarized in Table 2.

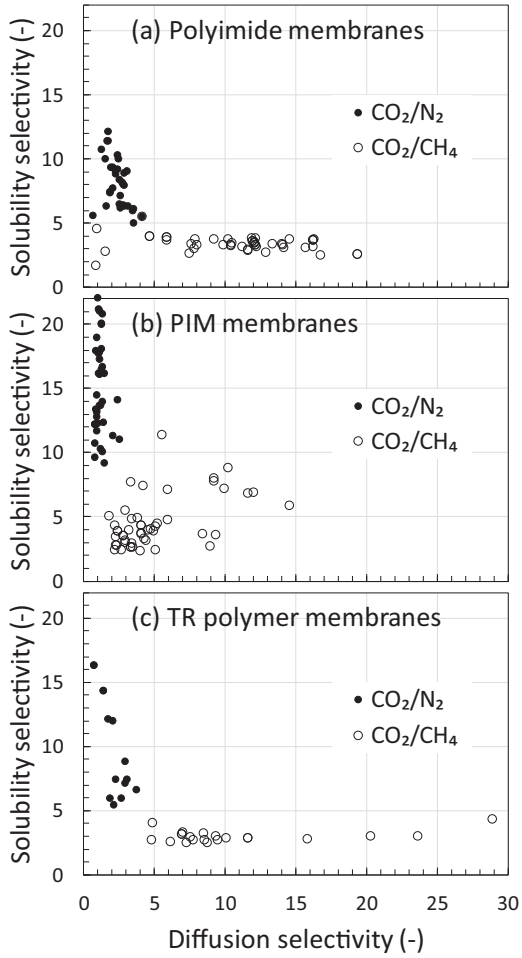

Figure 8. Relationship between solubility and diffusion selectivities of polyimide-based polymer membranes, PIM membranes, and TR polymer membranes.

For the CO_2/CH_4 separation system, the permselectivity of the glassy polymer membranes was dominated by diffusion selectivity (Figure 8). This is the general trend for glassy polymer membranes for the following two reasons: (1) the difference in the kinetic diameters of CO_2 and CH_4 is greater than that between CO_2 and N_2 (the kinetic diameters of CO_2, CH_4, and N_2 are 0.33, 0.387, and 0.364 nm, respectively); (2) the difference in the boiling points (condensability) between CO_2 and CH_4 is smaller than that between CO_2 and N_2 (the Lennard–Jones temperature, i.e., ε/k, of CO_2, CH_4, and N_2 is 195, 149, and 71 K, respectively). In general, a higher kinetic diameter difference results in a high diffusion selectivity, and a lower difference in condensability results in a low solubility selectivity. Thus, it can be said that the CO_2/CH_4 permselectivity of these glassy polymer membranes are primarily dominated by the high CO_2 diffusivity due to the highly developed micropores. In addition to the above general trend, because of the smaller micropore diameter of TR polymers, certain TR polymer membranes have a greater CO_2/CH_4 diffusion selectivity than conventional glassy polymer membranes and PIM membranes (Figure 8). Furthermore, based on Eq. (8), TR polymers are expected to have a more rigid membrane matrix because the diffusion selectivity of CO_2 over gas species j is determined by the rigidity of the membrane matrix.

Table 2. Positron annihilation lifetime spectroscopy (PALS) data for glassy polymers with high CO_2 permeability.

	PIM-1[a]		TR-1[b]		PTMSP[a]		AF1600[a]		AF2400[a]	PMP[a]
			From tHPI	From aHPI						
PALS data	Fresh	Aged	Fresh	Fresh	Fresh	Aged	Fresh	Aged	Fresh	Fresh
τ_3(ns)	2.06	1.98	1.24	1.06	1.7	1.7	1.2	1.2	1.32	2.3
I_3(%)	6.15	5.72	5	7.1	7.4	7.4	5.51	5.85	4.87	8.4
Small pore diameter (nm)	0.581	0.567	0.404	0.351	0.512	0.512	0.393	0.393	0.425	0.623
τ_4(ns)	6.28	6.15	5.26	3.9	8.8	8.8	5.11	5.21	5.78	7.6
I_4(%)	18.6	17.4	6	12.7	34	31	17.3	15.1	13.6	29.4
Large pore diameter (nm)	1.06	1.049	0.973	0.837	1.238	1.238	0.96	0.969	1.019	1.158
Specific gravity	1.13	1.16	1.27	1.38	0.75	–	1.8	–	1.7	0.78
FFV	0.15	0.12	0.28	0.22	0.34	–	0.28	–	0.32	0.28

[a]Staiger et al. (2008)
[b]Han et al. (2010)

Owing to the small micropores and rigid polymer chains, TR polymer membranes have high CO_2/CH_4 diffusion selectivity and are particularly superior in CO_2/CH_4 separation based on the size-sieving effect (red line in Figure 6(b)).

On the other hand, for the CO_2/N_2 separation system, because of the close kinetic diameters and significant difference in condensability, the diffusion selectivity of glassy polymer membranes is quite limited and similar among the three types of glassy polymers that are shown in Figure 8. Moreover, unlike PIMs, TR polymers seem to exhibit no additional solubility enhancement for CO_2, and the CO_2/N_2 solubility selectivity is similar to that of conventional glassy polymers. Thus, the upper bound of the CO_2/N_2 separation performance of the TR polymer membranes is similar to that of conventional glassy polymer membranes (Figure 6(a)).

2.3.3 Rubbery polymer membranes and ionic liquid-based membranes developed in accordance with the design criterion (ii)

As mentioned above, PIM and TR polymer membranes are high-performance CO_2 separation membranes with rigid and intrinsic microporous structures relative to the above-mentioned design criterion (i) for the development of high-performance CO_2 separation membranes. Conversely, polymer membranes based on design criterion (ii) can be created using rubbery polymers such as PDMS. Soft and flexible polymer chains provide a large CO_2 diffusion coefficient for the membrane matrix, and the development of thin film formation technology has enabled the development of a CO_2 separation membrane with high CO_2 permeance (Li et al. 2013a, 2015; Liang and Chung 2018). However, because of the low solubility selectivity of PDMS, the CO_2/N_2 permselectivity is low (about 10). Thus, enhancement of the solubility selectivity of PDMS is highly desired. On the other hand, PEO-based polymers are another type of attractive rubbery polymer for CO_2 separation membrane. Because PEO has high solubility selectivity of CO_2 over other light gases, the PEO-based membranes have high CO_2 permselectivity over N_2 and CH_4. The CO_2 separation performances of some examples of PEO-based membranes (Bondar et al. 2000; Hirayama et al. 1999; Lin et al. 2006; Taniguchi et al. 2017; Yave et al. 2010; Yoshino et al. 2000) are shown in Figure 6(a) as a black solid line. The attractive feature of PEO-based

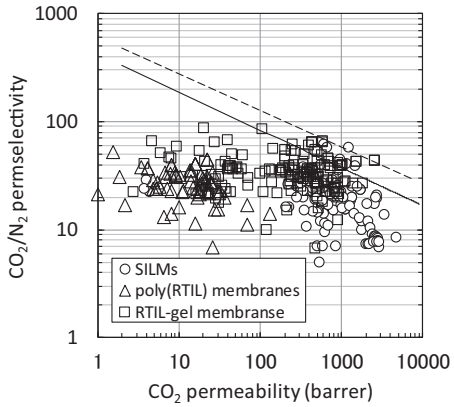

Figure 9. Relationship between $\alpha_{CO2/N2}$ and P_{CO2}. Solid and broken lines are the upper bounds reported by Robeson (2008) and Comesaña-Gándara et al. (2019), respectively.

membranes relates to the enhancement of improving the solubility selectivity of the design criterion (ii). If the concept of increasing in the softness of the design criterion (ii) can be further adopted for the PEO-based membrane, a CO_2 separation membrane with high CO_2 permeability based on design criterion (ii) and high CO_2 permselectivity derived from the PEO unit could be created.

The other CO_2 separation membrane that is being developed based on design criterion (ii) is ionic liquid-based membranes. ILs are low-molecular-weight liquids with significantly softer and more flexible properties than rubber polymers. Thus, the parameter c in Eq. (6) and the activation energy for solute diffusion can be considered as significantly small, and the diffusion coefficient of CO_2 in ILs is an order of magnitude higher than that in PIMs and TR polymers. In addition, because the physical and physicochemical properties of ILs can be controlled by tuning the chemical structure, some ILs have not only high diffusivity but also high CO_2 solubility selectivity. Thus, ILs can be regarded as the ultimate CO_2 separation medium for achieving design criterion (ii) for the development of high-performance CO_2 separation membranes. Figure 9 shows the relationship between the CO_2/N_2 permselectivity and CO_2 permeability of the IL-based CO_2 separation membranes that have been reported to date. The solid and broken lines shown in this figure are the upper bound lines reported in 2008 and 2019, respectively (Comesaña-Gándara et al. 2019; Robeson 2008). This figure shows that some IL-based CO_2 separation membranes, especially ion gel membranes, show

outstanding CO_2 separation performance beyond the upper bound that was redefined in 2019. Thus, it can be said that the ion gel membrane is a high-performance CO_2 separation membrane developed by pursuing the flexibility of the diffusion field based on structural design criterion (ii).

2.4 Facilitated Transport Membranes

Apart from the design criteria based on the theoretical considerations of Freeman, the strategy of increasing the CO_2 absorbability using chemical reactions to increase CO_2 permeability and CO_2 permselectivity over other light gases is also attractive and effective. This concept has been applied to well-known facilitated transport membranes. In this section, the facilitated transport mechanism is reviewed and three types of facilitated transport membranes for CO_2 separation are introduced.

2.4.1 Facilitated transport mechanism

Facilitated transport membranes are functional membranes that contain chemical compounds that can chemically and reversibly react with specific molecules (gases or ions). The chemical compound incorporated into the membrane is called a carrier. Because the carrier can chemically react with CO_2 but not with other light gases, CO_2 permeates through the membrane based on the facilitated transport mechanism; however, the permeation of other light gases such as N_2, CH_4, and H_2 is not facilitated by the carrier. A schematic illustration of the facilitated CO_2 transport mechanism is shown in Figure 10. In a facilitated transport membrane, both of the CO_2-carrier complexes formed via chemical reactions and the physically dissolved CO_2 permeate through the membrane. Conversely, other light gases such as N_2, CH_4, and H_2 can only permeate through the membrane based on the solution-diffusion mechanism. Thus, facilitated transport membranes achieve high selectivity and significantly faster CO_2 permeation as compared to other CO_2 separation membranes.

In facilitated transport membranes, the transmembrane diffusion of CO_2-carrier complexes formed by chemical reactions promotes CO_2 permeation. Therefore, the CO_2 permeability and permselectivity of facilitated transport membranes are affected by the concentration gradient of the CO_2-carrier complexes in the membrane and the chemical reaction rate in complex formation. When the complex formation reaction is significantly faster than the CO_2-carrier complex diffusion in the membrane, the rate-determining step of CO_2 permeation becomes an intermembrane diffusion-controlled process. In this case, the concentration of each gas component in the facilitated transport membrane can be described by the concentration profile shown in Figure 11. Figure 11(a–c) show the concentration profiles of CO_2 and N_2 for low, middle, and high CO_2 partial pressures in the feed gas, respectively. Figure 11(d–f) show the typical absorption isotherms of CO_2 and N_2 in the facilitated transport membranes. CO_2 is predominantly absorbed via chemical reactions, whereas N_2 is only absorbed by physical dissolution. Thus, the CO_2 absorption isotherm shows significant and moderate increases in the absorption amount under low and high CO_2 partial pressure conditions,

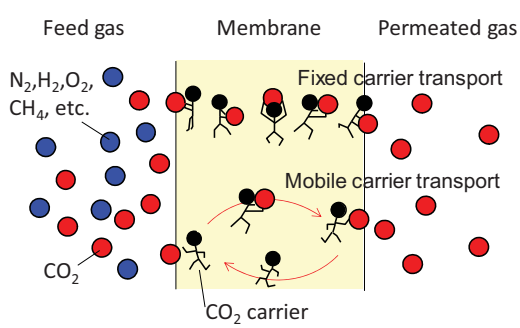

Figure 10. Schematic illustration of facilitated transport mechanism.

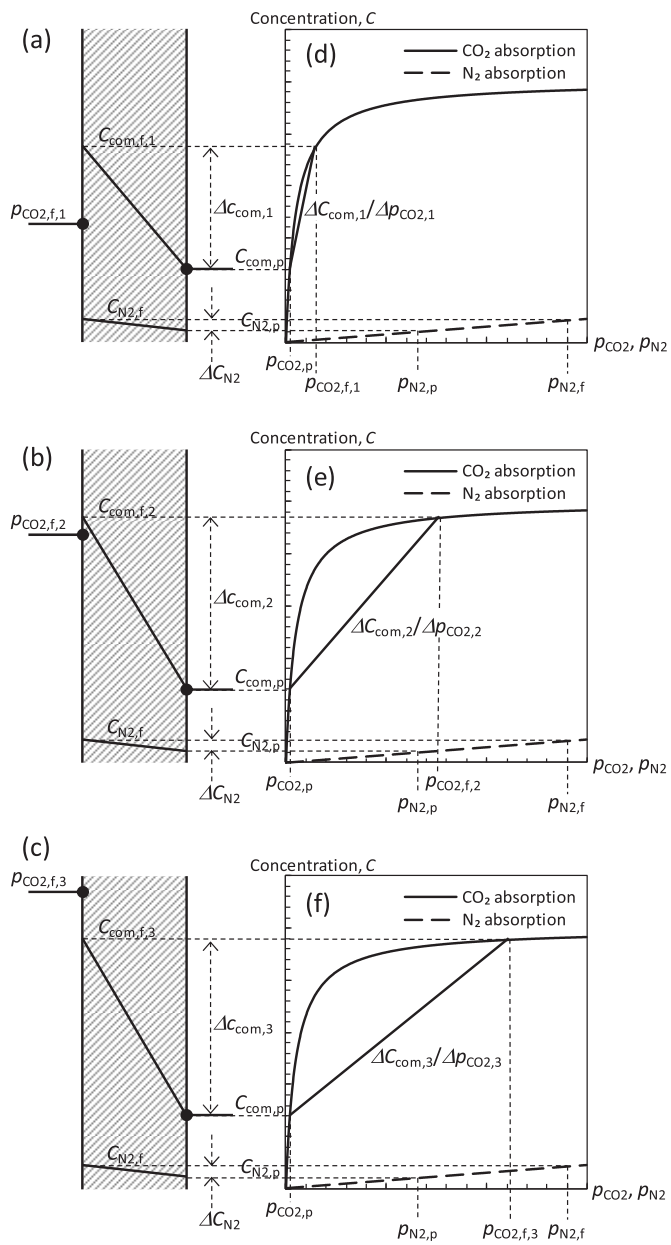

Figure 11. (a-c) Concentration profiles of CO_2 and N_2 for the cases of low, middle, and high CO_2 partial pressure in the feed gas, respectively. (d-f) typical absorption isotherms of CO_2 and N_2 in facilitated transport membranes for each case of (a-c), respectively.

respectively. The moderate increase in the absorption amount under high CO_2 partial pressure conditions is due to the saturation of the carrier by a sufficient amount of CO_2 in the gas phase. Conversely, N_2 is absorbed based on Henry's law, and the absorption amount increases proportionally with the increase in N_2 partial pressure. Other light gases, such as CH_4, O_2, and H_2, are also adsorbed in the facilitated transport membrane based on Henry's law, and the absorption isotherms are similar to Henry's type. Therefore, the amount of absorption is significantly lower than that of CO_2.

When diffusion-controlled gas permeation occurs across the membrane, the CO_2 and N_2 permeabilities, P_{CO2} and P_{N2}, respectively, are expressed by the following equations:

$$P_{CO_2} = D_{CO_2}\frac{\Delta C_{CO_2}}{\Delta p_{CO_2}} + D_{com}\frac{\Delta C_{com}}{\Delta p_{CO_2}}, \tag{13}$$

$$P_{N_2} = D_{N_2}\frac{\Delta C_{N_2}}{\Delta p_{N_2}}, \tag{14}$$

where D_{CO2} and D_{N2} are the effective diffusion coefficients of CO_2 and N_2 that are physically dissolved in the membrane, respectively; ΔC_{CO2} and ΔC_{N2} are the concentration gradients of CO_2 and N_2 in the membrane, respectively; moreover, Δp_{CO2} and ΔpN_2 are the transmembrane partial pressure differences of CO_2 and N_2, respectively. Because the amounts of physically absorbed CO_2 and N_2 show a proportional relationship with the partial pressures of each gas, the values of $\Delta C_{CO2}/\Delta p_{CO2}$ and $\Delta C_{N2}/\Delta pN_2$ are constant regardless of the partial pressures of each gas in the feed- and permeate-side streams. Assuming that the membrane structure does not change owing to gas absorption and that D_{CO2} and D_{N2} do not change, the permeability coefficients of the physically dissolved CO_2 and N_2 can be considered constant, independent of the transmembrane partial pressure difference. Conversely, the effect of facilitated CO_2 transport is described by the second term on the right-hand side of Eq. (13), where D_{com} and ΔC_{com} are the effective diffusion coefficient and concentration gradient of the CO_2-carrier complex in the membrane, respectively. Based on the chemical absorption isotherm of CO_2, we can observe that the amount of chemically absorbed CO_2 drastically increases under low CO_2 partial pressure conditions because of the strong chemical interaction between CO_2 and the carrier and becomes constant under high CO_2 partial pressure conditions because of carrier saturation. Thus, as indicated in Figure 11(d–f), when the CO_2 partial pressure in the permeate gas is constant, $\Delta C_{com}/\Delta p_{CO2}$ decreases with an increase in Δp_{CO2}. Consequently, the CO_2 permeability strongly depends on the CO_2 partial pressure and decreases with increasing CO_2 partial pressure in the feed stream. This is a general phenomenon of facilitated transport membranes, and they are considered to be particularly effective for gases with low CO_2 partial pressures.

2.4.2 Materials of facilitated transport membranes

As carriers for facilitated transport membranes for CO_2 separation, chemical compounds containing amino groups and alkali metal carbonates are generally used. For example, the reaction between primary or secondary amines and CO_2 is based on the following equilibrium reaction, where 2 mol of amine reacts with 1 mol of CO_2 to produce 1 mol of carbamate ions.

$$\text{Primary amine}: \quad CO_2 + 2RNH_2 \rightleftharpoons RHNCOO^- + RNH_3^+ \tag{15}$$

$$\text{Secondary amine}: CO_2 + 2RR'NH \rightleftharpoons RR'NCOO^- + RR'NH_2^+ \tag{16}$$

In the presence of water molecules, bicarbonate ions are generated based on the following equilibrium reaction, which is further accelerated.

$$\text{Primary amine}: \quad 2CO_2 + 2RNH_2 + H_2O \rightleftharpoons RHNCOOH + RNH_3^+ + HCO_3^- \tag{17}$$

$$\text{Secondary amine}: \quad CO_2 + RR'NH + H_2O \rightleftharpoons RR'NH_2^+ + HCO_3^- \tag{18}$$

Although tertiary amines cannot react with CO_2 in a dry atmosphere, they produce bicarbonate ions based on the following equilibrium reaction under humid condition.

$$\text{Tertiary amine}: \quad CO_2 + RR'R''N + H_2O \rightleftharpoons RR'R''HN^+ + HCO_3^- \tag{19}$$

Alkali metal carbonate, which is the other typical CO_2 carrier, also reacts with CO_2 under humid conditions to form bicarbonate ions. Moreover, the carboxylate group ($-COO^-$) is also an effective CO_2-reactive functional group and polymers with carboxylate groups can be used as materials for facilitated transport membranes. A carboxylate group reacts with CO_2 under humid conditions to produce bicarbonate ions, according to the following equilibrium equation.

$$CO_2 + -COO^- + H_2O \rightleftharpoons -COOH + HCO_3^- \tag{20}$$

As described above, in the general facilitated transport membranes, CO_2 permeation is facilitated by the intramembrane transportation of CO_2-carrier complexes, such as carbamate and bicarbonate ions. Thus, to maximize the facilitated transport effect, the use of a carrier with a large chemical absorption capacity for CO_2 is vital.

Conversely, the reaction rate of complex formation between carriers and CO_2 also influences the facilitated transport effect (Matsuyama et al. 1999a). If the reaction rates of complex formation and/or decomposition are significantly slower than the diffusion rate of the CO_2-carrier complex in the membrane, the chemical reaction becomes the rate-determining step of CO_2 permeation. In this case, to achieve effective facilitated transport, a CO_2 carrier with a

fast reaction rate for CO_2-carrier complex formation is required.

Furthermore, to maximize the facilitated transport effect, optimization of not only the CO_2 carrier but also the membrane material holding the CO_2 carrier is important. The use of a material that can hold a large amount of CO_2 carriers is vital. Moreover, flexibility is desirable so that the diffusion resistance of the CO_2-carrier complex becomes as small as possible. Furthermore, as mentioned above, as several carriers require water molecules to react with CO_2, a highly hydrophilic material that can easily absorb water vapor from the feed gas is preferable. In addition, when a chemical compound with amine or carboxylate groups is used as the CO_2 carrier, they must be maintained in a deprotonated state so that they can react with CO_2. Thus, adjusting the pH of the membrane is also important.

2.4.3 Fixed-carrier-type facilitated transport membranes

Facilitated transport membranes are broadly classified into fixed- and mobile-carrier-type facilitated transport membranes (hereafter referred to as fixed and mobile carrier membranes, respectively). A fixed carrier membrane is composed of a polymer with a functional group that chemically reacts with CO_2. Because the CO_2 carrier is immobilized in the polymer matrix, a fixed carrier membrane is highly stable. Examples of fixed carrier membranes and their CO_2 permeation performances are listed in Table 3. Representative polymers for fixed carrier membranes include polyvinylamine (Kim et al. 2004b), poly(ethylenimine) (Ben Hamouda et al. 2010; Matsuyama et al. 1999b), poly(allylamine) (Zhao and Ho 2012), and chitosan (Liu et al. 2014c; Prasad and Mandal 2018; Prasad et al. 2019). A fixed carrier membrane is prepared by dissolving a functional polymer in a good solvent, spreading the solution on a porous support membrane by casting or dip coating, and then removing the good solvent by drying. In these membranes, because the CO_2 reactive functional groups are fixed to the polymer matrix, carbamate and bicarbonate ions formed by the reaction between the functional groups sequentially diffuse and react with adjacent functional groups (Noble 1992). This transportation mode is called as hopping mechanism. In a fixed carrier membrane, the membrane matrix is dense and tightly entangled; thus, the CO_2 permeability is low because of the low diffusivity of the carbamate ions and bicarbonate. However, a fixed carrier membrane can be prepared as a thin layer on a porous support membrane by casting and dip-coating methods (Deng and Hagg 2015; Sandru et al. 2009, 2010). A significantly thin separation layer containing tertiary amino groups can be formed via interfacial polymerization between trimesoyl chloride and diamine compounds (Li et al. 2012b). Another interesting fixed carrier membrane with an extraordinary thin separation layer was developed by spray-coating of microgel particles (Hoshino et al. 2021). Such thin fixed carrier membranes provide large CO_2 permeance and CO_2 permselectivity (Li et al. 2012b, 2015).

2.4.4 Mobile-carrier-type facilitated transport membranes

A mobile carrier membrane is a functional membrane containing a low-molecular-weight CO_2 carrier in the membrane matrix. Because the size of the CO_2 carrier and the formed CO_2-carrier complex are small, they can easily diffuse in the membrane matrix. Therefore, a mobile carrier membrane usually has a faster diffusion rate of the CO_2-carrier complex and a higher CO_2 permeability than a fixed carrier membrane. Examples of mobile carrier membranes and their CO_2 permeabilities are listed in Table 4. Despite the high CO_2 permeability, the CO_2 permeances of mobile carrier membranes are not very high. This is because the mobile carrier membranes listed in Table 4 are thicker than the fixed carrier membranes, which have higher CO_2 permeance. If the thickness of the mobile carrier membrane can be reduced to 1 μm and the chemical reaction rate between the carrier and CO_2 is sufficiently fast to not change the rate-limiting step along with the decrease in the membrane thickness, it is expected that a mobile carrier membrane with a higher CO_2 permeance than thin fixed carrier membranes can be developed.

A representative form of a mobile carrier film is a supported liquid membrane (SLM), in which a liquid CO_2 carrier is held in a porous support membrane by capillary force. Typical SLMs with carriers such as monoethanolamine, diethanolamine, diglycolamine, and diethylenetriamine have high CO_2 permeability (Ito et al. 2001; Teramoto et al. 1996; Yamaguchi et al. 1995). However, as described in the explanation of SILMs, the carrier solution easily leaks from a porous support membrane because SLMs also hold a carrier solution by weak capillary force. Therefore, SLMs have the problem of low-pressure resistance, which significantly restricts the use of SLMs for practical applications. When considering carrier leakage, it has been reported that the use of a charged polymer matrix, such as an ion-exchange membrane, as a support membrane, is effective in holding the carrier solution within the support owing to the strong electrostatic interaction (Matsuyama et al. 1996, 1999a; Way et al. 1987). A stability issue other than leakage of the carrier liquid is the volatilization loss of the carrier solution. Because the carriers in the mobile carrier membrane are not fixed in the membrane matrix, volatile carriers easily evaporate from the membrane. To prevent such volatilization loss, the use of crystalline carriers such as an alkali metal bicarbonate or an amino acid is effective. However, although the crystalline carrier is not evaporated and retained in the membrane matrix, the diffusivity of the carrier and CO_2-carrier complex in the membrane decreases because of the volatilization of the solvent in the carrier solution. Thus, the evaporation loss of the solvent leads to a decrease in the CO_2 permeability. When water is the solvent of the carrier, the decrease in diffusivity can be prevented by the absorption of water vapor from the humid gas into the membrane. Moreover, water vapor absorbed by the membrane reacts with the carrier and CO_2 to form bicarbonate ions, which increases the amount of CO_2 absorbed and further facilitates the transport effect. As an example, Taniguchi et al. (2021) prepared facilitated

Table 3. CO_2 permeation properties of fixed carrier membranes.

Membrane material	p_{CO2} kPa	Temp K	RH %	CO_2 permeance GPU	CO_2 permeability barrer	Thickness µm	Feed gas –	Permselectivity of CO_2 –	Ref.
Polyvinylamine	0.2	298	Sat	766	920	1.2	CO_2/N_2	197	Sandru et al. (2009)
Polyvinylamine	0.11	308	Sat	1827	1520	0.83	CO_2/N_2	500	Kim et al. (2013b)
Polyvinylamine	12	298	Sat	570	850	1.5	CO_2/N_2	183	Sandru et al. (2010)
polyallylamine/polyvinylalcohol blend	40	383	58	2.2	55	25	CO_2/N_2	83	Zhao and Ho (2012)
poly-N-isopropylallylamine/ polyvinylalcohol blend	40	383	58	11.88	297	25	CO_2/N_2	341	Zhao and Ho (2012)
poly-N-isobutylallylamine/ polyvinylalcohol blend	40	383	58	6.4	159	25	CO_2/N_2	187	Zhao and Ho (2012)
poly-N-tertbutylallylamine/ polyvinylalcohol blend	40	383	58	4.8	119	25	CO_2/N_2	179	Zhao and Ho (2012)
Chitosan	15	383	28.6	7.4	482	65	CO_2/N_2	250	El-Azzami and Grulke (2009)
poly(2-N,N-dimethyl aminoethyl -methacrylate-co-acrylic sodium)	1.7	299	Sat	784	–	–	CO_2/CH_4	254	Shen et al. (2008)
hydrolyzed polyVinylpyrrolidone	1.3	299	Sat	793	–	–	CO_2/CH_4	212	Zhang et al. (2002)
Polyvinylamine	22.5	298	Sat	1887	377	0.2	CO_2/N_2	83	Li et al. (2015)
Copolymer synthesized from trimesoyl chloride, diethylene glycol bis(3-aminopropyl) ether, and 3,3′-diamino-N-methyldipropylamine	16.5	295	Sat	1610	–	–	CO_2/N_2	138	Li et al. (2012b)
Copolymer synthesized from *N*-[3-(dimethylamino)propyl]methacrylamide, *tert*-butyl acrylamide, and *N,N′*-methylenebisacrylamide	8	337	85	1010	30.5–50.5	0.03–0.05	CO_2/N_2	216	Hoshino et al. (2021)

transport membranes composed of piperazine derivatives as a mobile carrier and poly(vinyl alcohol) as a hygroscopic membrane matrix. Superabsorbent polymers (SAPs) are also preferable materials for the matrices of mobile carrier membranes. Mobile carrier membranes composed of an SAP as a gel matrix and a crystalline carrier exhibit superior CO_2 permeation performance for humid gases (Kamio et al. 2020a, 2020c; Yegani et al. 2007). Moreover, because the SAP, which is a component of the gel matrix, is a polyelectrolyte such as polyacrylic acid, it is effective in preventing carrier leakage even under pressurized conditions. However, under low-humidity conditions, the facilitated transport effect significantly decreases because of the decrease in the absorption amount of water vapor, which limits the formation of bicarbonate and decreases the diffusivity of the CO_2-carrier complex.

2.4.5 Facilitated transport membrane with an IL-based carrier

As mentioned above, conventional facilitated transport membranes exhibit significantly high CO_2 permeability under highly humid conditions, but the facilitated transport effect disappears under low-humidity conditions. The main reason for this is the decrease in the amount of water vapor absorbed, which limits bicarbonate formation and decreases the diffusivity of the CO_2-carrier complex. Thus, if a carrier that can absorb a sufficient amount of CO_2 without water molecules and a nonvolatile solvent are used, the decrease in CO_2 permeability under low-humidity conditions can be improved. Based on this concept, a facilitated transport membrane with a nonvolatile IL-based CO_2 carrier has been developed in recent years (Kasahara et al. 2012a). As mentioned before, ILs are organic molten salts with diverse molecular structures and properties. Thus, CO_2-reactive functional groups such as amino groups can be introduced into the molecule. Such amine-functionalized ILs can act not only as CO_2 carriers but also as the diffusion medium of a mobile carrier membrane (Hanioka et al. 2008). Examples of amino-functionalized ILs and their CO_2 permeation performance are summarized in Table 5. Among the IL-based CO_2 carriers listed in Table 5, ILs with amino acidates (AAILs) and ILs with aprotic heterocyclic anions can react with CO_2 to form carbamate ions according to Eq. (15) (or Eq. (17)) even under dry conditions (Gouveia et al. 2016; Kamio et al. 2017a; Kasahara et al. 2012a, 2012b, 2014a, 2014b, 2016; Myers et al. 2008). Moreover, the formed carbamate ions diffuse through the ILs incorporated in the membrane. Thus, these ILs act not only as CO_2 carriers but also as diffusion media and provide high CO_2 permeability and high CO_2 permselectivity over other light gases under dry and low-humidity conditions (Kasahara et al. 2012a).

In recent years, an ion gel membrane containing a large amount of amine-functionalized ILs has been developed (Kasahara et al. 2014c). The IL content of the ion gel membrane was more than 70 wt%. Because of the high IL content, the ion gel membrane can chemically absorb a large amount of CO_2. Further, the diffusivity of the CO_2-carrier

Table 4. CO_2 permeation properties of mobile carrier membranes.

Membrane material	p_{CO2} kPa	Temp K	RH %	CO_2 permeance GPU	CO_2 permeability barrer	Thickness μm	Feed gas –	Permselectivity of CO_2 –	Ref.
poly(amidoamine) dendrimer	0.35	r.t.	Sat	41	4100	100	CO_2/N_2	ca. 20000	Kovvali et al. (2000)
Glycine-Na	0.7	r.t.	Sat	101	10100	100	CO_2/N_2	3980	Chen et al. (2000)
Glycine-Na/Na_2CO_3 blend	0.7	r.t.	Sat	54.8	5480	100	CO_2/N_2	2003	Chen et al. (2000)
polyallyamine/2-aminoisobutyric acid potassium salt	40	110	41	207	6196	30	CO_2/N_2	493	Huang et al. (2008)
DL-2,3-Diaminopropionic acid hydrochloride	3.65	125	Sat	ca. 900	ca. 30000	35	CO_2/N_2	ca. 1000	Yegani et al. (2007)
DL-2,3-Diaminopropionic acid hydrochloride	21.9	160	61.5	600	20900	35	CO_2/N_2	700	Yegani et al. (2007)
monoethanolamine	5	298	Sat	ca. 60	ca. 6000	100	CO_2/CH_4	ca. 2000	Teramoto et al. (1996)
diethanolamine	5	298	Sat	ca. 70	ca. 7000	100	CO_2/CH_4	ca. 2000	Teramoto et al. (1996)
poly(amidoamine) dendrimer	5	313	80	6.3	2520	400	CO_2/N_2	ca. 1200	Duan et al. (2012)
poly(amidoamine) dendrimer	560	313	80	0.54	216	400	CO_2/N_2	ca. 35	Duan et al. (2012)

complex in the ion gel membrane is also high. Thus, the CO_2 permeability of amine-functional IL-based facilitated transport membrane has a significantly high CO_2 permeability and permselectivity of CO_2 over other light gases. Moreover, by forming a DN in the amino-functionalized ILs, the mechanical strength, IL content, and CO_2 permeability of the gel membrane can be further increased (Kamio et al. 2017b; Moghadam et al. 2015). The facilitated transport membranes composed of a large amount of amino-functionalized ILs and the characteristic gel network can be used under significantly harsh conditions such as high temperature, high pressure, and low humidity (Moghadam et al. 2017a, 2017b). Figure 12 shows the CO_2 permeability of the DN ion gel membrane containing 80 wt% AAIL measured at a temperature of 373 K, transmembrane pressure of 400 kPa, CO_2 partial pressure of 10 kPa, and humidity of 0%. The ion gel membrane maintained a CO_2 permeability >6000 barrers and CO_2/N_2 selectivity >120 even after 120 h of continuous operation. Ion gel membranes are expected to overcome the stability issues associated with conventional facilitated transport membranes.

3. Inorganic CO_2 Separation Membranes

Inorganic CO_2 separation membranes are being studied and developed, focusing on their advantages over organic materials in terms of thermal resistance, chemical resistance, mechanical strength, and high permeance. As a large-scale project aimed at developing a full-scale CO_2 separation technology for inorganic CO_2 separation membranes in Japan, the "Research and Development of High-Temperature CO_2 Separation, Recovery, and Reuse Technology" was conducted as part of the New Sunshine Project between 1992 and 2000. The project was led by New Energy and Industrial Technology Development Organization (NEDO), with the participation of national research institutes, universities, and companies related to ceramic materials at the time. The Kyoto Protocol was issued in 1997, mandating a 6% reduction of greenhouse gases in Japan as a measure against global warming, and thus interest in efficient CO_2 capture technology was growing. Since then, studies have been conducted to determine the applicability of membrane separation as an efficient separation and recovery method for CO_2 as a greenhouse gas in processes such as separation from combustion exhaust gas (CO_2/N_2), separation from natural gas and biogas (CO_2/CH_4), and improvement of energy efficiency in coal-fired power plants ($H_2/CO/CO_2$) (Haraya 1998).

CO_2 separation membranes using inorganic materials include ceramic membranes, organic-inorganic composite membranes, and carbon membranes. Ceramic membranes are made of various metal oxides, while carbon membranes are mainly made of organic polymers that are sintered at high temperatures to convert organic materials into inorganic carbon. Organic-inorganic composite membranes include the following: covalently bonded inorganic elements such as Si and organic elements at the molecular level; organic molecules attached to metal elements through coordination bonds; metal oxide membranes modified with organic functional groups such as amines; membranes in which inorganic material is added as a filler to an organic polymer matrix, generally referred to as a Mixed Matrix Membranes (MMMs). For organic-inorganic composite membranes, only inorganic-based membranes will be presented in this section. Readers can consult previous reviews for the Metal-organic framework (MOF) membranes (Chakrabarty et al. 2022; Demir et al. 2022; Kamble et al. 2021; Kang et al. 2022; Wong and Jawad 2019).

Table 6 summarizes the classification of the various inorganic membranes for carbon dioxide separation presented in this paper. These membranes are classified into crystalline (regular) and amorphous membranes in terms of regularity of membrane structure, and into porous and dense membranes in terms of porosity of membrane structure. For example, zeolite membranes are porous regular membranes made of ceramic, while silica, organosilica, and carbon membranes are porous amorphous membranes made of ceramic, organic-inorganic composite, and carbon, respectively. The general fabrication methods for porous silica, zeolite, and carbon membranes are described in detail in the review by Yeo et al. (2013). Ceramic membranes, such as those of Perovskite, and supported molten salt membranes are non-porous dense membranes, while MOFs are porous crystalline membranes made of organic-inorganic composite materials. As described above, carbon dioxide separation membranes based on inorganic materials have a wide variety of materials and structures, each of which has been studied and developed for application to unique separation systems. The following is an overview of the research and development of CO_2 separation membranes made of inorganic materials.

Table 5. CO_2 permeation properties of mobile carrier-type facilitated transport membranes containing ionic-liquid-based carrier.

IL-based carrier Cation Anion	p_{CO2} kPa	Temp K	RH %	CO_2 permeance GPU*	CO_2 permeability barrer**	Thickness μm	Feed gas –	Permselectivity of CO_2 –	Ref.
N-aminopropyl-3-methylimidazolium trifluoromethanesulfone	2	298	Sat.	ca. 75	ca. 2600	35	CO_2/CH_4	ca. 130	Hanioka et al. (2008)
N-aminopropyl-3-methylimidazolium bis(trifluoromethylsulfonyl)imide	2	298	Sat.	ca. 35	ca. 1200	35	CO_2/CH_4	ca. 95	Hanioka et al. (2008)
N-aminopropyl-3-methylimidazolium bis(trifluoromethylsulfonyl)imide	21.6	368	Dry	–	ca. 1000	–	CO_2/N_2	ca. 10	Myers et al. (2008)
triethylbutylammonium maleate	0.1	313	Sat.	19	2840	150	CO_2/N_2	265	Huang et al. (2014)
triethylbutylammonium malonate	0.1	313	Sat.	14.3	2150	150	CO_2/N_2	178	Huang et al. (2014)
tetrabutylphosphonium glycinate	10	373	Dry	132	4960	37.5	CO_2/N_2	48	Kasahara et al. (2012a)
1-ethyl-3-methylimidazolium Glycinate	10	373	Dry	220	8290	37.5	CO_2/N_2	146	Kasahara et al. (2012a)
tetrabutylphosphonium alaniate	10	373	Dry	195	7320	37.5	CO_2/N_2	54	Kasahara et al. (2012b)
tetrabutylphosphonium prolinate	10	373	Dry	376	14,110	37.5	CO_2/N_2	102	Kasahara et al. (2012b)
tetrabutylphosphonium 2-cyanopyrrolide	10	323	Dry	66	2490	37.5	CO_2/N_2	55	Kasahara et al. (2014b)
triethyl(pentyl)phosphonium glycinate	10	373	Dry	181	6810	37.5	CO_2/N_2	97	Kasahara et al. (2014a)
triethyl(pentyl)phosphonium prolinate	10	373	Dry	11	6510	600	CO_2/N_2	109	Moghadam et al. (2015)
tetrabutylphosphonium prolinate	10	373	Dry	112	6490	58	CO_2/N_2	102	Moghadam et al. (2015)

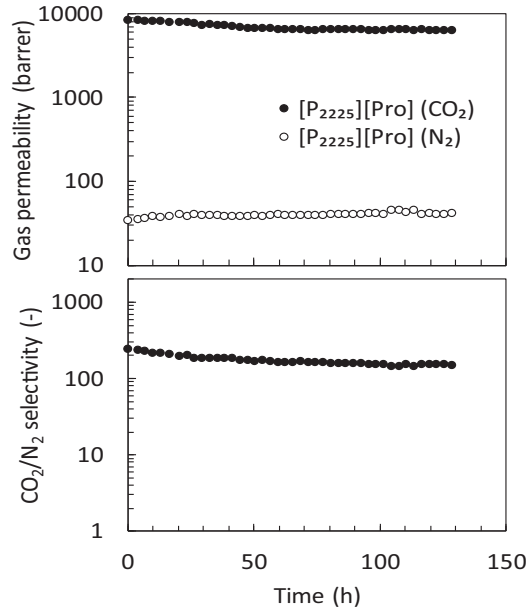

Figure 12. CO_2 permeation performance of a DN ion gel membrane containing an ionic liquid with amino acidates (AAIL) (AAIL: triethyl(pentyl)phosphonium prolinate ([P_{2225}][Pro]; temperature: 373 K; transmembrane pressure difference: 400 kPa; CO_2 partial pressure of the feed gas: 10 kPa; humidity of the feed gas: 0% (dry)).

3.1 Porous ceramic membranes

CO_2 separation performance by microporous membranes depends on the pore size of the membrane, surface properties and operating conditions such as CO_2 partial pressure and temperature. According to the Henry-like adsorption relationship between the pore concentration c and the bulk gas phase pressure p, expressed as $c = (p/RT)\exp(-E_P/RT)$, which assumes that the diffusivity in the micropores is governed by the thermal motion of the permeating molecules, the temperature dependence of the gas permeation rate is expressed by Eq. (21) (Yoshioka et al. 2001).

$$P_P = \frac{k_g}{\sqrt{MRT}}\exp\left(-\frac{E_P}{RT}\right) \tag{21}$$

E_P is not the true activation energy for permeation, but the apparent interaction between the permeating molecules and the pore surface; the greater the affinity between the pore surface and the permeating gas molecules, the smaller (larger absolute value) the potential at the negative value for the same pore diameter. In molecular-order micropores in size, the potential at the centre of the pore is smaller in negative values (larger in absolute values) as the pore diameter decreases due to the effect of superposition of neighboring pore walls but conversely increases in positive values as the pore diameter decreases to the extent that repulsion from the pore walls is effective. The value of k_g depends on the pore structure, such as porosity and pore diameter, and is considered to be a unique value when permeating through the same pore. For the separation of carbon dioxide and nitrogen, a high affinity between carbon dioxide and the membrane material is preferred, which corresponds to a small value of E_P for carbon dioxide (negative and large absolute value) and a large permeance at low temperatures

Table 6. Inorganic membranes for carbon dioxide separation.

		Inorganic	Inorganic/Organic
Amorphous	Porous	SiO_2	Organosilica
		Al_2O_3	Modified ceramic (SiO_2, TiO_2-ZrO_2)
		Carbon	
Crystalline	Porous	TiO_2	
		ZrO_2	Modified mesoporous silica
		Zeolite	Metal organic framework
	Dense (Molten salt)	Lithium silicate	
		Perovskite	
		Yttrium Stabilized Zirconia	

due to the large temperature dependency of the permeance. The smaller pore size should inhibit the permeation of nitrogen, and the pore size should be controlled so that nitrogen does not diffuse by surface diffusion or Knudsen diffusion, but by activation diffusion. In this case, the value of the E_P of nitrogen is positive and large. In such membranes, high permselectivity of carbon dioxide is achieved, especially at low temperatures. In general, Vycor glass membranes prepared by the phase separation and dissolution method and γ-alumina membranes prepared by the sol-gel method have relatively larger pore diameters for gas separation, and in these membranes gases are permeated by the Knudsen mechanism. The gas permeance is determined by the square root of the molecular weight, so that the permeance ratio of carbon dioxide to nitrogen is 0.8, resulting in almost no separation. Therefore, pore size control and surface modification with affinity materials by employing suitable materials preparation methodology are necessary to demonstrates the molecular sieving effect and surface diffusion.

3.1.1 Al_2O_3, TiO_2, and ZrO_2-based membranes

Ceramic materials such as Al_2O_3, TiO_2, and ZrO_2 have been studied as high-temperature CO_2 separation membranes because they are stable and form porous structures, which are partially crystalline. Since they do not have sub-nano-sized pores like zeolite, silica or carbon materials, precise separation by molecular sieving cannot be expected. Therefore, separation membranes based on CO_2 affinity and composite membranes with controlled pores were developed.

Horiuchi et al. (1998) fabricated γ-alumina and various metal-modified γ-alumina membranes and evaluated the CO_2 permeability from the heat of CO_2 adsorption in order to understand the possibility of CO_2 separation by surface diffusion using ceramic membranes at high temperature. It was found that metal oxides such as rare earth metals (La, Ce, Nd, Pr), alkaline earth metals (Mg, Ca, Sr, Ba), and alkali metals (Na, K, Rb, Cs) react with Al_2O_3 to form surface aluminate layers. The interaction with CO_2 increased in the order of rare earth oxides, alkaline earth oxides, and alkali metal oxides (maximum value 167 kJ/mol for Rb_2O). The results indicated that a very strong affinity between the membrane and CO_2 resulted in low CO_2 mobility, but that the dominant permeation was due to the so-called surface diffusion, which was dependent on the affinity. The CO_2 permeation coefficient estimated from the adsorption and diffusion properties was about 10^{-12} mol m/(m^2 s Pa), but the actual CO_2 permeability was 10^{-8} to 10^{-9} mol m/(m^2 s Pa) because the membrane thickness was not precisely determined.

Van Gestel et al. (2010) fabricated dense H_2/CO_2 separation membranes by sol-gel coating of various ceramic layers, such as ZrO_2, $8Y_2O_3$-ZrO_2, on α-Al_2O_3 as a support material with thicknesses ranging from 50 to 200 nm. The formation of a crack-free non-silica top layer had been considered extremely difficult, but by optimizing the sol synthesis and coating method and keeping the layer thickness below 100 nm, an ultra-thin, homogeneous separation active layer was successfully fabricated. In particular, the membranes sintered at 400 °C or higher showed low permeation of He and H_2, suggesting the formation of a denser separation layer than in silica membranes. Although H_2 permeability is an issue for application to H_2/CO_2 separation membranes in power plants, the stability of the membranes is expected to be superior to those of amorphous silica membranes. Franz and Scherer (2011) also discussed the carbon capture potential of ceramic membranes with H_2 permselectivity in the Integrated Gasification Combined Cycle (IGCC).

In addition, some studies have been conducted to improve the performance of such ceramic materials as CO_2 separation membranes by compositing them with organic materials. Fukumoto et al. (2014) employed isoeugenol (2-methoxy-4-propenyl-phenol, ISOH), which is an Organic Chelating Ligand (OCL), as a reaction inhibitor for the hydrolysis and condensation of Ti- and Zr-alkoxides during the sol preparaton procedure. The TiO_2-ZrO_2-ISOH membranes were successfully formed with a thickness of about 50 nm, on a SiO_2-ZrO_2 intermediate layer, as the top layer of an asymmetric membrane. A microporous structure was formed due to the residual organic matter derived from ISOH, resulting in high permeance and selectivity as a gas separation membrane. TiO_2-ZrO_2-ISOH membranes calcined at 350 °C in N_2 atmosphere showed a CO_2 permeability of 2.0 x 10^{-7} mol/(m^2 s Pa) at 200 °C and CO_2/N_2 permeance ratios of 6.4 and 46 at 200 °C and 35 °C, respectively. Tachibana et al. (2020) reported that the pore structure of TiOs-ZrO_2-OCL membranes can be controlled by using aromatic compounds with different side-chain molecular structures as OCLs, which changes the gas separation performance. For composite membranes with organic chelate ligands, SiO_2-ZrO_2-acetylacetonate membranes with residual carbon were also reported (Lawal et al. 2020). At 300 °C, the membrane exhibited molecular sieve-like gas

separation performance; at 50 °C, however, a decrease in H_2 permeance due to CO_2 adsorption was observed. Various applications based on this separation principle that is different from the molecular sieving mechanism of a porous membrane would be promising.

3.1.2 Silica membranes

High CO_2 permeance and moderate CO_2/N_2 selectivity have been reported for amorphous and metal-doped silica membranes (Asaeda and Yamasaki 2001; Yoshioka et al. 2001, 2007). However, the stability against water vapor and difficulties in membrane formation have prevented practical application. In order to improve the stability of silica membranes, silica-zirconia CO_2 separation membranes have also been investigated, but their performance has not been satisfactory due to difficulties in pore size control (Coterillo et al. 2011; Osada and Kato 2002).

The advantage of this type of membrane is its high CO_2 permeance. In general, however, the interaction of amorphous silica-based membranes with CO_2 molecules is not as strong as that of organic membrane systems, and advanced pore size control technology is required to take advantage of the molecular sieving property (Yoshioka et al. 2001). Therefore, new amorphous CO_2 separation membranes have been explored and developed from the viewpoints of sub-nano-order pore size control and CO_2 affinity control. Nomura et al. (2014) investigated the pore size control of silica membranes using chemical vapor deposition (CVD). Propyltrimethoxysilane (PrTMOS) was used as the silica precursor, and the counter diffusion method, in which PrTMOS and O_3 were supplied from opposite sides of a porous alumina substrate, was used to fabricate dense and thin silica membranes. The membranes deposited at 270 °C had a CO_2 permeance of 2×10^{-8} mol/(m^2 s Pa) and a CO_2/N_2 permeance ratio of 20, which was attributed to the presence of PrTMOS-derived alkyl groups on the membrane that promoted CO_2 adsorption. Karimi et al. (2020) prepared functionalized silica membranes by introducing five organic functional groups into the silica matrix, including acetic acid groups, trifluoromethyl groups, methacrylic acid groups, urea groups, and vinyl groups, and investigated their CO_2 separation performance. Among those functionalized membranes, the trifluoromethyl group modified silica membrane showed the highest performance due to both the highest (82%) microporosity and the possible CF_3-CO_2 attractive interaction owing to the three fluorine atoms. The CO_2 permeance of the silica membrane with trifluoromethyl groups was 5.5×10^{-7} mol/(m^2 s Pa), representing a permeance ratio of 10.

Inherently, the amorphous network structure of silica polymer has a pore distribution mainly consisting of oxygen six-membered rings, as shown in Figure 13, and its average pore size is about 0.3 nm (Yoshioka et al. 2004). Therefore, it has excellent permselectivity for small molecules such as He and H_2. However, the structure is too dense for CO_2 permeation. Therefore, Rana et al. (2022) attempted to control the silica network pore size by adding fluorine (NH_4F) to conventional tetraethoxysilane (TEOS) derived silica membranes. An optimum amount of fluorine was found, and a membrane with a CO_2/N_2 permeance ratio of 30 and a CO_2 permeance of 1.6×10^{-7} mol/(m^2 s Pa) at 50 °C was successfully fabricated at F/Si = 0.1/9.9. The hydrothermal stability of the silica membranes was also found to increase with increasing fluorine concentration under a high partial pressure of water vapor (300 °C, H_2O partial pressure 30 kPa).

From the viewpoint of controlling CO_2 affinity, attempts have been made to add organic functional groups having an affinity for CO_2 to silica membranes. A typical functional group is the amino group, which is also present in the components of CO_2 absorbent solutions.

As shown in Eqs. (15)–(19), there are three types of interaction between CO_2 molecules and amino groups, and all of the amino groups, primary, secondary, and tertiary, have CO_2 affinity, so the introduction of amino groups into the porous membrane is considered effective for improving selective permeation performance of CO_2. Since the adsorption enthalpy of CO_2 onto amino groups is larger in the order of primary, secondary and tertiary, porous membranes with primary amine groups are assumed to be advantageous in terms of CO_2 affinity, therefore, in increasing the CO_2 permeation and separation performance. However, it has been reported that the secondary amine has a larger adsorption enthalpy than primary one when CO_2 is adsorbed once more after CO_2 is desorbed (Yu et al. 2017b). In membrane separation operations where adsorption at the feed side and desorption at the permeate side proceed simultaneously, the amount of CO_2 adsorbed and ease of desorption as equilibrium theory should also be considered, and from the perspective of kinetics, the porous structure should be appropriately designed to affect the diffusivity of adsorbed CO_2 molecules (Yu et al. 2018).

Typically, 3-aminopropyltriethoxysilane, a primary amine, has been used as a reagent. It has been reported that one CO_2 molecule is adsorbed on the amine-modified membrane by forming alkylammonium carbamate with two amino groups, even in the dry state, as shown by the equation for a facilitated transport membrane (Eq. (15)) (Hiyoshi et al. 2005).

It has also been reported that even secondary amines develop CO_2 affinity by reacting reversibly with CO_2 as the same equation in Eq. (16) (Yu et al. 2017b)

Mesoporous silica (Jang et al. 2011; Kim et al. 2004a; Miyamoto et al. 2011; Sakamoto et al. 2007) and Vycor glass (Ostwal et al. 2011) were the preferred supports for amino groups. This is because the properties of mesoporous silica materials, such as large surface area, high pore volume, and tunable pore size with two- or three-dimensional porous structure, were considered effective for CO_2 separation membranes in terms of adsorption and molecular transport. However, it is difficult to produce continuous, defect-free mesoporous silica membranes with high yields (Kim et al. 2015a). To improve the defects in mesoporous support-amino group structures, homogeneous amino-silica structures, in which amino groups were highly and homogeneously dispersed, were studied.

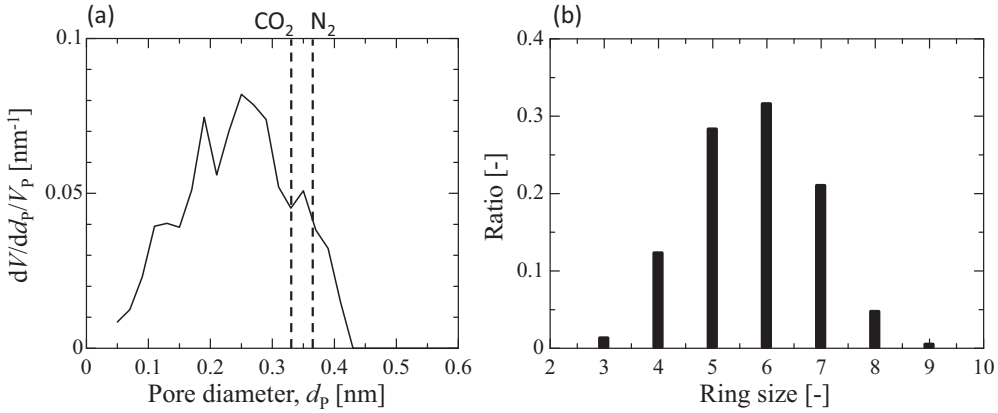

Figure 13. Pore size distribution of amorphou silica* (a) and ring size ditribution of silica polymer network** (b). *Yoshioka et al. (2004), **Calculated by the authors for a silica model simulated using molecular dynamics, similar with the results reported by Feuston and Garofalini (1988).

Xomeritakis et al. (2005) developed a novel sol-gel derived aminosilicate microporous inorganic membrane to facilitate CO_2 separation. The membrane was formed using a silica sol with sodium glycinate salt (CH_2NH_2COONa (GlyNa)) as the source of amine functional groups. The membrane is assumed to be composed of amine (-NH_2) functional groups randomly dispersed in an amorphous silica matrix with a pore size of 4–5 Å. The membrane is characterized by a high degree of dispersion of the amine functional groups. The characteristic feature of this membrane is that CO_2 is preferentially adsorbed to the highly dispersed amine functional groups in the membrane pores, while other gases (O_2, N_2, CH_4) are blocked by molecular sieving due to the inherent pore structure of amorphous silica, thereby improving the CO_2 permselectivity. The membrane exhibited a CO_2 permeance of 7.3×10^{-9} to 1.1×10^{-7} mol/(m^2 s Pa) and a CO_2/N_2 separation factor of about 100 at 22 °C in a feed of 1–20% CO_2 by volume and 0–40% relative humidity. Messaoud et al. (2015) investigated the effect of the incorporation of primary and secondary amine functional groups on CO_2/CH_4 separation performance. Dense aminosilica membranes were deposited by chemical vapor deposition (CVD) using 3-aminopropyltrimethoxysilane (APTMS) and (3-methylaminopropyl)trimethoxysilane (MAPTMS) as primary and secondary alkylamine-silica precursors, respectively. The pore size of the membrane prepared using propyl trimethoxysilane (PTMS) without amino groups as a precursor was 0.37 nm, the CO_2 permeance at 393 K was 2.1×10^{-8} mol/(m^2 s Pa), and the CO_2/CH_4 selectivity was 4. On the other hand, the primary aminosilica membrane had a pore size of 0.36 nm, a CO_2 permeance of 2.1×10^{-8} mol/(m^2 s Pa) at 393 K, and a CO_2/CH_4 selectivity of 70. The secondary aminosilica membrane had a pore size of 0.43 nm and achieved a CO_2 permeance of 1.3×10^{-7} mol/(m^2 s Pa) and a CO_2/CH_4 selectivity of 140. The CO_2 transport mechanism of the aminosilica hybrid membrane was surface diffusion, and the membrane was stable for 60 h under 20% relative humidity. Yu et al. (2017b) prepared three types of amino-silica membranes with amino functional groups and different functional group structures by using 3-(triethoxysilyl)propan-1-amine (primary amine, PA-Si), 3-(triethoxysilyl)-N-methylpropan-1-amine (secondary amine, SA-Si), and 3-(triethoxysilyl)-N,N-dimethylpropan-1-amine (tertiary amine, TA-Si) as silicon alkoxides for membrane materials, and investigated their CO_2 permeation properties. The tertiary amine-Si membranes showed faster adsorption and desorption processes due to the decrease in CO_2 binding energy caused by the steric hindrance effect of the functional groups, which contributed to their higher CO_2 permeability. On the other hand, it is interesting to note that the effect of the basicity of the amine functional group on CO_2 permeability is not significant. This finding may serve as a guideline for the future improvement of the performance of inorganic porous membranes by loading CO_2-affinity functional groups.

In H_2/CO_2 separation, silica membranes are generally used to selectively permeate H_2 and block CO_2 due to their microporous structure. Since silica membranes are inherently advantageous for H_2 selective permeation, modifications have been studied mainly to improve hydrothermal stability and to reduce CO_2 permeability. A fluorocarbon-modified silica membrane coated by the sol-gel method on a γ-Al_2O_3/α-Al_2O_3 substrate exhibited a H_2 permeance of 3.1×10^{-6} mol/(m^2 s Pa) and H_2/CO_2 selectivity of 15.2 at 200 °C. The membrane was sufficiently hydrophobic and hydrothermally stable (Wei et al. 2008).

In an attempt to improve the H_2 permselectivity, silica membranes doped with metallic elements such as niobium (Boffa et al. 2009), cobalt (Diniz da Costa et al. 2009) and magnesium (Karakilic et al. 2017) have been reported. A simple method was also developed to fabricate ultrathin silica-like membranes (~3 nm) by oxygen plasma treatment of polydimethylsiloxane thin composite membranes at room temperature (Zhu et al. 2021). These modified H_2/CO_2 separation membranes showed an improvement in performance to some extent. In the application of H_2/CO_2 separation membranes to the IGCC process, it is desirable to permeate the CO_2, leaving the high-pressure H_2 on the retentate for feeding to a gas turbine, so silica-based H_2 permselective membranes do not appear to be practical in principle. In the Integrated Coal Gasification Fuel Cell Combined Cycle

(IGFC), it makes sense as a means of obtaining H_2 to feed the fuel cell, but for this purpose, further improvement of membrane performance to obtain high-purity H_2 is required. The reported performances of porous ceramic membranes are shown in Figure 14.

3.1.3 Organosilica membranes

Organosilica membranes are composed of amorphous materials as ordinal silica membranes but have a chemical structure in which hydrocarbon groups are inserted between Si-Si atoms in the silica matrix (Figure 15), resulting in a porous structure different from that of amorphous silica membranes. This is characterized by possible high gas permeability (Kanezashi et al. 2009). The hydrocarbon groups can be designed according to the purpose, and the high degree of freedom in controlling the pore structure makes the membrane promising for the precise separation of various molecular mixtures.

For H_2 permeselective organosilica membranes, Qi et al. decreased membrane affinity for CO_2 by increasing the acidity of the membrane by doping ethylene group-bridged organosilica (2-bis(triethoxysilyl)ethane, BTESE) with niobium, thereby improving the H_2/CO_2 selectivity (Qi et al. 2011). It has also been shown that Nb doping to a BTESE membrane contributed to the improvement of hydrothermal stability (Qi et al. 2012). In addition, the membrane performance was improved by controlling the porous structure through firing conditions (Song et al. 2017) and by doping palladium, which has an H_2 absorption property, in addition to niobium, and a membrane with H_2/CO_2 selectivity of 107 and CO_2 permeance of 1.12×10^{-7} mol/(m^2 s Pa) was reported (Zhang et al. 2020, 2021a).

To improve the CO_2 permselectivity of organosilica membranes, it is important to precisely control the porous structure and improve the affinity for CO_2 as in amorphous silica membranes. Yang et al. (2016) prepared two different types of BTESE sols by controlling the amount of acid added during the preparation of the sols for coating. A dense separation layer with excellent CO_2 permeability was produced by a two-step hot coating method in which these two types of sols were combined and coated onto a preheated substrate. The CO_2 permeance was as high as 1.3×10^{-6} mol/(m^2 s Pa), and the CO_2/N_2 and CO_2/CH_4 permeance ratios were 23.5 and 31.5, respectively.

The studies on organosilica membranes described above have focused on the development of organosilica membranes of Si-R-Si cross-linked with linear alkanes (for "R"), and there have been only a few studies on organosilica membranes with aromatic groups. Guo et al. (2022) prepared organosilica membranes by using phenyltriethoxysilane (PhTES) with (pendant) benzene groups as side chains, bis(triethoxysilyl)benzene cross-linked with benzene groups (BTESB), and 4,4′-bis(triethoxysilyl)-1,1′-biphenyl cross-linked with biphenyl groups (BTESBPh) as precursors, and studied their CO_2 separation performance. They found that the position of aromatic benzene groups (bridged or

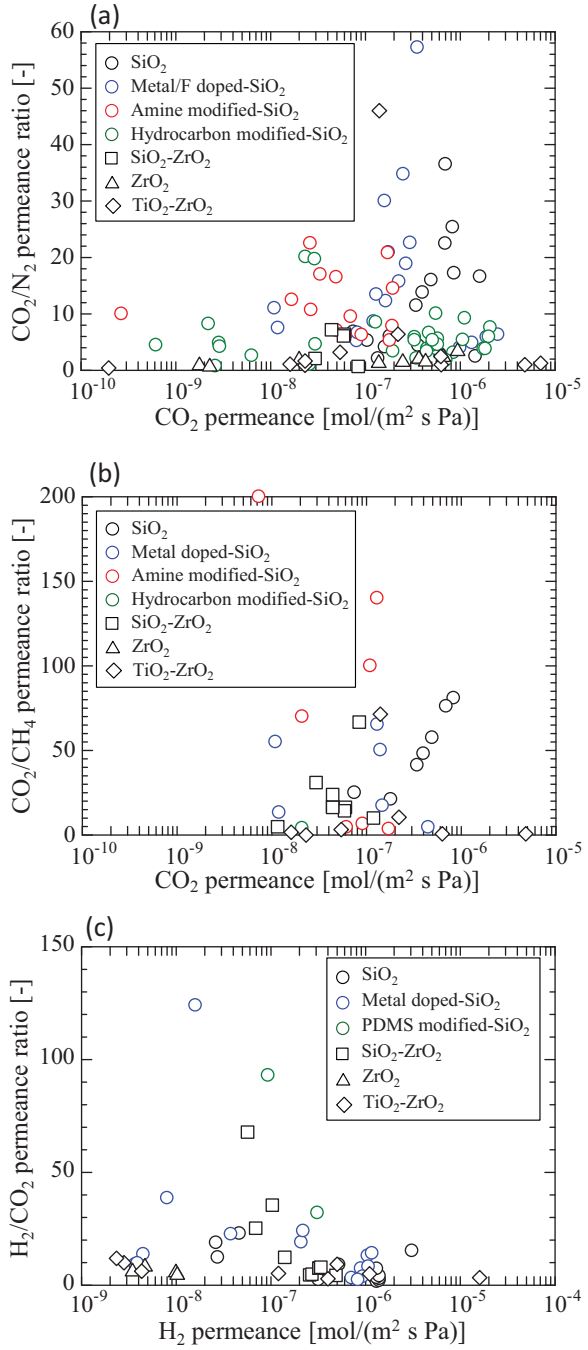

Figure 14. (a) CO_2 permeance vs. CO_2/N_2, (b) CO_2 permeance vs. CO_2/CH_4, and (c) H_2 permeance vs. H_2/CO_2 for porous ceramic membranes.

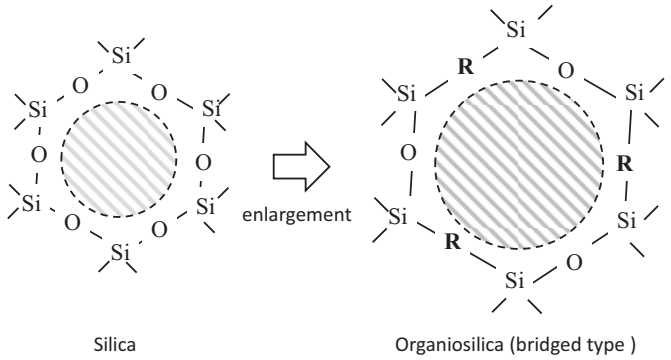

Figure 15. Pore size control by introducing hydrocarbon group (R) as Si-R-Si, partially replacing Si-O-Si (ex. **R** = CH_2, C_2H_2, C_2H_4, C_3H_6, C_6H_4, etc.).

pendant) and the number of aromatic bridges (single benzene or biphenyl bridge) affected the CO_2 permeance. In a CO_2/N_2 mixed gas separation at 50 °C, the PhTES membrane exhibited a CO_2 permeance of 3.64×10^{-7} mol/(m^2 s Pa) and a CO_2/N_2 permeance ratio of 30. On the other hand, the BTESB membrane exhibited a CO_2/N_2 permeance ratio of 34, but a CO_2 permeance of 8.7×10^{-7} mol/(m^2 s Pa), about 2.5 times higher. The BTESBPh membrane showed a CO_2/N_2 selectivity of 13, which was rather small, but a very high CO_2 permeance of 1.83×10^{-6} mol/(m^2 s Pa). The use of organosilica precursor functionalized with aromatic groups enhances the stability of the membrane network structure, and furthermore, by tuning the number of aromatic benzene groups and side chains, various porous structures can be formed, which is expected to lead to the development of high-performance CO_2 separation membranes.

Similar to silica membranes, the introduction of amine functional groups into organosilica membranes has been investigated as a way to increase the affinity for CO_2. Yu et al. prepared a sol with a secondary amine functional group, 4,6-bis(3-(triethoxysilyl)-1-propoxy)-1,3-pyrimidine (BTPP), where the BTPP membranes were prepared by the sol-gel method (Yu et al. 2018, 2019). The membranes showed higher permeance than those prepared from (3-aminopropyl)triethoxysilane (APTES) with primary amines, indicating that a membrane with a very strong affinity for CO_2 does not necessarily lead to high CO_2 permeance. They proposed the concept of "mild affinity membranes," which are membranes with moderate interaction with CO_2, to improve CO_2 transport efficiency (Yu et al. 2017a). In addition, amine-organosilica membranes consisting of APTES complexed with organosilica (bis(triethoxysilyl)acetylene, BTESA), which has a triple bonded acetylene group as a cross-linking group, have shown high-performance with CO_2 permeance of 2550–3230 GPU (1 GPU = 3.35×10^{-10} mol/(m^2 s Pa)), CO_2/N_2 selectivity of 31–42, and CO_2/CH_4 of 70 (Guo et al. 2020). It was concluded that this was the result of moderate control of CO_2 affinity and pore structure. On the other hand, Ren et al. (2021) used polyhedral oligomeric silsesquioxanes (POSS) with eight $-(CH_2)_3$-NH-$(CH_2)_3$-NH_2 groups at the vertices as nanocomposites to prepare BTESE-PNEN composite membranes with the 1.2-bis(triethoxy)-2-$(CH_2)_3$-NH-(PNEN) bond. Although slightly inferior to the BTESE-APTES membrane in terms of membrane performance, the pore size of the BTESE-PNEN membrane was larger than that of the BTESE-APTES membrane, indicating its potential for use in mixed matrix membranes with amine-POSS particles.

Since amorphous silica-based membranes do not have a fixed pore size like regular porous media, they do not exhibit clear molecular sieving properties, and selectivity is determined by the pore size distribution. Therefore, it is difficult to separate CO_2 and N_2, which have similar molecular sizes. However, the dominant pore size is precisely controlled by the membrane formation method and sol preparation method, and affinity to selectively permeable molecules can be provided to some extent by suitably selecting dope components. The reported performances of organosilica membranes are shown in Figure 16.

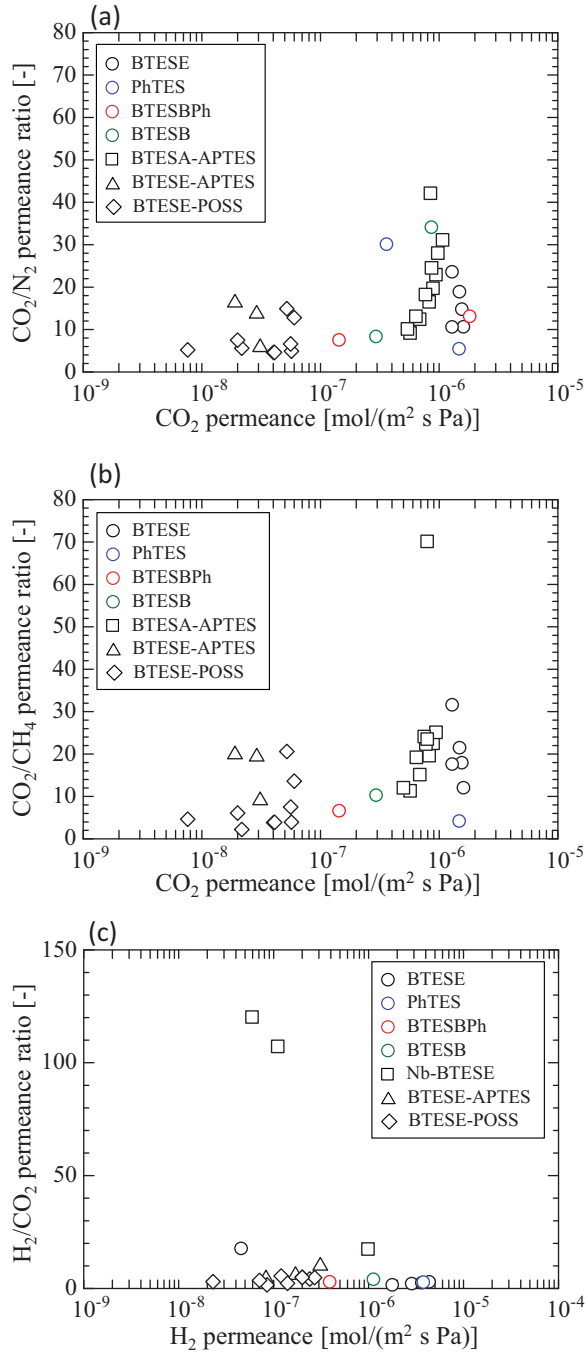

Figure 16. (a) CO_2 permeance vs. CO_2/N_2, (b) CO_2 permeance vs. CO_2/CH_4, and (c) H_2 permeance vs. H_2/CO_2 for organosilica membranes.

3.2 Zeolite membranes

Zeolite membranes are characterized by their regular pore structure. The pore size is clearly defined by the crystalline framework structure, and a zeolite membrane is expected to function as an ideal molecular sieve membrane because of its sharp and narrow pore size distribution. Another advantage is that the adsorption property derived from high porosity and high specific surface area can be used for

Table 7. Typical crystalline structures of zeolite membranes for gas separation.

Type	Property: Max. diameter of sphere that can diffuse along (a:, b:, c:)	Property: Accessible volume %	Framework			
SOD	2.5 Å, 2.53 Å, 2.53 Å	0.00%	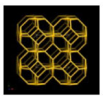	Viewed along [001]	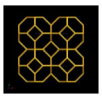	Projection along [001]
DDR	3.65 Å, 3.65 Å, 2.63 Å	9.21%	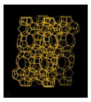	Viewed along [110]		8-ring along [100]
CHA	3.72 Å, 3.72 Å, 3.72, Å	17.27%	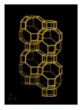	Viewed normal to [001]		Projection along [001]
LTA	4.21 Å, 4.21 Å, 4.21 Å	21.43%	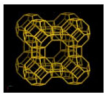	Viewed along [100]		Alpha-cage, sodalite cage and 4MR
MFI	4.7 Å, 4.46 Å, 4.46 Å	9.81%		Viewed along [010]		Projection along [010]
FAU	7.35 Å, 7.35 Å, 7.35 Å	27.42%		Viewed along [111]	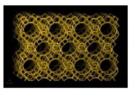	Viewed along [110]

Baerlocher et al. (2007), Baerlocher and McCusker (2023) (https://jpn01.safelinks.protection.outlook.com/?url=http%3A%2F%2Fwww.iza-structure.org%2Fdatabases%2F&data=05%7C01%7C%7C1e257823984f44e4d71a08db6ce79436%7C20ee4c8087bd422ca5063a2b0aca0615%7C0%7C0%7C638223514246461814%7CUnknown%7CTWFpbGZsb3d8eyJWIjoiMC4wLjAwMDAiLCJQIjoiV2luMzIiLCJBTiI6Ik1haWwiLCJXVCI6Mn0%3D%7C3000%7C%7C%7C&sdata=HwtV%2Fv%2F6TlWI9Wz86c0Lq5%2BTJ6s4BeQt7f3wqyt2v4g%3D&reserved=0).

separation. The basic crystal structures of typical zeolite membranes that have been successfully fabricated into homogeneous dense thin membranes used as separation membranes are summarized in Table 7. In reality, however, only a limited number of zeolite structures have been successfully used to form dense thin membranes, and there are unfortunately no zeolite membranes suitable for CO_2 (0.33 nm)/N_2 (0.364 nm) separation by molecular sieving based on the relation between their molecular sizes and zeolite pore sizes. Therefore, it is necessary to modify the pores of existing zeolite membranes that can permeate both CO_2 and N_2 or to replace cations appropriately to achieve effective pore size control. In addition, pinholes originating from crystalline grain boundaries degrade separation performance, so it is a challenge to form membranes without such pinholes.

3.2.1 CO_2/N_2 separation

To the best of the author's knowledge, the first zeolite membrane with high performance for CO_2/N_2 separation was reported by Kusakabe et al. in 1998 (Kusakabe et al. 1998). At 40 °C, the CO_2 permeance of the NaY-type (FAU) membrane was 0.4×10^{-6} to 2.5×10^{-6} mol/(m^2 s Pa), and the CO_2/N_2 selectivity ranged from 20 to 50. The permeance of CO_2 according to the exchange cation species was in the order of $Li^+ \approx K^+ > Na^+ \approx Ba^{2+} > Ca^{2+} \approx Mg^{2+}$, and the KY-type membrane showed the highest CO_2/N_2 selectivity. Lara-Medina et al. (2012) prepared CO_2 separation membranes by modifying silicalite-1 membranes (0.55 nm) with Li solution, which have a smaller pore size than the FAU type (0.74 nm). Surface diffusion was shown to be the major transport mechanism in the lithium-modified silicalite-1 membrane, with preferential adsorption and diffusion of CO_2 preventing N_2 permeation; at 400 °C, the CO_2/N_2 separation factor was 1.46 for the unmodified silicalite-1 membrane, whereas it was 6 for the Li^+ modified silicalite-1 membrane. Zhang et al. (2013) produced T-type zeolite membranes, which are composed of intergrown crystal structures of erionite and offretite with Si/Al ratios of 3 to 4, by controlling the hydrothermal synthesis temperature to optimize nucleation and crystallization conditions. The membrane exhibited a CO_2 permeance of 6.2×10^{-8} mol/(m^2 s Pa), CO_2/N_2 selectivity of 43, and CO_2/CH_4 selectivity of 80. In terms of organic polymer-zeolite composite membranes that are not mixed matrix membranes for CO_2/N_2 separation, membranes with polydimethylsiloxane (PDMS) support and FAU-type zeolite crystals synthesized within their pores have been reported (Wang et al. 2015). This membrane showed relatively high performance with a separation factor of 35–45 and CO_2 permeance of 1600–2200 GPU, but it is not clear to what extent the FAU-type zeolite membrane contributes to CO_2 separation because of the thin coating of 200–300 nm PDMS on the top layer.

However, the membrane is interesting from an application standpoint because of its 3-d stability and flexible mechanical properties.

3.2.2 H_2/CO_2 separation

In terms of H_2/CO_2 separation, as well as CO_2/N_2 separation, molecular sieving separation by the original zeolite membrane is difficult. This is because even the pore size of LTA-type (NaA-type) zeolite, which is in practical use as a dehydration membrane for alcohol-aqueous solutions, is 0.42 nm, and both H_2 and CO_2 molecules can permeate through this membrane, owing to the smaller molecular sizes of H2 (0.29 nm) and CO_2 (0.33 nm). Of course, DDR-type and CHA-type zeolites, which have a pore size of about 0.38 nm and are expected to be suitable for CO_2/CH_4 (0.38 nm) separation, cannot be applied to H_2/CO_2 separation because they are permeable to both H_2 and CO_2. The pore size of MFI type (ZSM-5) zeolite is 0.55 nm, so it is difficult to apply this membrane to H_2/CO_2 and CO_2/N_2 separations for the same reason. Therefore, attempts have been made to control the pore size of zeolite membranes, which have a slightly larger pore size than those of the separation target, by modifying the existing zeolite pore surface by some method.

Hong et al. (2005) silylated boron-substituted ZSM-5 and SAPO-34 membranes by catalytic decomposition of methyldiethoxysilane (MDES) to improve the selectivity of H_2 separation from light gas. MDES reacted within the pores of B-ZSM-5 and reduced the effective pore size, which led to H_2/CO_2 and H_2/CH_4 selectivities increasing from 1.4 to 37 and from 1.6 to 33 at 473 K, respectively. However, silylation decreased the H_2 permeance of the B-ZSM-5 membrane by more than an order of magnitude. At higher temperatures, the membranes performed better; at 673 K, the H_2 permeance was 1.0×10^{-7} mol/(m^2 s Pa), and H_2/CO_2 selectivity was 47. Since methyldiethoxysilane does not enter the pores of SAPO-34, silylation reduced the pore size of the non-zeolite pores in the SAPO-34 membrane, resulting in attaining the original selectivity of the SAPO-34 pore. Therefore, the H_2 permeability and H_2/CO_2 selectivity of the silylated SAPO-34 membrane remained almost the same, but the CO_2/CH_4 separation selectivity increased from 73 to 110. Wang and Lin (2011) also reported that modifying MFI zeolite membranes with methyldiethoxysilane (MDES) improved the H_2/CO_2 separation factor from 4.2 to 8.6, although the H_2 permeance decreased by about 40%. Subsequently, several reports on the modification of MFI membranes by catalytic cracking deposition (CCD) of methyldiethoxysilane (MDES) to improve H_2/CO_2 separation performance have been published (Hong et al. 2013a; Wang and Lin 2012). The H_2/CO_2 separation factor was 42.6, and the H_2 permeance was 2.82×10^{-7} mol/(m^2 s Pa) at 500 °C by CCD modification of cation-exchanged MFI membranes (Hong et al. 2013b). The membrane was applied to an actual water gas shift reaction as a membrane reactor, and high CO conversion and stability over 100 h were achieved (Zhang et al. 2012, 2015).

Other zeolite membrane modification methods include the preparation of SiO_2/ZSM-5 composite membranes by dip-coating of SiO_2 sol onto ZSM-5 membranes, mainly to fill grain boundaries (Shin et al. 2005), and preparation of Al_2O_3/SAPO-34 composite membranes (Yu et al. 2011), which showed improved CO_2/N_2 and H_2/CO_2 selectivity, respectively. An unexpected and interesting effect of MFI zeolite pore size control by chemical vapor deposition (CVD) using methyl diethoxysilane (MDES) has also been reported. It was shown that CO_2 adsorbs in the zeolite pores and blocks the pore channels effective for H_2 diffusion, resulting in a membrane that is more selective for CO_2 molecules than H_2 at room temperature (Zhu et al. 2010).

Recently, it has been reported that CO_2/CH_4 selectivity can be increased by a factor of 2.5 by modifying SAPO-34 membranes with bis(triethoxysilyl)ethane (BTESE)-derived organosilica by vacuum-assisted deposition (VAD) (Mu et al. 2019), and that graphite amine (Ga) in NaX zeolite membranes simultaneously improves H_2 permeance and H_2/CO_2 selectivity (Roy and Das 2019). Although the membrane production technology has been established, it has been shown that zeolite membranes can be applied to CO_2 separation membranes by devising post-treatment and composite methods when the inherent pores of the zeolite are not suitable for CO_2 separation, which is important as a technology to increase the potential of zeolite membranes for CO_2 separation operations. On the other hand, sodalite (SOD) is known as a zeolite with a regular structure suitable for selective H_2 diffusion. The main cage of sodalite is composed of oxygen six-membered rings, and its pore size is approximately 0.3 nm, creating a dense SOD membrane that can be ideal for H_2 separation. Eterigho-Ikelegbe et al. (2020) prepared a defect-free SOD/Al_2O_3 nanocomposite membrane by synthesizing sodalite crystals in the pores of an α-Al_2O_3 support. They found that the H_2 permeance was relatively high at 100 °C, at 7.97×10^{-7} mol/(m^2 s Pa), while the H_2/CO_2 permeance ratio was not so high as 8.76. It cannot be said that a sufficiently dense SOD membrane structure has been formed yet, and further improvement of the membrane formation technology is desired to achieve higher performance.

As mentioned above, hydrogen is normally a permselective component in H_2/CO_2 separation due to the molecular sieving mechanism, which depends on the pore size of the zeolite structure and the size of the gas molecules. However, it has been reported that in MFI membranes, CO_2 can be selectively adsorbed into the pores at low temperatures and high pressures (Korelskiy et al. 2015; Lindmark and Hedlund 2010) or when accompanied by a third component such as water (Zhou et al. 2014b), which can inhibit H_2 diffusion in the pore, and selective permeation of CO_2 is also possible. Although the results are very interesting considering the application to actual processes such as IGCC, the reliability of the results should be carefully examined for the unusually high CO_2 permeability (10^{-5} mol/(m^2 s Pa)) observed. The detailed mechanism of permeation separation, which depends on the membrane structure and operating conditions of the membranes, is still awaited.

3.2.3 CO_2/CH_4 separation

Since the effective inner diameter of oxygen 8-membered rings is about 0.36–0.38 nm, zeolites with a pore structure composed of oxygen 8-membered rings have CO_2/CH_4 separation properties. DDR, SAPO-34, and CHA are examples of such zeolites. DDR and SAPO-34 zeolites have been reported to provide high-performance CO_2/CH_4 separation for nearly 20 years. DDR-type zeolite membranes are molecular sieving membranes with apertures of 0.36×0.44 nm.

Tomita et al. (2004) reported that at 301 and 373 K, the permeance decreased by more than three orders of magnitude with the kinetic diameter of the permeating gas molecules between 0.35 nm and 0.40 nm, and that the CO_2/CH_4 separation factors for a 50% CO_2/50% CH_4 mixture at a total pressure of 0.5 MPa were 220 and 100 at 301 and 373 K, respectively. The DDR membranes were shown to have a molecular sieving ability with few defects. Furthermore, they succeeded in fabricating a highly permeable DDR membrane with a 10-fold improvement in CO_2 permeance while maintaining CO_2 selectivity (Himeno et al. 2007). The CO_2 permeance and separation factor were also reported to decrease under high pressure and in the presence of water vapor.

van den Bergh et al. (2008) measured the permeance of various gases through deca-dodecasil 3 rhombohedral (DD3R) membranes, which are Al-free all-silica DDR, over a wide temperature range and found that molecular sieving at the pore entrance, and competitive adsorption and diffusion in zeolite micropores largely affected the gas permselectivity. The DD3R membrane showed high adsorptivity for CO_2 molecules and high CO_2 selectivity, especially for mixtures of CO_2 and other gases at low temperatures. In the CO_2/Air and CO_2/CH_4 separations in the temperature range 250–350 K, CO_2 permeability of 0.3×10^{-8} to 2×10^{-8} mol/(m^2 s Pa), and CO_2/Air and CO_2/CH_4 selectivities of 10–20 and 200–1000, respectively, were obtained. It has also been reported that dense DD3R membranes exhibited H_2/CO and CO_2/CO selectivities of 3 and 12 (303 K), respectively, and could be CO_2-selective for CO_2/H_2 separation, and that isobutane permeates slightly through the grain boundaries (1×10^{-10} mol/(m^2 s Pa)) (van den Bergh et al. 2010).

The DDR membrane has already been scaled up to a large monolithic structure of 180 mm in diameter and 1000 mm in length by NGK Co., Japan. This membrane element achieved a CO_2/CH_4 selectivity of over 100 for a gas mixture of 8.0 MPa, 45 °C, and 70 mol% CO_2 (Hasegawa et al. 2017). It is expected to be applied to CO_2 separation in natural gas fields with high CO_2 concentrations. Recently, the possibility of CO_2/N_2 and CO_2/CH_4 separation using ZSM-58 membranes, a type of DDR zeolite, has been investigated (Hayakawa and Himeno 2020, 2021). ZSM-58 is expected to exhibit varying DDR membrane performances because it is possible, depending on the fabrication method, to form mixed crystalline structures with DOH zeolite or to introduce Al atoms. The performances of ZSM-58 membranes in the separation of CO_2/CH_4 mixed gas are 1.7×10^{-7} mol/(m^2 s Pa) for CO_2 permeance and 290 for CO_2/CH_4 selectivity, and values of 2.9×10^{-7} mol/(m^2 s Pa) for CO_2 permeance and 44 for CO_2/N_2 selectivity were obtained in the CO_2/N_2 system.

The zeolite SAPO-34 containing phosphorus atoms also has an oxygen 8-membered ring structure similar to the DDR type, and its pore size is 0.38 nm, so it can function as a CO_2 separation membrane. The crystal structure of zeolite SAPO-34 belongs to the CHA type described below. The performance of the SAPO-34 membrane was about 1.6×10^{-7} mol/(m^2 s Pa) for CO_2 permeance and 67 for CO_2/CH_4 selectivity (Li et al. 2004). However, by forming a thin membrane with uniformly sized zeolite crystals, a highly permeation-selective membrane with CO_2 permeance of 2×10^{-6} mol/(m^2 s Pa) and CO_2/CH_4 selectivity of 170 was reported in 2008 (Carreon et al. 2008). As a result of optimization of the membrane preparation method, a CO_2 permeance of 1.85×10^{-6} mol/(m^2 s Pa) and CO_2/N_2 selectivity of 29 were obtained by utilizing the high affinity of SAPA-34 with CO_2, especially in the separation of CO_2/N_2 mixed gas at around room temperature (Liu et al. 2020). This performance far exceeded the trade-off upper boundary of zeolite membranes in the CO_2 permeance vs. CO_2/N_2 selectivity plot, and stability under high temperature steam was also observed, indicating that the SAPO-34 membrane has potential for application to CO_2 separation in power generation flue gas.

As far as the authors know, the first CHA-type membrane consisting only of Si and Al was developed by Noble and Falconer's group as the SSZ-13 zeolite membrane with a Si/Al ratio of 14 (Kalipcilar et al. 2002). This membrane was characterized with a CO_2 permeance of 2.4×10^{-7} mol/(m^2 s Pa) and CO_2/CH_4 selectivity of 13. Although the performance of the SSZ-13 membrane for CO_2 separation was not satisfactory, it is interesting to note that the CO_2/N_2 selectivity was already surprisingly high at 11 at that time, suggesting the high affinity of the SSZ-13 membrane for CO_2. Subsequently, optimization of CHA membranes has also progressed, and a CO_2 permeability of 1.17×10^{-6} mol/(m^2 s Pa) and a CO_2/CH_4 separation factor of 210 were demonstrated for a CHA membrane formed on an alumina hollow fiber substrate (Yang et al. 2019). Other performance results were reported for all-silica CHA membranes (Zhou et al. 2020) or high-silica CHA membranes (Hasegawa et al. 2021; Liu et al. 2021a), with CO_2 permeability of 0.3×10^{-6} to 1.2×10^{-6} mol/(m^2 s Pa) and CO_2/CH_4 selectivity of 120–480. Compared to DDR membranes, CHA membranes exhibit relatively high CO_2 permeability. This may be due in part to the fact that the accessible volume of the CHA structure is inherently higher than that of the DDR structure. Although the development of CHA membranes is currently more vigorous than that of DDR membranes, large-scale-area DDR membranes have already been produced and are expected to be put into practical use as CO_2 separation membranes in the near future.

Permeation and separation mechanisms in various zeolite membranes applicable to CO_2 separation have been reported for Silicalite-I (Tawalbeh et al. 2021), SAPO-34 (Zito et al.

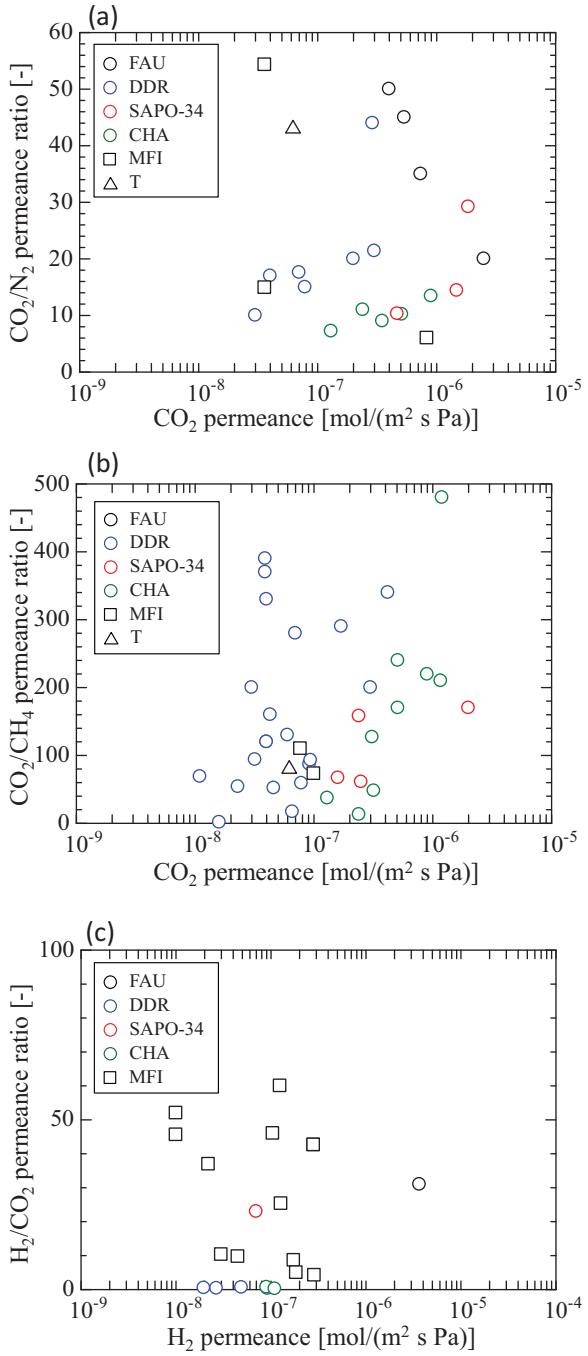

Figure 17. (a) CO_2 permeance vs. CO_2/N_2, (b) CO_2 permeance vs. CO_2/CH_4, and (c) H_2 permeance vs. H_2/CO_2 for zeolite membranes.

2020a), DDR (Zito et al. 2020b), and SSZ-13 (Aydani et al. 2021). Basically, a model is used to estimate the permeability of a single gas or the permeability and separation factor of each component in a mixed system from the adsorption and diffusion coefficients of a single gas. Most of those models reported are based on the generalized Maxwell-Stefan model (Krishna 1990; Krishna and Paschek 2002; Krishna and Wesselingh 1997) and are useful for predicting permeation and separation performance under various operating conditions.

Reported performances of zeolite membranes are shown in Figure 17.

3.3 Molten salt/ceramic membranes

To supply combustion exhaust gases to the membrane at temperatures above 500 °C for CO_2 separation, ceramic membranes operating at high temperatures are required. The CO_2 should be absorbed and permeated by a chemical reaction rather than the physical interaction between the membrane and CO_2 that is more pronounced at lower temperatures. The microporous membranes mentioned in earlier sections are not suitable for this purpose. Other thermally stable membranes based on a different concept of CO_2 separation from that of microporous molecular sieving or CO_2 affinity membranes should be studied.

Yamaguchi et al. (2007) proposed a new CO_2 separation membrane in which CO_2 dissolves into the membrane as carbonate ions (CO_3^{2-}) and permeates through the membrane by using lithium orthosilicate (Li_4SiO_4) as the membrane material. Li_4SiO_4 reacts reversibly with CO_2 under high temperature. The proposed membrane is called as a mixed conducting membrane. (Figure 18(a)). Carbonate ions diffuse through the membrane as Li_2CO_3 and carbonate ions are desorbed as CO_2 on the permeate side of the membrane by flowing a sweep gas downstream of the membrane, and O_2^- diffuses from downstream to upstream in the solid phase framework of Li_2SiO_3 to ensure charge balance. The membranes operated at high temperatures around 525–625 °C. Modeling of such a membrane was also reported by (Wade et al. 2007).

Subsequently, for O_2^- conduction, a dual-phase membrane was developed using porous perovskite (ex. $La_{0.6}Sr_{0.4}Co_{0.8}Fe_{0.2}O_{3-\delta}$ (LSCF)) or yttrium stabilized zirconia

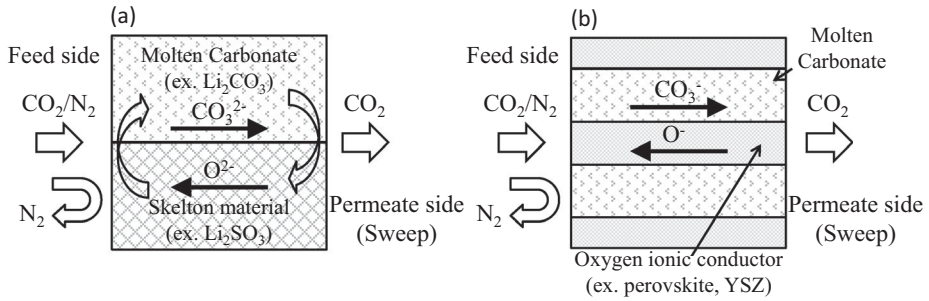

Figure 18. Schematic image of mixed conducting membrane (a) and dual-phase membrane (b) for selective CO_2 permeation.

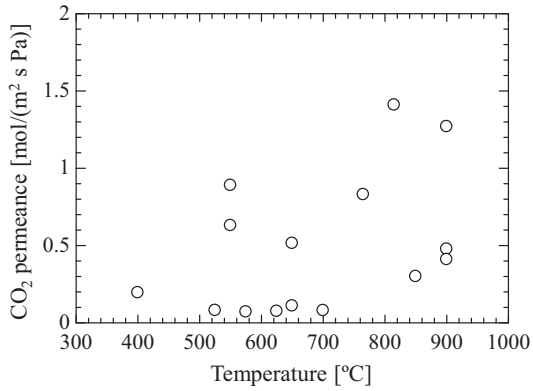

Figure 19. Temperature dependency of CO_2 permeance of molten salt/Ceramic membranes.

(YSZ) as a substrate, in which a molten carbonate eutectic salt (ex. $Li_2CO_3/Na_2CO_3/K_2CO_3$) mixture was composited for CO_2 reaction and CO_3^{2-} diffusion (Anderson and Lin 2010; Ceron et al. 2018; Dong et al. 2013; Lan et al. 2014; Rui et al. 2012; Wade et al. 2011)(Figure 18(b)). These membranes operate in the 500–900 °C range, and the CO_2 permeability can be predicted by a model that accounts for oxygen ion conduction in the solid support phase, which is the oxygen conductor. Recent dual-phase membranes have been formed into hollow-fiber shapes, and CO_2 permeability values as high as 2.3×10^{-7} mol/(m^2 s Pa) at 700 °C for a 50% CO_2 feed composition and stability of over 85 h were reported (Chen et al. 2020). Attempts have been made to control the porous structure of the carrier for molten salts to obtain even higher permeability (Grima et al. 2021; Kazakli et al. 2021).

Since the CO_2/X-selectivity of molten salt/ceramic membranes should be theoretically infinite and there is wide variation in reported values among membranes, here we compare the CO_2 permeance against temperature as an index of membrane performance, as shown in Figure 19.

Hydrogen-selective permeation membranes have also been investigated by applying the concept of dual-phase membranes (Jin et al. 2021). Dual-phase membranes with a sulfonated graphene nanosheet as the electronic conductor and crosslinked polybenzimidazole (PBI)-triglycidylisocyanurate (TGIC) as the electronic conductor showed a hydrogen permeation flux of 0.22 mL/(min cm^2) and 99.99% hydrogen selectivity at 300 °C.

3.4 Carbon membranes

Carbon membranes are a type of inorganic porous membrane in which the separation active layer is formed of carbon or carbides. Carbon membranes with micro-pores of 0.3–0.5 nm are known to exhibit excellent gas separation performance due to the molecular sieving effect (Ismail and David 2001; Saufi and Ismail 2004). Although the concept of carbon membranes was discovered in the early 1970s, interest in the development of carbon membranes actually increased after Koresh and Soffer succeeded in fabricating a crack-free molecular sieve carbon membrane (Koresh and Sofer 1983). Carbon membranes are produced by the pyrolysis of appropriate polymer precursors under controlled conditions using a variety of polymeric materials. In the development and production of carbon membranes, the following issues need to be considered: precursor selection, polymeric membrane preparation, precursor pretreatment, pyrolysis process, post-treatment of the pyrolized membrane, and module construction.

Due to its molecular sieving property, carbon membranes are expected to be applied to the separation of H_2/CO_2, CO_2/CO, CO_2/N_2, CO_2/CH_4, etc. in CO_2-related separation systems. Aromatic polymers with high carbon yields are mainly used as precursors for carbon membranes. Aromatic polyimides, cellulose derivatives, polyacrylonitrile (PAN), and polyphenylene oxide (PPO) are mainly used as precursors for freestanding membranes. On the other hand, composite membranes with supports include phenolic resin, resorcinol resin, lignocresol, polyfurfuryl alcohol (PFA), polyvinylidene chloride (PVDC), and wood tar. The following is a description of several self-standing carbon membranes using organic polymers as precursors that have been often reported in relation to CO_2 separation.

3.4.1 Polyimide based

For the preparation of polyimide-based carbon membranes applicable to CO_2 separation, rigid organic polymers such as 6FDA/BPDA-X (Arab et al. 2021; Jones and Koros 1994), Kapton (Suda and Haraya 1997), PI-BTCOOMe (Kai et al. 2009), and BTDA-TDI/MDI (Sazali et al. 2018a, 2018b) are used as precursors.

Carbon membranes with 6FDA/BPDA-TMPD as precursor showed better selectivity for membranes produced at higher temperatures than at lower temperatures, with membranes produced at 500–550 °C showing performance with CO_2 permeance of 100 GPU, CO_2/N_2 selectivity of 55 and CO_2/CH_4 selectivity of 160 (Jones and Koros 1994). Polyimide is a highly stable material, but carbon membranes using plyimide as a precursor exhibit performance changes due to aging.

Arab et al. (2021) showed that the CO_2/CH_4 separation performance of carbon hollow fiber membranes with 6FDA:BPDA-DAM polyimide precursor changed with the aging environment in a vacuum, allowing control of membrane lifetime.

Commercially available Kapton films are also made of polyimide. By pyrolyzing it under a vacuum and controlling the pore size, CO_2/N_2 separation membranes can be fabricated. The observed permeance ratio of such a membrane was 122 for CO_2/N_2 and 36 for O_2/N_2 separation at 308 K (Suda and Haraya 1997).

Kai et al. (2009) prepared carbon membranes with a precursor of cardo-type polyimide (PI-BTCOOMe) and $CsCO_3$ as a Cs source to suppress the degradation of separation performance under humidity conditions. The Cs-incorporated carbon membrane exhibited higher CO_2 permeance (9.8×10^{-9} mol/(m^2 s Pa)) and CO_2/N_2 separation factor (44) under high humidity conditions, whereas the original carbon membrane without Cs exhibited lower CO_2 permeance and CO_2/N_2 separation factor under humid conditions

than under dry conditions. It was revealed that the incorporation of Cs into the carbon membrane makes the pores of the carbon hydrophilic and increases the pore size distribution.

Sazali et al. (2018a) used BTDA-TDI/MDI P84 copolyimide as a carbon precursor and coated it with a dope solution consisting of NMP by the dip coating method to prepare carbon membranes for CO_2 separation. The CO_2 permeance of the carbon tubular membrane prepared by stabilization at 300 °C after coating and carbonizing at 800 °C was 206 GPU, and this membrane showed high values of CO_2/N_2 and CO_2CH_4 selectivity of 66.0 and 69.5, respectively. The performance of membranes made of BTDA-TDI/MDI P84 copolyimide precursor solutions with additives such as polyvinylpyrrolidone (PVP), microcrystalline cellulose (MCC) and nanocrystalline cellulose (NCC) has also been investigated (Sazali et al. 2018b). The addition of 7 wt% NCC as a pore-forming agent increased the pore structure channels of the carbon membranes, resulting in high selectivity and high permeability. The PI/NCC carbon membrane exhibited a CO_2 permeance of 214 GPU and CO_2/N_2 and CO_2/CH_4 selectivities of 66.3 and 68.2, respectively, while the pristine PI carbon membrane exhibited a permeability of 157 GPU and CO_2/N_2 selectivity of 56.3. The results indicate that the membrane formation method of carbonization by adding thermally unstable additives such as NCC is promising.

3.4.2 Cellulose based

As described above, the development of high-performance carbon membranes using polyimide as a precursor is underway. However, in general, polymer precursors such as polyimide are expensive, which is one of the factors preventing the wide industrial use of carbon membranes (Araújo et al. 2020). On the other hand, cellulose is an inexpensive bioreducible raw material, and carbon membranes using cellulosic precursors are very promising alternatives, especially in carbon molecular sieve (CMS) membranes for O_2/N_2 and CO_2/CH_4 separation, which have been reported to significantly overcome Robeson's upper limit of membrane performance.

Lie and Hägg (2005) prepared CMS membranes by vacuum carbonizing cellulose, a low-cost precursor, with metals such as oxides of Ca, Mg, Fe(III), and Si and nitrates of Ag, Cu, and Fe(III). Carbon membranes containing Fe nitrate showed good separation performance for O_2/N_2 and CO_2/CH_4 gas pairs. On the other hand, carbon-containing Cu or Ag nitrates showed high selectivity but lower permeance for O_2 and CO_2 compared to carbon-containing Fe nitrates. This was due to the formation of a blocking layer of gas transport on the carbon surface by the metal additives. Membranes containing Ag and Cu exhibit high H_2 permeance and are expected to be applied to H_2/CO_2 separation membranes. In addition, hydrolysis of cellulose with trifluoroacetic acid (TFA) before carbonization suppresses weight loss during carbonization and improves CO_2/CH_4 separation performance (Lie and Hägg 2006).

The carbonized cellulose hollow fiber membranes prepared by the dry-wet spinning phase inversion method have excellent mechanical strength, and showed CO_2 permeability of 110 barrer and CO_2/N_2 selectivity of 42, and CO_2 permeability of 45 barrer and CO_2/CH_4 selectivity of 150 at a pressure difference of 8 bar. Furthermore, the CO_2 permeability and CO_2/N_2 selectivity increased to 180 and 55, respectively, when the applied pressure was increased to 20 bar while the pressure difference across the membranes was kept at 8 bar. Process simulations using this membrane have shown that a two-stage membrane system can produce methane with a composition of 96% with a loss of less than 4%. Further improvement of the permeance is expected to significantly reduce the cost of natural gas processing (Karousos et al. 2020). CMS membranes prepared from cellulose hollow fiber precursors have been reported for H_2/CO_2 separation, showing excellent H_2 permeance of 111 GPU and H_2/CO_2 selectivity of 36.9 under dry mixed gas conditions of 10 atm and 110 °C. The membranes were stable under humidified conditions of 90 °C and 14 bar (Lei et al. 2021). Simulations show that this membrane can be used in a two-stage carbon membrane system to produce high-purity H_2 (>99.5 vol %) in a methane steam reforming process.

Recently, CMS membranes with excellent separation performance and stability have been reported using ionic liquid regenerated cellulose as a precursor (Araújo et al. 2022). Although the H_2 and CO_2 permeabilities were not very high (200 and 10 barrer, respectively), extremely high selectivities of H_2/CH_4 (> 206,000) and CO_2/CH_4 (> 14,600) were achieved. Furthermore, post-treatment of the membranes with propylene was found to improve their stability. This is an interesting research result that will enhance the practical use of cellulosic carbon membranes.

3.4.3 PPO based

Polyphenylene oxide (PPO) and its derivatives are also important precursor polymers for self-standing carbon membranes. Yoshimune et al. at the National Institute of Advanced Industrial Science and Technology (AIST) in Japan have successfully fabricated novel CMS membranes from PPO and its derivatives as carbon hollow fibers. The PPO CMS membrane exhibited higher gas permeability than the polymer precursor, with CO_2/N_2 selectivity of 42–54, compared to 26–32 for the PPO precursor membrane. The CO_2 permeability was also improved by a factor of several times (Yoshimune et al. 2005). Subsequently, monovalent, divalent, and trivalent metal cations such as Na^+, Mg^{2+}, Al^{3+}, Ag^+, Cu^{2+}, and Fe^{3+} were substituted into sulfonated poly(phenylene oxide) (SPPO) by ion exchange with the protons of the sulfonic acid groups of SPPO to investigate their effects on the gas transport properties of SPPO CMS membranes. The SPPO membranes with these metal cations showed CO_2 permeability of several hundred to 1500 barrer and CO_2/N_2 selectivity of 20–30 (Yoshimune et al. 2006). When trimethylsilyl (TMS) substituents were introduced into the PPO precursor, the TMS groups were found to increase the pore volume and improve gas diffusivity (Yoshimune et al. 2007). This carbon membrane exhibited

excellent CO_2/CH_4 separation performance (CO_2 permeability 529 barrer, CO_2/CH_4 selectivity 102), comparable to polyimide carbon membranes.

In 2010, flexible carbon hollow fiber membranes were developed by carbonizing sulfonated polyphenylene oxide (SPPO) at 450–600 °C using SPPO as a carbon precursor (Yoshimune and Haraya 2010). Pyrolyzed membranes at 700 °C became less flexible and rather brittle due to the sintering of the carbon matrix, while carbon hollow fiber membranes pyrolyzed at 600 °C showed excellent mechanical stability and excellent performance in CO_2 separation (CO_2 permeance: about 2×10^{-8} mol/(m^2 s Pa), CO_2/N_2 selectivity: 43, CO_2/CH_4 selectivity: 118). In fact, a carbon membrane module with an effective membrane area of 259 cm^2 was successfully fabricated by installing 195 SPPO hollow fiber carbon membranes, each 18 cm long, in a 2 cm diameter tubular holder (Yoshimune and Haraya 2013). The CO_2 permeance of the module was 5×10^{-9} mol/(m^2 s Pa), which was slightly lower than that of single hollow fiber CMS membrane, while the CO_2/N_2 selectivity was 58 and CO_2/CH_4 selectivity was 170–200, maintaining high-performance. These flexible hollow-fiber carbon membranes are superior to other inorganic membranes in terms of module preparation and are highly practical.

Other CO_2 permeation and separation properties of carbon membranes using phenolic resins (Bera and Das 2022; Katsaros et al. 2007; Kita et al. 1997; Torres et al. 2021), polyetherimide (PEI) (Bakonyi et al. 2021; Salleh and Ismail 2012), and Resorcinol-Formaldehyde Resin (Rahimalimamaghani et al. 2022) as precursors have been investigated.

Compared to polymeric membranes, carbon membranes have the characteristics of inorganic membranes, especially in terms of selectivity and thermal and chemical stability, and have advantages over inorganic membranes in terms of membrane formation and module preparation, such as those of organic membranes. In the future, the development of advanced carbon membrane materials based on renewable precursors and simple carbonization processes, as well as the development of module designs and process optimization, are expected to facilitate the introduction of carbon membranes in various industrial processes (Lei et al. 2020).

Reported performances of polyimide-, cellulose-, and polyphenylene oxide-based carbon membranes are shown in Figure 20.

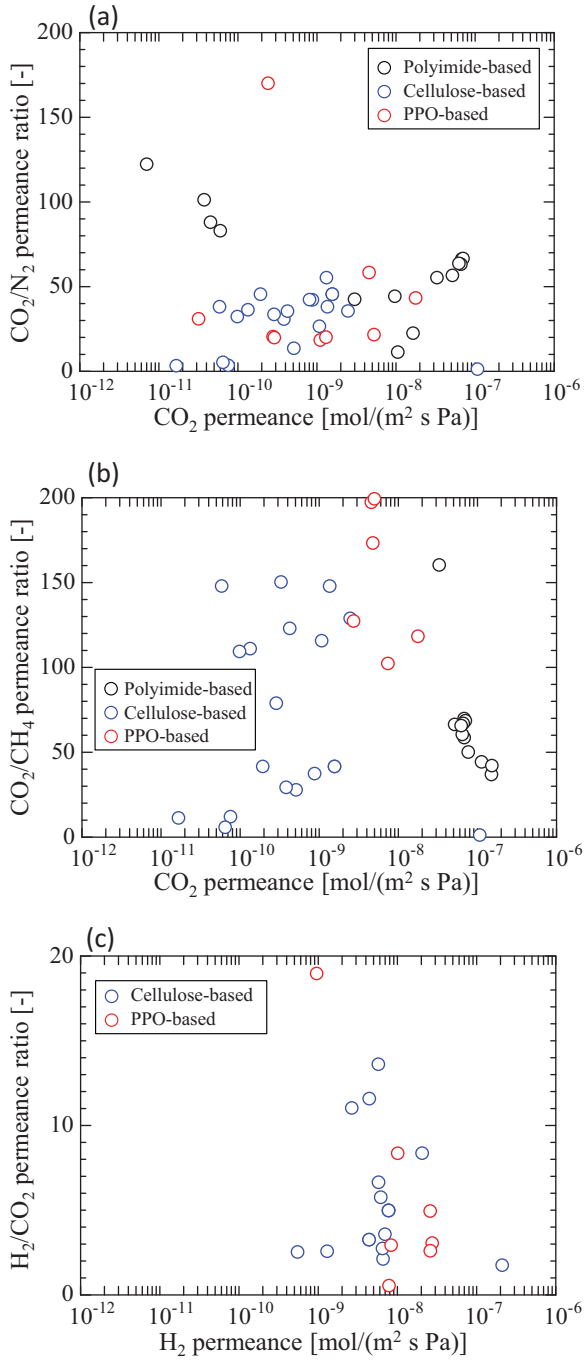

Figure 20. (a) CO_2 permeance vs. CO_2/N_2, (b) CO_2 permeance vs. CO_2/CH_4, and (c) H_2 permeance vs. H_2/CO_2 for carbon membranes.

4. Conclusions and Outlook

In this review, several new materials for high-performance CO_2 separation membranes were reviewed. Novel materials with high CO_2 separation performance are still continuously being developed. The upper bound for CO_2 separation showing the relationship between CO_2/other light gases permselectivity and CO_2 permeability of polymer membranes presented by Robeson in 1991 has been updated several times and is expected to be further updated in the future. Theoretical considerations of the upper bound have provided useful guideline for the development of new and effective membrane materials for CO_2 separation, and contributed greatly to the development of high-performance CO_2 separation membranes. In the next stage, understanding of the correlation between the physical, chemical, and physico-chemical properties of the membrane materials and the CO_2 diffusivity and solubility, which are the basic parameters for the CO_2 permeability and CO_2 permselectivity, is highly desired. A unified understanding of the dependence of CO_2 diffusivity on the micropore size of each membrane material is expected to deepen by using advanced analytical techniques such as PALS. On the other hand, there is a lack of basic knowledge about the relationship between selective CO_2 absorbability and membrane properties. A basic understanding of the properties of a membrane

material that affect the selective CO_2 absorption are highly desired. If the diffusivity and absorbability can be well correlated with the properties of the membrane materials, there is no doubt that membrane materials with much higher CO_2 separation performance will be developed in the future. Expertise and technology in various fields such as polymer chemistry, organic chemistry, inorganic chemistry, and material science could open the doors for the development of next-generation membrane materials with even higher CO_2 separation performance.

The use of computational science technologies such as molecular simulation has recently attracted much attention in predicting membrane properties and the absorption and diffusion of permeating molecules. Improved computer performance and the force fields that govern molecular interactions have enabled the reproduction of absorption/adsorption quantities and improved the accuracy of diffusivity predictions for various membrane materials, such as polymeric, mixmatrix and inorganic porous membranes, so that the combination of adsorption and diffusion models and simulation results is now being used to predict the permeability. In actual separation membranes, the membrane structure is not always homogeneous, with pore size distribution and grain boundaries, and permeation resistance may exist not only in the pores but also on the membrane surface. In order to simulate gas permeation phenomena in such systems more directly, the boundary-controlled Non-Equilibrium Molecular Dynamics (NEMD) method has also been developed as a calculation method that maintains a steady chemical potential gradient. It is expected that the computer-assisted development of various separation membranes, including CO_2 separation membranes, will be accelerated in the near future.

From the perspective of developing a CO_2 separation process using membrane separation technology, it is important to accumulate knowledge about the membrane properties required to use it in practical applications. One of them is the evaluation and accumulation of CO_2 permeance. For this purpose, it is also important to develop thin membrane fabrication methods. Experimental techniques to correctly determine the separation layer thickness should be also developed. Accumulation of the data of minimum membrane thickness achieved for each membrane material would be helpful to use membranes for practical applications.

Determination of the CO_2 permeance and CO_2 permselectivity using mixed gases is also important for practical use. This is because the CO_2 permeance and CO_2 permselectivity depend on temperature, total pressure, CO_2 partial pressure, and humidity. In particular, it is necessary to pay attention to humidity. The permeation rate of water vapor through most membranes is faster than that of most other light gases, and the relative humidity in the feed gas would change from upstream to downstream in the membrane module during practical operation. Therefore, the data for humidity dependence of CO_2 permeance and CO_2 permselectivity is necessary for a process simulation. Similar to humidity, the data for CO_2 partial pressure dependence on CO_2 permeance and CO_2 permselectivity are important for some kinds of CO_2 separation membranes. Especially for facilitated transport membranes and glassy polymer membranes, CO_2 absorption follows the dual sorption model, and the CO_2 permeance and CO_2 permselectivity depend on CO_2 partial pressure. Regarding the experimental conditions of the mixed gas permeation test, in order to compare the performances of the membranes easily, the evaluation should be conducted under certain representative standard conditions, which should be determined for each gas species from various CO_2 sources.

Besides these aspects, examination on the effects of trace gas components contained in the gas to be separated is also important. For example, NO_x and SO_2 in thermal power plant flue gas and H_2S in biogas can affect CO_2 permeance, CO_2 permselectivity, and life of the CO_2 separation membranes. On the other hand, if the membrane is used to separate CO_2 from a gas with high pressure, the effect of plasticization under high-pressure conditions should also be evaluated.

The successful development of the materials for high-performance CO_2 separation membranes has greatly increased the possibility of realizing energy-saving and compact CO_2 separation and capture processes using CO_2 separation membranes. In the next stage, it is necessary not only to make further progress in materials development, but also to simultaneously conduct performance evaluation, data accumulation, and data organization in order to apply the developed high-performance CO_2 separation membranes for practical processes.

CO_2 capture using CO_2 separation membranes is a technology full of possibilities. We strongly hope that membranes will contribute to the preservation of the global environment and the sustainable development of human beings.

References

Aitken CL, Koros WJ, Paul DR. 1992. Gas transport properties of biphenol polysulfones. Macromolecules. 25:3651–3658. doi: 10.1021/ma00040a008.

Aki SNVK, Mellein BR, Saurer EM, Brennecke JF. 2004. High-pressure phase behavior of carbon dioxide with imidazolium-based ionic liquids. J Phys Chem B. 108:20355–20365. doi: 10.1021/jp046895+.

Al-Masri M, Fritsch D, Kricheldorf HR. 2000. New polyimides for gas separation. 2. polyimides derived from substituted catechol bis(etherphthalic anhydride)s. Macromolecules. 33:7127–7135. doi: 10.1021/ma9920745.

Al-Masri M, Kricheldorf HR, Fritsch D. 1999. New polyimides for gas separation. 1. Polyimides derived from substituted terphenylenes and 4,4'-(hexafluoroisopropylidene)diphthalic anhydride. Macromolecules. 32:7853–7858. doi: 10.1021/ma9910742.

Alentiev AY, Yampolskii YP. 2000. Free volume model and tradeoff relations of gas permeability and selectivity in glassy polymers. J Membr Sci. 165:201–216. doi: 10.1016/S0376-7388(99)00229-X.

Alghunaimi F, Ghanem B, Alaslai N, Swaidan R, Litwiller E, Pinnau I. 2015. Gas permeation and physical aging properties of iptycene diamine-based microporous polyimides. J Membr Sci. 490:321–327. doi: 10.1016/j.memsci.2015.05.010.

Anderson M, Lin YS. 2010. Carbonate-ceramic dual-phase membrane for carbon dioxide separation. J Membr Sci. 357:122–129. doi: 10.1016/j.memsci.2010.04.009.

Anthony JL, Anderson JL, Maginn EJ, Brennecke JF. 2005. Anion effects on gas solubility in ionic liquids. J Phys Chem B. 109:6366–6374. doi: 10.1021/jp046404l.

Araújo T, Andrade M, Bernardo G, Mendes A. 2022. Stable cellulose-based carbon molecular sieve membranes with very high selectivities. J Membr Sci. 641:119852. doi: 10.1016/j.memsci.2021.119852.

Araújo T, Bernardo G, Mendes A. 2020. Cellulose-based carbon molecular sieve membranes for gas separation: a review. Molecules. 25:3532. doi: 10.3390/molecules25153532.

Arab P, Liu Z, Nasser M, Qiu W, Martinez M, Flick D, Roy A, Liu J, Koros WJ. 2021. Subtle penetrant size effects on separation of carbon molecular sieve membranes derived from 6FDA:BPDA-DAM polyimide. Carbon. 184:214–222. doi: 10.1016/j.carbon.2021.08.005.

Ariyoshi M, Fujikawa S, Kunitake T. 2021. Robust, hyper-permeable nanomembrane composites of poly(dimethylsiloxane) and cellulose nanofibers. ACS Appl Mater Interfaces. 13:61189–61195. doi: 10.1021/acsami.1c19220.

Asaeda M, Yamasaki S. 2001. Separation of inorganic/organic gas mixtures by porous silica membranes. Sep Purif Technol. 25:151–159. doi: 10.1016/S1383-5866(01)00099-5.

Aydani A, Brunetti A, Maghsoudi H, Barbieri G. 2021. CO_2 separation from binary mixtures of CH_4, N_2, and H_2 by using SSZ-13 zeolite membrane. Sep Purif Technol. 256:117796. doi: 10.1016/j.seppur.2020.117796.

Babarao R, Dai S, Jiang D-E. 2011. Understanding the high solubility of CO_2 in an ionic liquid with the tetracyanoborate anion. J Phys Chem B. 115:9789–9794. doi: 10.1021/jp205399r.

Baerlocher C, McCusker LB. 2023. Structure commission of the international zeolite association (IZA-SC). Database of Zeolite Structures. https://jpn01.safelinks.protection.outlook.com/?url=http%3A%2F%2Fwww.iza-structure.org%2Fdatabases%2F&data=05%7C01%7C%7C1e257823984f44e4d71a08db6ce79436%7C20ee4c8087bd422ca5063a2b0aca0615%7C0%7C0%7C638223514246461814%7CUnknown%7CTWFpbGZsb3d8eyJWIjoiMC4wLjAwMDAiLCJQIjoiV2luMzIiLCJBTiI6Ik1haWwiLCJXVCI6Mn0%3D%7C3000%7C%7C%7C&sdata=HwtV%2Fv%2F6TlWl9Wz86c0Lq5%2BTJ6s4BeQt7f3wqyt2v4g%3D&reserved=0

Baerlocher C, Mccusker LB, Olson DH. 2007. Atlas of zeolite framework types. 6th ed. Amsterdam: Elsevier Science.

Bakonyi P, Peter J, Nemestothy N, Maly D, Kumar G, Koter S, Kim S-H, Kujawski W, Belafi-Bako K, Pientka Z. 2021. Feasibility study of polyetherimide membrane for enrichment of carbon dioxide from synthetic biohydrogen mixture and subsequent utilization scenario using microalgae. Int J Energy Res. 45:8327–8334. doi: 10.1002/er.5732.

Bandehali S, Ebadi Amooghin A, Sanaeepur H, Ahmadi R, Fuoco A, Jansen JC, Shirazian S. 2021. Polymers of intrinsic microporosity and thermally rearranged polymer membranes for highly efficient gas separation. Sep Purif Technol. 278:119513. doi: 10.1016/j.seppur.2021.119513.

Bara JE, Hatakeyama ES, Gin DL, Noble RD. 2008. Improving CO_2 permeability in polymerized room-temperature ionic liquid gas separation membranes through the formation of a solid composite with a room-temperature ionic liquid. Polym Adv Technol. 19:1415–1420. doi: 10.1002/pat.1209.

Ben Hamouda S, Nguyen QT, Langevin D, Roudesli S. 2010. Poly(vinylalcohol)/poly(ethyleneglycol)/poly(ethyleneimine) blend membranes - structure and CO_2 facilitated transport. C R Chim. 13:372–379. doi: 10.1016/j.crci.2009.10.009.

Benito J, Vidal J, Sánchez-Laínez J, Zornoza B, Téllez C, Martín S, Msayib KJ, Comesaña-Gándara B, Mckeown NB, Coronas J, et al. 2019. The fabrication of ultrathin films and their gas separation performance from polymers of intrinsic microporosity with two-dimensional (2D) and three-dimensional (3D) chain conformations. J Colloid Interface Sci. 536:474–482. doi: 10.1016/j.jcis.2018.10.075.

Bera B, Das N. 2022. Synthesis of SBA 15 graphene oxide composite membrane using phenol-formaldehyde resin pore modifier for CO_2 separation. J Am Ceram Soc. 105:913–928. doi: 10.1111/jace.18181.

Bernardo P, Bazzarelli F, Tasselli F, Clarizia G, Mason CR, Maynard-Atem L, Budd PM, Lanc M, Pilnacek K, Vopicka O, et al. 2017. Effect of physical aging on the gas transport and sorption in PIM-1 membranes. Polymer. 113:283–294. doi: 10.1016/j.polymer.2016.10.040.

Bezzu CG, Carta M, Ferrari M-C, Jansen JC, Monteleone M, Esposito E, Fuoco A, Hart K, Liyana-Arachchi TP, Colina CM, et al. 2018. The synthesis, chain-packing simulation and long-term gas permeability of highly selective spirobifluorene-based polymers of intrinsic microporosity. J Mater Chem A. 6:10507–10514. doi: 10.1039/C8TA02601G.

Blanchard LA, Hancu D, Beckman EJ, Brennecke JF. 1999. Green processing using ionic liquids and CO_2. Nature. 399:28–29. doi: 10.1038/19887.

Boffa V, Ten Elshof JE, Garcia R, Blank DHA. 2009. Microporous niobia-silica membranes: Influence of sol composition and structure on gas transport properties. Microporous Mesoporous Mater. 118:202–209. doi: 10.1016/j.micromeso.2008.08.038.

Bondar VI, Freeman BD, Pinnau I. 2000. Gas transport properties of poly(ether-b-amide) segmented block copolymers. J Polym Sci B Polym Phys. 38:2051–2062. doi: 10.1002/1099-0488(20000801)38:15<2051::AID-POLB100>3.0.CO;2-D.

Brinkmann T, Lillepärg J, Notzke H, Pohlmann J, Shishatskiy S, Wind J, Wolff T. 2017. Development of CO_2 selective poly(ethylene oxide)-based membranes: from laboratory to pilot plant scale. Engineering. 3:485–493. doi: 10.1016/J.ENG.2017.04.004.

Brunetti A, Cersosimo M, Dong G, Woo KT, Lee J, Kim JS, Lee YM, Drioli E, Barbieri G. 2016. In situ restoring of aged thermally rearranged gas separation membranes. J Membr Sci. 520:671–678. doi: 10.1016/j.memsci.2016.07.030.

Budd PM, Elabas ES, Ghanem BS, Makhseed S, Mckeown NB, Msayib KJ, Tattershall CE, Wang D. 2004a. Solution-processed, organophilic membrane derived from a polymer of intrinsic microporosity. Adv Mater. 16:456–459. doi: 10.1002/adma.200306053.

Budd PM, Ghanem BS, Makhseed S, Mckeown NB, Msayib KJ, Tattershall CE. 2004b. Polymers of intrinsic microporosity (PIMs): robust, solution-processable, organic nanoporous materials. Chem Commun. 2:230–231. doi: 10.1039/b311764b.

Budd PM, Msayib KJ, Tattershall CE, Ghanem BS, Reynolds KJ, Mckeown NB, Fritsch D. 2005. Gas separation membranes from polymers of intrinsic microporosity. J Membr Sci. 251:263–269. doi: 10.1016/j.memsci.2005.01.009.

Cadena C, Anthony JL, Shah JK, Morrow TI, Brennecke JF, Maginn EJ. 2004. Why is CO_2 so soluble in imidazolium-based ionic liquids? J Am Chem Soc. 126:5300–5308. doi: 10.1021/ja039615x.

Calle M, Lee YM. 2011. Thermally rearranged (TR) poly(ether-benzoxazole) membranes for gas separation. Macromolecules. 44:1156–1165. doi: 10.1021/ma102878z.

Carlisle TK, Nicodemus GD, Gin DL, Noble RD. 2012. CO_2/light gas separation performance of cross-linked poly(vinylimidazolium) gel membranes as a function of ionic liquid loading and cross-linker content. J Membr Sci. 397-398:24–37. doi: 10.1016/j.memsci.2012.01.006.

Carreon MA, Li S, Falconer JL, Noble RD. 2008. Alumina-supported SAPO-34 membranes for CO_2/CH_4 separation. J Am Chem Soc. 130:5412–5413. doi: 10.1021/ja801294f.

Carta M, Croad M, Malpass-Evans R, Jansen JC, Bernardo P, Clarizia G, Friess K, Lanc M, Mckeown NB. 2014. Triptycene induced enhancement of membrane gas selectivity for microporous Troeger's base polymers. Adv Mater. 26:3526–3531. doi: 10.1002/adma.201305783.

Carta M, Malpass-Evans R, Croad M, Rogan Y, Jansen JC, Bernardo P, Bazzarelli F, Mckeown NB. 2013. An efficient polymer molecular sieve for membrane gas separations. Science. 339:303–307. doi: 10.1126/science.1228032.

Carvalho PJ, Coutinho JaP 2011. The polarity effect upon the methane solubility in ionic liquids: a contribution for the design of ionic liquids for enhanced CO_2/CH_4 and H_2S/CH_4 selectivities. Energy Environ Sci. 4:4614–4619. doi: 10.1039/c1ee01599k.

Ceron MR, Lai LS, Amiri A, Monte M, Katta S, Kelly JC, Worsley MA, Merrill MD, Kim S, Campbell PG. 2018. Surpassing the conventional limitations of CO_2 separation membranes with

hydroxide/ceramic dual-phase membranes. J Membr Sci. 567:191–198. doi: 10.1016/j.memsci.2018.09.028.

Chakrabarty T, Giri AK, Sarkar S. 2022. Mixed-matrix gas separation membranes for sustainable future: a mini review. Polym Adv Technol. 33:1747–1761. doi: 10.1002/pat.5645.

Chen H, Kovvali AS, Sirkar KK. 2000. Selective CO_2 separation from CO_2-N_2 mixtures by immobilized glycine-Na-glycerol membranes. Ind Eng Chem Res. 39:2447–2458. doi: 10.1021/ie9908736.

Chen T, Wang Z, Hu J, Wai MH, Kawi S, Lin YS. 2020. High CO_2 permeability of ceramic-carbonate dual-phase hollow fiber membrane at medium-high temperature. J Membr Sci. 597:117770. doi: 10.1016/j.memsci.2019.117770.

Chiou JS, Maeda Y, Paul DR. 1987. Gas permeation in poly(ether sulfone). J Appl Polym Sci. 33:1823–1828. doi: 10.1002/app.1987.070330533.

Cho YJ, Park HB. 2011. High performance polyimide with high internal free volume elements. Macromol Rapid Commun. 32:579–586. doi: 10.1002/marc.201000690.

Choi JI, Jung CH, Han SH, Park HB, Lee YM. 2010. Thermally rearranged (TR) poly(benzoxazole-co-pyrrolone) membranes tuned for high gas permeability and selectivity. J Membr Sci. 349:358–368. doi: 10.1016/j.memsci.2009.11.068.

Comesaña-Gándara B, Ansaloni L, Lee YM, Lozano AE, De Angelis MG. 2017. Sorption, diffusion, and permeability of humid gases and aging of thermally rearranged (TR) polymer membranes from a novel ortho-hydroxypolyimide. J Membr Sci. 542:439–455. doi: 10.1016/j.memsci.2017.08.009.

Comesaña-Gándara B, Chen J, Bezzu CG, Carta M, Rose I, Ferrari M-C, Esposito E, Fuoco A, Jansen JC, Mckeown NB. 2019. Redefining the Robeson upper bounds for CO_2/CH_4 and CO_2/N_2 separations using a series of ultrapermeable benzotriptycene-based polymers of intrinsic microporosity. Energy Environ Sci. 12:2733–2740. doi: 10.1039/C9EE01384A.

Coterillo CC, Yokoo T, Yoshioka T, Tsuru T, Asaeda M. 2011. Synthesis and characterization of microporous ZrO_2 membranes for gas permeation at 200 °C. Sep Sci Technol. 46:1224–1230. doi: 10.1080/01496395.2011.556098.

Cowan MG, Gin DL, Noble RD. 2016. Poly(ionic liquid)/ionic liquid ion-gels with high "free" ionic liquid content: platform membrane materials for CO_2/light gas separations. Acc Chem Res. 49:724–732. doi: 10.1021/acs.accounts.5b00547.

De Abajo J, De La Campa JG, Lozano AE, Espeso J, Garcia C. 2003. Designing aromatic polyamides and polyimides for gas separation membranes. Macromol Symp. 199:293–306. doi: 10.1002/masy.200350925.

Demir H, Aksu GO, Gulbalkan HC, Keskin S. 2022. MOF membranes for CO_2 capture: past, present and future. Carbon Capture Sci Technol. 2:100026. doi: 10.1016/j.ccst.2021.100026.

Deng L, Hagg M-B. 2015. Fabrication and evaluation of a blend facilitated transport membrane for CO_2/CH_4 separation. Ind Eng Chem Res. 54:11139–11150. doi: 10.1021/acs.iecr.5b02971.

Diniz Da Costa JC, Reed GP, Thambimuthu K. 2009. High temperature gas separation membranes in coal gasification. Energy Procedia. 1:295–302. doi: 10.1016/j.egypro.2009.01.041.

Do YS, Seong JG, Kim S, Lee JG, Lee YM. 2013. Thermally rearranged (TR) poly(benzoxazole-co-amide) membranes for hydrogen separation derived from 3,3'-dihydroxy-4,4'-diamino-biphenyl (HAB), 4,4'-oxydianiline (ODA) and isophthaloyl chloride (IPCl). J Membr Sci. 446:294–302. doi: 10.1016/j.memsci.2013.06.059.

Dong X, Ortiz Landeros J, Lin YS. 2013. An asymmetric tubular ceramic-carbonate dual phase membrane for high temperature CO_2 separation. Chem Commun. 49:9654–9656. doi: 10.1039/c3cc45949g.

Du N, Park HB, Robertson GP, Dal-Cin MM, Visser T, Scoles L, Guiver MD. 2011. Polymer nanosieve membranes for CO_2-capture applications. Nat Mater. 10:372–375. doi: 10.1038/nmat2989.

Du N, Robertson GP, Dal-Cin MM, Scoles L, Guiver MD. 2012. Polymers of intrinsic microporosity (PIMs) substituted with methyl tetrazole. Polymer. 53:4367–4372. doi: 10.1016/j.polymer.2012.07.055.

Du N, Robertson GP, Song J, Pinnau I, Guiver MD. 2009. High-performance carboxylated polymers of intrinsic microporosity (PIMs) with tunable gas transport properties. Macromolecules. 42:6038–6043. doi: 10.1021/ma9009017.

Duan S, Taniguchi I, Kai T, Kazama S. 2012. Poly(amidoamine) dendrimer/poly(vinyl alcohol) hybrid membranes for CO_2 capture. J Membr Sci. 423–424:107–112. doi: 10.1016/j.memsci.2012.07.037.

El-Azzami LA, Grulke EA. 2009. Parametric study of CO_2 fixed carrier facilitated transport through swollen chitosan membranes. Ind Eng Chem Res. 48:894–902. doi: 10.1021/ie7016916.

Embaye AS, Martínez-Izquierdo L, Malankowska M, Téllez C, Coronas J. 2021. Poly(ether-block-amide) copolymer membranes in CO_2 separation applications. Energy Fuels. 35:17085–17102. doi: 10.1021/acs.energyfuels.1c01638.

Eterigho-Ikelegbe O, Bada SO, Daramola MO. 2020. Preparation and evaluation of nanocomposite sodaliteα-Al2O3 tubular membranes for H_2/CO_2 separation. Membranes. 10:312. doi: 10.3390/membranes10110312.

Feuston BP, Garofalini SH. 1988. Empirical three-body potential for vitreous silica. J. Chem. Phys. 89:5818–5824. doi: 10.1063/1.455531.

Figueroa JD, Fout T, Plasynski S, Mcilvried H, Srivastava RD. 2008. Advances in CO_2 capture technology. The U.S. department of energy's carbon sequestration program. Int J Greenh Gas Control. 2:9–20. doi: 10.1016/S1750-5836(07)00094-1.

Franz J, Scherer V. 2011. Impact of ceramic membranes for CO_2 separation on IGCC power plant performance. Energy Procedia. 4:645–652. doi: 10.1016/j.egypro.2011.01.100.

Freeman BD. 1999. Basis of permeability/selectivity tradeoff relations in polymeric gas separation membranes. Macromolecules. 32:375–380. doi: 10.1021/ma9814548.

Fujii K, Asai H, Ueki T, Sakai T, Imaizumi S, Chung U-I, Watanabe M, Shibayama M. 2012. High-performance ion gel with tetra-PEG network. Soft Matter. 8:1756–1759. doi: 10.1039/C2SM07119C.

Fujii K, Makino T, Hashimoto K, Sakai T, Kanakubo M, Shibayama M. 2015. Carbon dioxide separation using a high-toughness ion gel with a tetra-armed polymer network. Chem Lett. 44:17–19. doi: 10.1246/cl.140795.

Fujikawa S, Ariyoshi M, Selyanchyn R, Kunitake T. 2019. Ultra-fast, selective CO_2 permeation by free-standing siloxane nanomembranes. Chem Lett. 48:1351–1354. doi: 10.1246/cl.190558.

Fujikawa S, Selyanchyn R, Kunitake T. 2021. A new strategy for membrane-based direct air capture. Polym J. 53:111–119. doi: 10.1038/s41428-020-00429-z.

Fukumoto T, Yoshioka T, Nagasawa H, Kanezashi M, Tsuru T. 2014. Development and gas permeation properties of microporous amorphous TiO_2-ZrO_2-organic composite membranes using chelating ligands. J Membr Sci. 461:96–105. doi: 10.1016/j.memsci.2014.02.031.

Gan F, Dong J, Xu X, Li M, Zhao X, Zhang Q. 2019. Preparation of thermally rearranged poly(benzoxazole-co-imide) membranes containing heteroaromatic moieties for CO_2/CH_4 separation. Polymer. 185:121945. doi: 10.1016/j.polymer.2019.121945.

Gan F, Dong J, Zheng S, Zhao X, Zhang Q. 2020. Constructing gas molecule transport channels in thermally rearranged multiblock poly(benzoxazole-co-imide) membranes for effective CO_2/CH_4 separation. ACS Sustainable Chem Eng. 8:9669–9679. doi: 10.1021/acssuschemeng.0c01224.

Ghanem BS, Mckeown NB, Budd PM, Al-Harbi NM, Fritsch D, Heinrich K, Starannikova L, Tokarev A, Yampolskii Y. 2009. Synthesis, characterization, and gas permeation properties of a novel group of polymers with intrinsic microporosity: PIM-polyimides. Macromolecules. 42:7881–7888. doi: 10.1021/ma901430q.

Ghanem BS, Mckeown NB, Budd PM, Fritsch D. 2008a. Polymers of intrinsic microporosity derived from bis(phenazyl) monomers. Macromolecules. 41:1640–1646. doi: 10.1021/ma071846r.

Ghanem BS, Mckeown NB, Budd PM, Selbie JD, Fritsch D. 2008b. High-performance membranes from polyimides with intrinsic microporosity. Adv Mater. 20:2766–2771. doi: 10.1002/adma.200702400.

Ghanem BS, Swaidan R, Litwiller E, Pinnau I. 2014a. Ultra-microporous triptycene-based polyimide membranes for high-performance gas separation. Adv Mater. 26:3688–3692. doi: 10.1002/adma.201306229.

Ghanem BS, Swaidan R, Ma X, Litwiller E, Pinnau I. 2014b. Energy-efficient hydrogen separation by AB-type ladder-polymer molecular sieves. Adv Mater. 26:6696–6700. doi: 10.1002/adma.201401328.

Ghosal K, Chern RT, Freeman BD, Daly WH, Negulescu II. 1996. Effect of basic substituents on gas sorption and permeation in polysulfone. Macromolecules. 29:4360–4369. doi: 10.1021/ma951310i.

Gouveia ASL, Tome LC, Marrucho IM. 2016. Towards the potential of cyano and amino acid-based ionic liquid mixtures for facilitated CO_2 transport membranes. J Membr Sci. 510:174–181. doi: 10.1016/j.memsci.2016.03.008.

Grima L, Mutch GA, Oliete PB, Bucheli W, Merino RI, Papaioannou EI, Bailey JJ, Kok MD, Brett DJL, Shearing PR, et al. 2021. High CO_2 permeability in supported molten-salt membranes with highly dense and aligned pores produced by directional solidification. J Membr Sci. 630:119057. doi: 10.1016/j.memsci.2021.119057.

Gu Y-Y, Lodge TP. 2011. Synthesis and gas separation performance of triblock copolymer ion gels with a polymerized ionic liquid midblock. Macromolecules. 44:1732–1736. doi: 10.1021/ma2001838.

Gu Y, Cussler EL, Lodge TP. 2012. ABA-triblock copolymer ion gels for CO_2 separation applications. J Membr Sci. 423-424:20–26. doi: 10.1016/j.memsci.2012.07.011.

Guo M, Kanezashi M, Nagasawa H, Yu L, Ohshita J, Tsuru T. 2020. Amino-decorated organosilica membranes for highly permeable CO_2 capture. J Membr Sci. 611:118328. doi: 10.1016/j.memsci.2020.118328.

Guo M, Qian J, Xu R, Ren X, Zhong J, Kanezashi M. 2022. Boosting the CO_2 capture efficiency through aromatic bridged organosilica membranes. J Membr Sci. 643:120018. doi: 10.1016/j.memsci.2021.120018.

Han SH, Kwon HJ, Kim KY, Seong JG, Park CH, Kim S, Doherty CM, Thornton AW, Hill AJ, Lozano AE, et al. 2012. Tuning microcavities in thermally rearranged polymer membranes for CO_2 capture. Phys Chem Chem Phys. 14:4365–4373. doi: 10.1039/c2cp23729f.

Han SH, Misdan N, Kim S, Doherty CM, Hill AJ, Lee YM. 2010. Thermally rearranged (TR) polybenzoxazole: effects of diverse imidization routes on physical properties and gas transport behaviors. Macromolecules. 43:7657–7667. doi: 10.1021/ma101549z.

Hanioka S, Maruyama T, Sotani T, Teramoto M, Matsuyama H, Nakashima K, Hanaki M, Kubota F, Goto M. 2008. CO_2 separation facilitated by task-specific ionic liquids using a supported liquid membrane. J Membr Sci. 314:1–4. doi: 10.1016/j.memsci.2008.01.029.

Haraya K. 1998. Possibility of utilization of gas-separation membranes as countermeasure for global warming. Bunri Gijutsu. 28:299–303.

Hasegawa H, Nishida K, Oguro S, Fujimura Y, Yajima K, Niino M, Isomura M, Tomita T. 2017. Gas separation process for CO_2 removal from natural gas with DDR-type zeolite membrane. Energy Procedia. 114:32–36. doi: 10.1016/j.egypro.2017.03.1143.

Hasegawa Y, Abe C, Natsui M, Ikeda A. 2021. Gas permeation properties of high-silica CHA-type zeolite membrane. Membranes. 11:249. doi: 10.3390/membranes11040249.

Hayakawa E, Himeno S. 2020. Synthesis of all-silica ZSM-58 zeolite membranes for separation of CO_2/CH_4 and CO_2/N_2 gas mixtures. Microporous Mesoporous Mater. 291:109695. doi: 10.1016/j.micromeso.2019.109695.

Hayakawa E, Himeno S. 2021. Preparation of Al-containing ZSM-58 zeolite membranes using rapid thermal processing for CO_2/CH_4 mixture separation. Membranes. 11:623. doi: 10.3390/membranes11080623.

Hayashi E, Thomas ML, Hashimoto K, Tsuzuki S, Ito A, Watanabe M. 2019. Application of protic ionic liquids to CO_2 separation in a sulfonated polyimide-derived ion gel membrane. ACS Appl Polym Mater. 1:1579–1589. doi: 10.1021/acsapm.9b00383.

Hiarayama Y, Kazama S, Fujisawa E, Nakabayashi M, Matsumiya N, Takagi K, Okabe K, Mano H, Haraya K, Kamizawa C. 1995. Novel membranes for carbon dioxide separation. Energy Convers Mgmt. 36:435–438. doi: 10.1016/0196-8904(95)00038-F.

Himeno S, Tomita T, Suzuki K, Nakayama K, Yajima K, Yoshida S. 2007. Synthesis and permeation properties of a DDR-type zeolite membrane for separation of CO_2/CH_4 gaseous mixtures. Ind Eng Chem Res. 46:6989–6997. doi: 10.1021/ie061682n.

Hirayama Y, Kase Y, Tanihara N, Sumiyama Y, Kusuki Y, Haraya K. 1999. Permeation properties to CO_2 and N_2 of poly(ethylene oxide)-containing and crosslinked polymer films. J Membr Sci. 160:87–99. doi: 10.1016/S0376-7388(99)00080-0.

Hiyoshi N, Yogo K, Yashima T. 2005. Adsorption characteristics of carbon dioxide on organically functionalized SBA-15. Microporous Mesoporous Mater. 84:357–365. doi: 10.1016/j.micromeso.2005.06.010.

Hong M, Falconer JL, Noble RD. 2005. Modification of zeolite membranes for H_2 separation by catalytic cracking of methyldiethoxysilane. Ind Eng Chem Res. 44:4035–4041. doi: 10.1021/ie048739v.

Hong Z, Sun F, Chen D, Zhang C, Gu X, Xu N. 2013a. Improvement of hydrogen-separating performance by on-stream catalytic cracking of silane over hollow fiber MFI zeolite membrane. Int J Hydrog Energy. 38:8409–8414. doi: 10.1016/j.ijhydene.2013.04.154.

Hong Z, Wu Z, Zhang Y, Gu X. 2013b. Catalytic cracking deposition of methyldiethoxysilane for modification of zeolitic pores in MFI/α-Al_2O_3 zeolite membrane with H + ion exchange pretreatment. Ind Eng Chem Res. 52:13113–13119. doi: 10.1021/ie4012563.

Horiuchi T, Osaki T, Sugiyama T, Suzuki K, Mori T. 1998. An estimate of surface mobility of CO_2 on γ-alumina and MgO-modified γ-alumina above 500 K. J Colloid Interface Sci. 204:217–218. doi: 10.1006/jcis.1998.5576.

Hoshino Y, Gyobu T, Imamura K, Hamasaki A, Honda R, Horii R, Yamashita C, Terayama Y, Watanabe T, Aki S, et al. 2021. Assembly of defect-free microgel nanomembranes for CO_2 separation. ACS Appl Mater Interfaces. 13:30030–30038. doi: 10.1021/acsami.1c06447.

Hou Y, Baltus RE. 2007. Experimental measurement of the solubility and diffusivity of CO_2 in room-temperature ionic liquids using a transient thin-liquid-film method. Ind Eng Chem Res. 46:8166–8175. doi: 10.1021/ie070501u.

Hu X, Lee WH, Bae JY, Kim JS, Jung JT, Wang HH, Park HJ, Lee YM. 2020. Thermally rearranged polybenzoxazole copolymers incorporating Troger's base for high flux gas separation membranes. J Membr Sci. 612:118437. doi: 10.1016/j.memsci.2020.118437.

Hu Y-F, Liu Z-C, Xu C-M, Zhang X-M. 2011. The molecular characteristics dominating the solubility of gases in ionic liquids. Chem Soc Rev. 40:3802–3823. doi: 10.1039/c0cs00006j.

Hu Y, Shiotsuki M, Sanda F, Freeman BD, Masuda T. 2008. Synthesis and properties of indan-based polyacetylenes that feature the highest gas permeability among all the existing polymers. Macromolecules. 41:8525–8532. doi: 10.1021/ma801845g.

Huang J, Zou J, Ho WSW. 2008. Carbon dioxide capture using a CO_2-selective facilitated transport membrane. Ind Eng Chem Res. 47:1261–1267. doi: 10.1021/ie070794r.

Huang K, Zhang X-M, Li Y-X, Wu Y-T, Hu X-B. 2014. Facilitated separation of CO_2 and SO_2 through supported liquid membranes using carboxylate-based ionic liquids. J Membr Sci. 471:227–236. doi: 10.1016/j.memsci.2014.08.022.

Huang Z, Yin C, Corrado T, Li S, Zhang Q, Guo R. 2022. Microporous pentiptycene-based polymers with heterocyclic rings for high-performance gas separation membranes. Chem Mater. 34:2730–2742. doi: 10.1021/acs.chemmater.1c04212.

Ismail AF, David LIB. 2001. A review on the latest development of carbon membranes for gas separation. J Membr Sci. 193:1–18. doi: 10.1016/S0376-7388(01)00510-5.

Ito A, Duan S, Ikenori Y, Ohkawa A. 2001. Permeation of wet CO_2/CH_4 mixed gas through a liquid membrane supported on surface of a hydrophobic microporous membrane. Sep Purif Technol. 24:235–242. doi: 10.1016/S1383-5866(01)00124-1.

Jami'an WNR, Hasbullah H, Mohamed F, Yusof N, Ibrahim N, Ali RR. 2016. Effect of evaporation time on cellulose acetate membrane for

gas separation. IOP Conf Ser: Earth Environ Sci. 36:012008. doi: 10.1088/1755-1315/36/1/012008.

Jang K-S, Kim H-J, Johnson JR, Kim W-G, Koros WJ, Jones CW, Nair S. 2011. Modified mesoporous silica gas separation membranes on polymeric hollow fibers. Chem Mater. 23:3025–3028. doi: 10.1021/cm200939d.

Jansen JC, Friess K, Clarizia G, Schauer J, Izak P. 2011. High ionic liquid content polymeric gel membranes: preparation and performance. Macromolecules. 44:39–45. doi: 10.1021/ma102438k.

Jeon JW, Kim D-G, Sohn E-H, Yoo Y, Kim YS, Kim BG, Lee J-C. 2017. Highly carboxylate-functionalized polymers of intrinsic microporosity for CO_2-selective polymer membranes. Macromolecules. 50:8019–8027. doi: 10.1021/acs.macromol.7b01332.

Jiang Y, Willmore FT, Sanders D, Smith ZP, Ribeiro CP, Doherty CM, Thornton A, Hill AJ, Freeman BD, Sanchez IC. 2011. Cavity size, sorption and transport characteristics of thermally rearranged (TR) polymers. Polymer. 52:2244–2254. doi: 10.1016/j.polymer.2011.02.035.

Jin Y, Gao B, Bian C, Meng X, Meng B, Wong SI, Yang N, Sunarso J, Tan X, Liu S. 2021. Elevated-temperature H_2 separation using a dense electron and proton mixed conducting polybenzimidazole-based membrane with 2D sulfonated graphene. Green Chem. 23:3374–3385. doi: 10.1039/D0GC04077K.

Jones CW, Koros WJ. 1994. Carbon molecular sieve gas separation membranes - I. Preparation and characterization based on polyimide precursors. Carbon. 32:1419–1425. doi: 10.1016/0008-6223(94)90135-X.

Jue ML, Breedveld V, Lively RP. 2017. Defect-free PIM-1 hollow fiber membranes. J Membr Sci. 530:33–41. doi: 10.1016/j.memsci.2017.02.012.

Kai T, Kazama S, Fujioka Y. 2009. Development of cesium-incorporated carbon membranes for CO_2 separation under humid conditions. J Membr Sci. 342:14–21. doi: 10.1016/j.memsci.2009.06.014.

Kalipcilar H, Bowen TC, Noble RD, Falconer JL. 2002. Synthesis and separation performance of SSZ-13 zeolite membranes on tubular supports. Chem Mater. 14:3458–3464. doi: 10.1021/cm020248i.

Kamble AR, Patel CM, Murthy ZVP. 2021. A review on the recent advances in mixed matrix membranes for gas separation processes. Renewable Sustainable Energy Rev. 145:111062. doi: 10.1016/j.rser.2021.111062.

Kamio E, Kasahara S, Moghadam F, Matsuyama H. 2020a. Development of facilitated transport membranes composed of a dense gel layer containing CO_2 carrier formed on porous cylindrical support membranes. Chem Eng Res Des. 153:284–293. doi: 10.1016/j.cherd.2019.10.046.

Kamio E, Kinoshita M, Yasui T, Lodge TP, Matsuyama H. 2020b. Preparation of inorganic/organic double-network ion gels using a cross-linkable polymer in an open system. Macromolecules. 53:8529–8538. doi: 10.1021/acs.macromol.0c01488.

Kamio E, Matsuki T, Kasahara S, Matsuyama H. 2017a. The effect of chemical structures of cyclic amino acid type ionic liquids as CO_2 carriers on facilitated transport membrane performances. Sep Sci Technol. 52:209–220. doi: 10.1080/01496395.2016.1216567.

Kamio E, Matsuki T, Moghadam F, Matsuyama H. 2017b. Development of facilitated transport membranes with low viscosity aprotic heterocyclic anion type ionic liquid as a CO_2 carrier. Sep Sci Technol. 52:197–208. doi: 10.1080/01496395.2016.1245330.

Kamio E, Minakata M, Iida Y, Yasui T, Matsuoka A, Matsuyama H. 2021. Inorganic/organic double-network ion gel membrane with a high ionic liquid content for CO_2 separation. Polym J. 53:137–147. doi: 10.1038/s41428-020-0393-y.

Kamio E, Minakata M, Nakamura H, Matsuoka A, Matsuyama H. 2022. Tough ion gels composed of coordinatively crosslinked polymer networks using ZIF-8 nanoparticles as multifunctional crosslinkers. Soft Matter. 18:4725–4736. doi: 10.1039/d2sm00410k.

Kamio E, Tanaka M, Shirono Y, Keun Y, Moghadam F, Yoshioka T, Nakagawa K, Matsuyama H. 2020c. Hollow fiber-type facilitated transport membrane composed of a polymerized ionic liquid-based gel layer with amino acidate as the CO_2 carrier. Ind Eng Chem Res. 59:2083–2092. doi: 10.1021/acs.iecr.9b05253.

Kamio E, Yasui T, Iida Y, Gong JP, Matsuyama H. 2017c. Inorganic/organic double-network gels containing ionic liquids. Adv Mater. 29:1704118. doi: 10.1002/adma.201704118.

Kanakubo M, Makino T, Taniguchi T, Nokami T, Itoh T. 2016. CO_2 solubility in ether functionalized ionic liquids on mole fraction and molarity scales. ACS Sustainable Chem Eng. 4:525–535. doi: 10.1021/acssuschemeng.5b00960.

Kanezashi M, Yada K, Yoshioka T, Tsuru T. 2009. Design of silica networks for development of highly permeable hydrogen separation membranes with hydrothermal stability. J Am Chem Soc. 131:414–415. doi: 10.1021/ja806762q.

Kang D-Y, Lee JS, Lin L-C. 2022. X-ray diffraction and molecular simulations in the study of metal-organic frameworks for membrane gas separation. Langmuir. 38:9441–9453. doi: 10.1021/acs.langmuir.2c01317.

Karakilic P, Huiskes C, Luiten-Olieman MWJ, Nijmeijer A, Winnubst L. 2017. Sol-gel processed magnesium-doped silica membranes with improved H_2/CO_2 separation. J Membr Sci. 543:195–201. doi: 10.1016/j.memsci.2017.08.055.

Karimi S, Mortazavi Y, Khodadadi AA, Holmgren A, Korelskiy D, Hedlund J. 2020. Functionalization of silica membranes for CO_2 separation. Sep Purif Technol. 235:116207. doi: 10.1016/j.seppur.2019.116207.

Karousos DS, Lei L, Lindbrathen A, Sapalidis AA, Kouvelos EP, He X, Favvas EP. 2020. Cellulose-based carbon hollow fiber membranes for high-pressure mixed gas separations of CO_2/CH_4 and CO_2/N_2. Sep Purif Technol. 253:117473. doi: 10.1016/j.seppur.2020.117473.

Kasahara S, Kamio E, Ishigami T, Matsuyama H. 2012a. Amino acid ionic liquid-based facilitated transport membranes for CO_2 separation. Chem Commun (Camb). 48:6903–6905. doi: 10.1039/c2cc17380h.

Kasahara S, Kamio E, Ishigami T, Matsuyama H. 2012b. Effect of water in ionic liquids on CO_2 permeability in amino acid ionic liquid-based facilitated transport membranes. J Membr Sci. 415-416:168–175. doi: 10.1016/j.memsci.2012.04.049.

Kasahara S, Kamio E, Matsuyama H. 2014a. Improvements in the CO_2 permeation selectivities of amino acid ionic liquid-based facilitated transport membranes by controlling their gas absorption properties. J Membr Sci. 454:155–162. doi: 10.1016/j.memsci.2013.12.009.

Kasahara S, Kamio E, Otani A, Matsuyama H. 2014b. Fundamental investigation of the factors controlling the CO_2 permeability of facilitated transport membranes containing amine-functionalized task-specific ionic liquids. Ind Eng Chem Res. 53:2422–2431. doi: 10.1021/ie403116t.

Kasahara S, Kamio E, Shaikh AR, Matsuki T, Matsuyama H. 2016. Effect of the amino-group densities of functionalized ionic liquids on the facilitated transport properties for CO_2 separation. J Membr Sci. 503:148–157. doi: 10.1016/j.memsci.2016.01.007.

Kasahara S, Kamio E, Yoshizumi A, Matsuyama H. 2014c. Polymeric ion-gels containing an amino acid ionic liquid for facilitated CO_2 transport media. Chem Commun (Camb). 50:2996–2999. doi: 10.1039/c3cc48231f.

Katsaros FK, Steriotis TA, Romanos GE, Konstantakou M, Stubos AK, Kanellopoulos NK. 2007. Preparation and characterisation of gas selective microporous carbon membranes. Microporous Mesoporous Mater. 99:181–189. doi: 10.1016/j.micromeso.2006.07.041.

Kazakli M, Mutch GA, Triantafyllou G, Gil AG, Li T, Wang B, Bailey JJ, Brett DJL, Shearing PR, Li K, et al. 2021. Controlling molten carbonate distribution in dual-phase molten salt-ceramic membranes to increase carbon dioxide permeation rates. J Membr Sci. 617:118640. doi: 10.1016/j.memsci.2020.118640.

Kazama S, Teramoto T, Haraya K. 2002. Carbon dioxide and nitrogen transport properties of bis(phenyl)fluorene-based cardo polymer membranes. J Membr Sci. 207:91–104. doi: 10.1016/S0376-7388(02)00112-6.

Kazarian SG, Briscoe BJ, Welton T. 2000. Combining ionic liquids and supercritical fluids: in situ ATR-IR study of CO_2 dissolved in two ionic liquids at high pressures. Chem Commun. 20:2047–2048. doi: 10.1039/b005514j.

Kim H-J, Yang H-C, Chung D-Y, Yang I-H, Choi YJ, Moon J-K. 2015a. Functionalized mesoporous silica membranes for CO_2 separation applications. J Chem. 2015:1–9. doi: 10.1155/2015/202867.

Kim I-W, Lee KJ, Jho JY, Park HC, Won J, Kang YS, Guiver MD, Robertson GP, Dai Y. 2001. Correlation between structure and gas transport properties of silyl-modified polysulfones and poly(phenyl sulfone)s. Macromolecules. 34:2908–2913. doi: 10.1021/ma002022b.

Kim S, Han SH, Lee YM. 2012. Thermally rearranged (TR) polybenzoxazole hollow fiber membranes for CO_2 capture. J Membr Sci. 403–404:169–178. doi: 10.1016/j.memsci.2012.02.041.

Kim S, Ida J, Guliants VV, Lin YS. 2004a. Functionalised mesoporous silica membrane for the separation of carbon dioxide. IJETM. 4:21–31. doi: 10.1504/IJETM.2004.004628.

Kim S, Jo HJ, Lee YM. 2013a. Sorption and transport of small gas molecules in thermally rearranged (TR) polybenzoxazole membranes based on 2,2-bis(3-amino-4-hydroxyphenyl)-hexafluoropropane (bisAPAF) and 4,4'-hexafluoroisopropylidene diphthalic anhydride (6FDA). J Membr Sci. 441:1–8. doi: 10.1016/j.memsci.2013.03.054.

Kim S, Seong JG, Do YS, Lee YM. 2015b. Gas sorption and transport in thermally rearranged polybenzoxazole membranes derived from polyhydroxylamides. J Membr Sci. 474:122–131. doi: 10.1016/j.memsci.2014.09.051.

Kim T-J, Li B, Hägg M-B. 2004b. Novel fixed-site-carrier polyvinylamine membrane for carbon dioxide capture. J Polym Sci B Polym Phys. 42:4326–4336. doi: 10.1002/polb.20282.

Kim T-J, Vrålstad H, Sandru M, Hägg M-B. 2013b. Separation performance of PVAm composite membrane for CO_2 capture at various pH levels. J Membr Sci. 428:218–224. doi: 10.1016/j.memsci.2012.10.009.

Kita H, Maeda H, Tanaka K, Okamoto K-I. 1997. Carbon molecular sieve membrane prepared from phenolic resin. Chem Lett. 26:179–180. doi: 10.1246/cl.1997.179.

Klahn M, Seduraman A. 2015. What determines CO_2 solubility in ionic liquids? A molecular simulation study. J Phys Chem B. 119:10066–10078. doi: 10.1021/acs.jpcb.5b03674.

Korelskiy D, Ye P, Fouladvand S, Karimi S, Sjöberg E, Hedlund J. 2015. Efficient ceramic zeolite membranes for CO_2/H_2 separation. J Mater Chem A. 3:12500–12506. doi: 10.1039/C5TA02152A.

Koresh JE, Sofer A. 1983. Molecular sieve carbon permselective membrane. Part I. Presentation of a new device for gas mixture separation. Sep Sci Technol. 18:723–734. doi: 10.1080/01496398308068576.

Koros WJ, Fleming GK, Jordan SM, Kim TH, Hoehn HH. 1988. Polymeric membrane materials for solution-diffusion based permeation separations. Prog Polym Sci. 13:339–401. doi: 10.1016/0079-6700(88)90002-0.

Kovvali AS, Chen H, Sirkar KK. 2000. Dendrimer membranes: a CO_2-selective molecular gate. J Am Chem Soc. 122:7594–7595. doi: 10.1021/ja0013071.

Krishna R. 1990. Multicomponent surface diffusion of adsorbed species: a description based on the generalized Maxwell-Stefan equations. Chem Eng Sci. 45:1779–1791. doi: 10.1016/0009-2509(90)87055-W.

Krishna R, Paschek D. 2002. Verification of the Maxwell-Stefan theory for tracer diffusion in zeolites. Chem Eng J. 85:7–15. doi: 10.1016/S1385-8947(01)00136-X.

Krishna R, Wesselingh JA. 1997. The Maxwell-Stefan approach to mass transfer. Chem Eng Sci. 52:861–911. doi: 10.1016/S0009-2509(96)00458-7.

Kusakabe K, Kuroda T, Morooka S. 1998. Separation of carbon dioxide from nitrogen using ion-exchanged faujasite-type zeolite membranes formed on porous support tubes. J Membr Sci. 148:13–23. doi: 10.1016/S0376-7388(98)00164-1.

Lan R, Abdallah SMM, Amar IA, Tao S. 2014. Preparation of dense $La_{0.5}Sr_{0.5}Fe_{0.8}Cu_{0.2}O_3$. δ-$(Li,Na)_2CO_3$-$LiAlO_2$ composite membrane for CO_2 separation. J Membr Sci. 468:380–388. doi: 10.1016/j.memsci.2014.06.030.

Lara-Medina JJ, Torres-Rodriguez M, Gutierrez-Arzaluz M, Mugica-Alvarez V. 2012. Separation of CO_2 and N_2 with a lithium-modified silicalite-1 zeolite membrane. Int J Greenh Gas Control. 10:494–500. doi: 10.1016/j.ijggc.2012.07.014.

Lawal SO, Yu L, Nagasawa H, Tsuru T, Kanezashi M. 2020. A carbon-silica-zirconia ceramic membrane with CO_2 flow-switching behaviour promising versatile high-temperature H_2/CO_2 separation. J Mater Chem A. 8:23563–23573. doi: 10.1039/D0TA07065C.

Lee J, Kim JS, Kim JF, Jo HJ, Park H, Seong JG, Lee YM. 2019. Densification-induced hollow fiber membranes using crosslinked thermally rearranged (XTR) polymer for CO_2 capture. J Membr Sci. 573:393–402. doi: 10.1016/j.memsci.2018.12.023.

Lee M, Bezzu CG, Carta M, Bernardo P, Clarizia G, Jansen JC, Mckeown NB. 2016. Enhancing the gas permeability of Troger's base derived polyimides of intrinsic microporosity. Macromolecules. 49:4147–4154. doi: 10.1021/acs.macromol.6b00351.

Lee WH, Seong JG, Hu X, Lee YM. 2020. Recent progress in microporous polymers from thermally rearranged polymers and polymers of intrinsic microporosity for membrane gas separation: pushing performance limits and revisiting trade-off lines. J Polym Sci. 58:2450–2466. doi: 10.1002/pol.20200110.

Lei L, Bai L, Lindbråthen A, Pan F, Zhang X, He X. 2020. Carbon membranes for CO_2 removal: Status and perspectives from materials to processes. Chem Eng J. 401:126084. doi: 10.1016/j.cej.2020.126084.

Lei L, Lindbråthen A, Hillestad M, He X. 2021. Carbon molecular sieve membranes for hydrogen purification from a steam methane reforming process. J Membr Sci. 627:119241. doi: 10.1016/j.memsci.2021.119241.

Li FY, Xiao Y, Chung T-S, Kawi S. 2012a. High-performance thermally self-cross-linked polymer of intrinsic microporosity (PIM-1) membranes for energy development. Macromolecules. 45:1427–1437. doi: 10.1021/ma202667y.

Li P, Chen HZ, Chung T-S. 2013a. The effects of substrate characteristics and pre-wetting agents on PAN-PDMS composite hollow fiber membranes for CO_2/N_2 and O_2/N_2 separation. J Membr Sci. 434:18–25. doi: 10.1016/j.memsci.2013.01.042.

Li P, Pramoda KP, Chung T-S. 2011. CO_2 separation from flue gas using polyvinyl-(room temperature ionic liquid)-room temperature ionic liquid composite membranes. Ind Eng Chem Res. 50:9344–9353. doi: 10.1021/ie2005884.

Li P, Wang Z, Li W, Liu Y, Wang J, Wang S. 2015. High-performance multilayer composite membranes with mussel-inspired polydopamine as a versatile molecular bridge for CO_2 separation. ACS Appl Mater Interfaces. 7:15481–15493. doi: 10.1021/acsami.5b03786.

Li S, Falconer JL, Noble RD. 2004. SAPO-34 membranes for CO_2/CH_4 separation. J Membr Sci. 241:121–135. doi: 10.1016/j.memsci.2004.04.027.

Li S, Jo HJ, Han SH, Park CH, Kim S, Budd PM, Lee YM. 2013b. Mechanically robust thermally rearranged (TR) polymer membranes with spirobisindane for gas separation. J Membr Sci. 434:137–147. doi: 10.1016/j.memsci.2013.01.011.

Li S, Wang Z, Yu X, Wang J, Wang S. 2012b. High-performance membranes with multi-permselectivity for CO_2 separation. Adv Mater. 24:3196–3200. doi: 10.1002/adma.201200638.

Liang CZ, Chung T-S. 2018. Ultrahigh flux composite hollow fiber membrane via highly crosslinked PDMS for recovery of hydrocarbons: propane and propene. Macromol Rapid Commun. 39:1700535. doi: 10.1002/marc.201700535.

Liang CZ, Liu JT, Lai J-Y, Chung T-S. 2018. High-performance multiple-layer PIM composite hollow fiber membranes for gas separation. J Membr Sci. 563:93–106. doi: 10.1016/j.memsci.2018.05.045.

Lie JA, Hägg M-B. 2005. Carbon membranes from cellulose and metal loaded cellulose. Carbon. 43:2600–2607. doi: 10.1016/j.carbon.2005.05.018.

Lie JA, Hägg M-B. 2006. Carbon membranes from cellulose: synthesis, performance and regeneration. J Membr Sci. 284:79–86. doi: 10.1016/j.memsci.2006.07.002.

Lin H, Freeman BD. 2005. Materials selection guidelines for membranes that remove CO_2 from gas mixtures. J Mol Struct. 739:57–74. doi: 10.1016/j.molstruc.2004.07.045.

Lin H, Van Wagner E, Freeman BD, Toy LG, Gupta RP. 2006. Plasticization-enhanced hydrogen purification using polymeric membranes. Science. 311:639–642. doi: 10.1126/science.1118079.

Lindmark J, Hedlund J. 2010. Carbon dioxide removal from synthesis gas using MFI membranes. J Membr Sci. 360:284–291. doi: 10.1016/j.memsci.2010.05.025.

Liu B, Tang C, Li X, Wang B, Zhou R. 2020. High-performance SAPO-34 membranes for CO_2 separations from simulated flue gas. Microporous Mesoporous Mater. 292:109712. doi: 10.1016/j.micromeso.2019.109712.

Liu H, Dai S, Jiang D-E. 2014a. Molecular dynamics simulation of anion effect on solubility, diffusivity, and permeability of carbon dioxide in ionic liquids. Ind Eng Chem Res. 53:10485–10490. doi: 10.1021/ie501501k.

Liu H, Dai S, Jiang D-E. 2014b. Structure and dynamics of CO_2 and N_2 in a tetracyanoborate based ionic liquid. Phys Chem Chem Phys. 16:1909–1913. doi: 10.1039/c3cp54326a.

Liu H, Gao X, Wang S, Hong Z, Wang X, Gu X. 2021a. SSZ-13 zeolite membranes on four-channel α-Al2O3 hollow fibers for CO_2 separation. Sep Purif Technol. 267:118611. doi: 10.1016/j.seppur.2021.118611.

Liu L, Doherty CM, Ricci E, Chen GQ, De Angelis MG, Kentish SE. 2021b. The influence of propane and n-butane on the structure and separation performance of cellulose acetate membranes. J Membr Sci. 638:119677. doi: 10.1016/j.memsci.2021.119677.

Liu Y, Yu S, Wu H, Li Y, Wang S, Tian Z, Jiang Z. 2014c. High permeability hydrogel membranes of chitosan/poly ether-block-amide blends for CO_2 separation. J Membr Sci. 469:198–208. doi: 10.1016/j.memsci.2014.06.050.

Lodge TP, Ueki T. 2016. Mechanically tunable, readily processable ion gels by self-assembly of block copolymers in ionic liquids. Acc Chem Res. 49:2107–2114. doi: 10.1021/acs.accounts.6b00308.

Longo M, De Santo MP, Esposito E, Fuoco A, Monteleone M, Giorno L, Comesaña-Gándara B, Chen J, Bezzu CG, Carta M, et al. 2020. Correlating gas permeability and young's modulus during the physical aging of polymers of intrinsic microporosity using atomic force microscopy. Ind Eng Chem Res. 59:5381–5391. doi: 10.1021/acs.iecr.9b04881.

Low Z-X, Budd PM, Mckeown NB, Patterson DA. 2018. Gas permeation properties, physical aging, and its mitigation in high free volume glassy polymers. Chem Rev. 118:5871–5911. doi: 10.1021/acs.chemrev.7b00629.

Ma X, Pinnau I. 2018. Effect of film thickness and physical aging on "intrinsic" gas permeation properties of microporous ethanoanthracene-based polyimides. Macromolecules. 51:1069–1076. doi: 10.1021/acs.macromol.7b02556.

Mahurin SM, Hillesheim PC, Yeary JS, Jiang D-E, Dai S. 2012. High CO_2 solubility, permeability and selectivity in ionic liquids with the tetracyanoborate anion. RSC Adv. 2:11813–11819. doi: 10.1039/c2ra22342b.

Mahurin SM, Lee J-S, Baker GA, Luo H-M, Dai S. 2010. Performance of nitrile-containing anions in task-specific ionic liquids for improved CO_2/N_2 separation. J Membr Sci. 353:177–183. doi: 10.1016/j.memsci.2010.02.045.

Makino T, Kanakubo M, Masuda Y, Mukaiyama H. 2014. Physical and CO_2-absorption properties of imidazolium ionic liquids with tetracyanoborate and bis(trifluoromethanesulfonyl)amide anions. J Solution Chem. 43:1601–1613. doi: 10.1007/s10953-014-0232-x.

Mason CR, Maynard-Atem L, Al-Harbi NM, Budd PM, Bernardo P, Bazzarelli F, Clarizia G, Jansen JC. 2011. Polymer of intrinsic microporosity incorporating thioamide functionality: preparation and gas transport properties. Macromolecules. 44:6471–6479. doi: 10.1021/ma200918h.

Mason CR, Maynard-Atem L, Heard KWJ, Satilmis B, Budd PM, Friess K, Lanc M, Bernardo P, Clarizia G, Jansen JC. 2014. Enhancement of CO_2 affinity in a polymer of intrinsic microporosity by amine modification. Macromolecules. 47:1021–1029. doi: 10.1021/ma401869p.

Masuda T, Iguchi Y, Tang BZ, Higashimura T. 1988. Diffusion and solution of gases in substituted polyacetylene membranes. Polymer. 29:2041–2049. doi: 10.1016/0032-3861(88)90178-4.

Masuda T, Isobe E, Higashimura T, Takada K. 1983. Poly[1-(trimethylsilyl)-1-propyne]: a new high polymer synthesized with transition-metal catalysts and characterized by extremely high gas permeability. J Am Chem Soc. 105:7473–7474. doi: 10.1021/ja00363a061.

Matsuyama H, Matsui K, Kitamura Y, Maki T, Teramoto M. 1999a. Effects of membrane thickness and membrane preparation condition on facilitated transport of CO_2 through ionomer membrane. Sep Purif Technol. 17:235–241. doi: 10.1016/S1383-5866(99)00047-7.

Matsuyama H, Terada A, Nakagawara T, Kitamura Y, Teramoto M. 1999b. Facilitated transport of CO_2 through polyethylenimine/poly(-vinyl alcohol) blend membrane. J Membr Sci. 163:221–227. doi: 10.1016/S0376-7388(99)00183-0.

Matsuyama H, Teramoto M, Sakakura H, Iwai K. 1996. Facilitated transport of CO_2 through various ion exchange membranes prepared by plasma graft polymerization. J Membr Sci. 117:251–260. doi: 10.1016/0376-7388(96)00072-5.

Mchattie JS, Koros WJ, Paul DR. 1991a. Gas transport properties of polysulfones. 1. Role of symmetry of methyl group placement on bisphenol. Polymer. 32:840–850. doi: 10.1016/0032-3861(91)90508-G.

Mchattie JS, Koros WJ, Paul DR. 1991b. Gas transport properties of polysulfones. 2. Effect of bisphenol connector groups. Polymer. 32:2618–2625. doi: 10.1016/0032-3861(91)90343-H.

Mchattie JS, Koros WJ, Paul DR. 1992. Gas transport properties of polysulfones: 3. Comparison of tetramethyl-substituted bisphenols. Polymer. 33:1701–1711. doi: 10.1016/0032-3861(92)91070-I.

Mckeown NB, Budd PM. 2006. Polymers of intrinsic microporosity (PIMs): organic materials for membrane separations, heterogeneous catalysis and hydrogen storage. Chem Soc Rev. 35:675–683. doi: 10.1039/b600349d.

Meckler SM, Bachman JE, Robertson BP, Zhu C, Long JR, Helms BA. 2018. Thermally rearranged polymer membranes containing Troeger's base units have exceptional performance for air separations. Angew Chem Int Ed Engl. 57:4912–4916. doi: 10.1002/anie.201800556.

Merkel TC, Freeman BD, Spontak RJ, He Z, Pinnau I, Meakin P, Hill AJ. 2003. Sorption, transport, and structural evidence for enhanced free volume in poly(4-methyl-2-pentyne)/fumed silica nanocomposite membranes. Chem Mater. 15:109–123. doi: 10.1021/cm020672j.

Merkel TC, Lin H, Wei X, Baker R. 2010. Power plant post-combustion carbon dioxide capture: an opportunity for membranes. J Membr Sci. 359:126–139. doi: 10.1016/j.memsci.2009.10.041.

Messaoud SB, Takagaki A, Sugawara T, Kikuchi R, Oyama ST. 2015. Alkylamine-silica hybrid membranes for carbon dioxide/methane separation. J Membr Sci. 477:161–171. doi: 10.1016/j.memsci.2014.12.022.

Miyamoto M, Takayama A, Uemiya S, Yogo K. 2011. Gas permeation properties of amine loaded mesoporous silica membranes for CO_2 separation. Desalin Water Treat. 34:266–271. doi: 10.5004/dwt.2011.2896.

Mizrahi Rodriguez K, Wu AX, Qian Q, Han G, Lin S, Benedetti FM, Lee H, Chi WS, Doherty CM, Smith ZP. 2020. Facile and time-efficient carboxylic acid functionalization of PIM-1: effect on molecular packing and gas separation performance. Macromolecules. 53:6220–6234. doi: 10.1021/acs.macromol.0c00933.

Moghadam F, Kamio E, Matsuyama H. 2017a. High CO_2 separation performance of amino acid ionic liquid-based double network ion gel membranes in low CO_2 concentration gas mixtures under humid conditions. J Membr Sci. 525:290–297. doi: 10.1016/j.memsci.2016.12.002.

Moghadam F, Kamio E, Yoshioka T, Matsuyama H. 2017b. New approach for the fabrication of double-network ion-gel membranes with high CO_2/N_2 separation performance based on facilitated transport. J Membr Sci. 530:166–175. doi: 10.1016/j.memsci.2017.02.032.

Moghadam F, Kamio E, Yoshizumi A, Matsuyama H. 2015. An amino acid ionic liquid-based tough ion gel membrane for CO_2 capture. Chem Commun. 51:13658–13661. doi: 10.1039/c5cc04841a.

Mu Y, Chen H, Xiang H, Lan L, Shao Y, Fan X, Hardacre C. 2019. Defects-healing of SAPO-34 membrane by post-synthesis modification using organosilica for selective CO_2 separation. J Membr Sci. 575:80–88. doi: 10.1016/j.memsci.2019.01.004.

Myers C, Pennline H, Luebke D, Ilconich J, Dixon JK, Maginn EJ, Brennecke JF. 2008. High temperature separation of carbon dioxide/hydrogen mixtures using facilitated supported ionic liquid membranes. J Membr Sci. 322:28–31. doi: 10.1016/j.memsci.2008.04.062.

Naderi A, Yong WF, Xiao Y, Chung T-S, Weber M, Maletzko C. 2018. Effects of chemical structure on gas transport properties of polyethersulfone polymers. Polymer. 135:76–84. doi: 10.1016/j.polymer.2017.12.014.

Nagai K, Freeman BD, Hill AJ. 2000. Effect of physical aging of poly(1-trimethylsilyl-1-propyne) films synthesized with TaCl5 and NbCl5 on gas permeability, fractional free volume, and positron annihilation lifetime spectroscopy parameters. J Polym Sci B Polym Phys. 38:1222–1239. doi: 10.1002/(SICI)1099-0488(20000501)38:9<1222::AID-POLB14>3.0.CO;2-P.

Nagai K, Masuda T, Nakagawa T, Freeman BD, Pinnau I. 2001. Poly[1-(trimethylsilyl)-1-propyne] and related polymers: synthesis, properties and functions. Prog Polym Sci. 26:721–798. doi: 10.1016/S0079-6700(01)00008-9.

Nagel C, Günther-Schade K, Fritsch D, Strunskus T, Faupel F. 2002. Free volume and transport properties in highly selective polymer membranes. Macromolecules. 35:2071–2077. doi: 10.1021/ma011028d.

Noble RD. 1992. Generalized microscopic mechanism of facilitated transport in fixed site carrier membranes. J Membr Sci. 75:121–129. doi: 10.1016/0376-7388(92)80011-8.

Nomura M, Matsuyama E, Ikeda A, Komatsuzaki M, Sasaki M. 2014. Preparation of silica hybrid membranes for high temperature CO_2 separation. J Chem Eng Japan. 47:569–573. doi: 10.1252/jcej.13we311.

Ogston AG. 1958. The spaces in a uniform random suspension of fibres. Trans Faraday Soc. 54:1754–1757. doi: 10.1039/tf9585401754.

Osada K, Kato T. 2002. Development of silica-zirconia membrane for gas separation. Kagaku Kogaku Ronbunshu. 28:67–72.

Ostwal M, Singh RP, Dec SF, Lusk MT, Way JD. 2011. 3-Aminopropyltriethoxysilane functionalized inorganic membranes for high temperature CO_2/N_2 separation. J Membr Sci. 369:139–147. doi: 10.1016/j.memsci.2010.11.053.

Park HB, Han SH, Jung CH, Lee YM, Hill AJ. 2010. Thermally rearranged (TR) polymer membranes for CO_2 separation. J Membr Sci. 359:11–24. doi: 10.1016/j.memsci.2009.09.037.

Park HB, Jung CH, Lee YM, Hill AJ, Pas SJ, Mudie ST, Van Wagner E, Freeman BD, Cookson DJ. 2007. Polymers with cavities tuned for fast selective transport of small molecules and ions. Science. 318:254–258. doi: 10.1126/science.1146744.

Patel HA, Yavuz CT. 2012. Noninvasive functionalization of polymers of intrinsic microporosity for enhanced CO_2 capture. Chem Commun. 48:9989–9991. doi: 10.1039/c2cc35392j.

Prasad B, Mandal B. 2018. Moisture responsive and CO_2 selective biopolymer membrane containing silk fibroin as a green carrier for facilitated transport of CO_2. J Membr Sci. 550:416–426. doi: 10.1016/j.memsci.2017.12.061.

Prasad B, Thakur RM, Mandal B, Su B. 2019. Enhanced CO_2 separation membrane prepared from waste by-product of silk fibroin. J Membr Sci. 587:117170. doi: 10.1016/j.memsci.2019.117170.

Puleo AC, Paul DR, Kelley SS. 1989. The effect of degree of acetylation on gas sorption and transport behavior in cellulose acetate. J Membr Sci. 47:301–332. doi: 10.1016/S0376-7388(00)83083-5.

Qi H, Chen H, Li L, Zhu G, Xu N. 2012. Effect of Nb content on hydrothermal stability of a novel ethylene-bridged silsesquioxane molecular sieving membrane for H_2/CO_2 separation. J Membr Sci. 421-422:190–200. doi: 10.1016/j.memsci.2012.07.010.

Qi H, Han J, Xu N. 2011. Effect of calcination temperature on carbon dioxide separation properties of a novel microporous hybrid silica membrane. J Membr Sci. 382:231–237. doi: 10.1016/j.memsci.2011.08.013.

Rahimalimamaghani A, Pacheco Tanaka DA, Llosa Tanco MA, Neira D'Angelo MF, Gallucci F. 2022. Ultra-selective CMSMs derived from resorcinol-formaldehyde resin for CO_2 separation. Membranes. 12:847. doi: 10.3390/membranes12090847.

Rahman MM, Abetz C, Shishatskiy S, Martin J, Müller AJ, Abetz V. 2018. CO_2 selective PolyActive membrane: thermal transitions and gas permeance as a function of thickness. ACS Appl Mater Interfaces. 10:26733–26744. doi: 10.1021/acsami.8b09259.

Rana I, Nagasawa H, Tsuru T, Kanezashi M. 2022. Tailoring the structure of a sub-nano silica network via fluorine doping to enhance CO_2 separation and evaluating CO_2 separation performance under dry or wet conditions. J Membr Sci. 658:120735. doi: 10.1016/j.memsci.2022.120735.

Ranjbaran F, Kamio E, Matsuyama H. 2017. Inorganic/organic composite ion gel membrane with high mechanical strength and high CO_2 separation performance. J Membr Sci. 544:252–260. doi: 10.1016/j.memsci.2017.09.036.

Raza A, Farrukh S, Hussain A, Khan I, Othman MHD, Ahsan M. 2021. Performance analysis of blended membranes of cellulose acetate with variable degree of acetylation for CO_2/CH_4 separation. Membranes. 11:245. doi: 10.3390/membranes11040245.

Ren X, Kanezashi M, Guo M, Xu R, Zhong J, Tsuru T. 2021. Multiple amine-contained POSS-functionalized organo silica membranes for gas separation. Membranes. 11:194. doi: 10.3390/membranes11030194.

Robeson LM. 1991. Correlation of separation factor versus permeability for polymeric membranes. J Membr Sci. 62:165–185. doi: 10.1016/0376-7388(91)80060-J.

Robeson LM. 2008. The upper bound revisited. J Membr Sci. 320:390–400. doi: 10.1016/j.memsci.2008.04.030.

Rogan Y, Malpass-Evans R, Carta M, Lee M, Jansen JC, Bernardo P, Clarizia G, Tocci E, Friess K, Lanc M, et al. 2014. A highly permeable polyimide with enhanced selectivity for membrane gas separations. J Mater Chem A. 2:4874–4877. doi: 10.1039/C4TA00564C.

Rose I, Bezzu CG, Carta M, Comesaña-Gándara B, Lasseuguette E, Ferrari MC, Bernardo P, Clarizia G, Fuoco A, Jansen JC, et al. 2017. Polymer ultrapermeability from the inefficient packing of 2D chains. Nat Mater. 16:932–937. doi: 10.1038/nmat4939.

Rose I, Carta M, Malpass-Evans R, Ferrari M-C, Bernardo P, Clarizia G, Jansen JC, Mckeown NB. 2015. Highly permeable benzotriptycene-based polymer of intrinsic microporosity. ACS Macro Lett. 4:912–915. doi: 10.1021/acsmacrolett.5b00439.

Roy P, Das N. 2019. Synthesis of NaX zeolite-graphite amine fiber composite membrane: role of graphite amine in membrane formation for H_2/CO_2 separation. Appl Surf Sci. 480:934–944. doi: 10.1016/j.apsusc.2019.03.038.

Rui Z, Anderson M, Li Y, Lin YS. 2012. Ionic conducting ceramic and carbonate dual phase membranes for carbon dioxide separation. J Membr Sci. 417-418:174–182. doi: 10.1016/j.memsci.2012.06.030.

Sakamoto Y, Nagata K, Yogo K, Yamada K. 2007. Preparation and CO_2 separation properties of amine-modified mesoporous silica membranes. Microporous Mesoporous Mater. 101:303–311. doi: 10.1016/j.micromeso.2006.11.007.

Salleh WNW, Ismail AF. 2012. Effects of carbonization heating rate on CO_2 separation of derived carbon membranes. Sep Purif Technol. 88:174–183. doi: 10.1016/j.seppur.2011.12.019.

Sandru M, Haukebø SH, Hägg M-B. 2010. Composite hollow fiber membranes for CO_2 capture. J Membr Sci. 346:172–186. doi: 10.1016/j.memsci.2009.09.039.

Sandru M, Kim T-J, Hägg M-B. 2009. High molecular fixed-site-carrier PVAm membrane for CO_2 capture. Desalination. 240:298–300. doi: 10.1016/j.desal.2008.01.053.

Satilmis B, Alnajrani MN, Budd PM. 2015. Hydroxyalkylaminoalkylamide PIMs: selective adsorption by ethanolamine- and diethanolamine-modified PIM-1. Macromolecules. 48:5663–5669. doi: 10.1021/acs.macromol.5b01196.

Satilmis B, Lanc M, Fuoco A, Rizzuto C, Tocci E, Bernardo P, Clarizia G, Esposito E, Monteleone M, Dendisova M, et al. 2018. Temperature and pressure dependence of gas permeation in amine-modified PIM-1. J Membr Sci. 555:483–496. doi: 10.1016/j.memsci.2018.03.039.

Saufi SM, Ismail AF. 2004. Fabrication of carbon membranes for gas separation – a review. Carbon. 42:241–259. doi: 10.1016/j.carbon.2003.10.022.

Sazali N, Salleh WNW, Ismail AF, Ismail NH, Sokri MNM, Nordin NaHM 2018a. CO_2 selective carbon tubular membrane: the effect of stabilization temperature on BTDA-TDI/MDI P84 co-polyimide. Int. J. Eng., Trans. B. 31:1356–1363.

Sazali N, Salleh WNW, Ismail AF, Nordin NaHM, Ismail NH, Mohamed MA, Aziz F, Yusof N, Jaafar J. 2018b. Incorporation of thermally labile additives in carbon membrane development for superior gas permeation performance. J Nat Gas Sci Eng. 49:376–384. doi: 10.1016/j.jngse.2017.10.026.

Scovazzo P. 2009. Determination of the upper limits, benchmarks, and critical properties for gas separations using stabilized room temperature ionic liquid membranes (SILMs) for the purpose of guiding future research. J Membr Sci. 343:199–211. doi: 10.1016/j.memsci.2009.07.028.

Selyanchyn O, Selyanchyn R, Fujikawa S. 2020. critical role of the molecular interface in double-layered pebax-1657/PDMS nanomembranes for highly efficient CO_2/N_2 gas separation. ACS Appl Mater Interfaces. 12:33196–33209. doi: 10.1021/acsami.0c07344.

Sen SK, Banerjee S. 2010. Spiro-biindane containing fluorinated poly (ether imide)s: synthesis, characterization and gas separation properties. J Membr Sci. 365:329–340. doi: 10.1016/j.memsci.2010.09.038.

Shannon MS, Tedstone JM, Danielsen SPO, Hindman MS, Irvin AC, Bara JE. 2012. Free volume as the basis of gas solubility and selectivity in imidazolium-based ionic liquids. Ind Eng Chem Res. 51:5565–5576. doi: 10.1021/ie202916e.

Shen J, Wu L, Wang D, Gao C. 2008. Sorption behavior and separation performance of novel facilitated transport membranes for CO_2/CH_4 mixtures. Desalination. 223:425–437. doi: 10.1016/j.desal.2007.01.186.

Shin DW, Hyun SH, Cho CH, Han MH. 2005. Synthesis and CO_2/N_2 gas permeation characteristics of ZSM-5 zeolite membranes. Microporous Mesoporous Mater. 85:313–323. doi: 10.1016/j.micromeso.2005.06.035.

Song H, Wei Y, Qi H. 2017. Tailoring pore structures to improve the permselectivity of organosilica membranes by tuning calcination parameters. J Mater Chem A. 5:24657–24666. doi: 10.1039/C7TA07117E.

Soo CY, Jo HJ, Lee YM, Quay JR, Murphy MK. 2013. Effect of the chemical structure of various diamines on the gas separation of thermally rearranged poly(benzoxazole-co-imide) (TR-PBO-co-I) membranes. J Membr Sci. 444:365–377. doi: 10.1016/j.memsci.2013.05.056.

Staiger CL, Pas SJ, Hill AJ, Cornelius CJ. 2008. Gas separation, free volume distribution, and physical aging of a highly microporous spirobisindane polymer. Chem Mater. 20:2606–2608. doi: 10.1021/cm071722t.

Stern SA. 1994. Polymers for gas separations: the next decade. J Membr Sci.,. 94:1–65.

Suda H, Haraya K. 1997. Gas permeation through micropores of carbon molecular sieve membranes derived from Kapton polyimide. J Phys Chem B. 101:3988–3994. doi: 10.1021/jp963997u.

Swaidan R, Ghanem BS, Litwiller E, Pinnau I. 2014. Pure- and mixed-gas CO_2/CH_4 separation properties of PIM-1 and an amidoxime-functionalized PIM-1. J Membr Sci. 457:95–102. doi: 10.1016/j.memsci.2014.01.055.

Tachibana T, Yoshioka T, Nakagawa K, Shintani T, Kamio E, Matsuyama H. 2020. Gas permeation characteristics of TiO_2-ZrO_2-aromatic organic chelating ligand (aOCL) composite membranes. Membranes. 10:388. doi: 10.3390/membranes10120388.

Taniguchi I, Kinugasa K, Toyoda M, Minezaki K, Tanaka H, Mitsuhara K. 2021. Piperazine-immobilized polymeric membranes for CO_2 capture: mechanism of preferential CO_2 permeation. Polym J. 53:129–136. doi: 10.1038/s41428-020-0389-7.

Taniguchi I, Wada N, Kinugasa K, Higa M. 2017. A strategy to enhance CO_2 permeability of well-defined hyper-branched polymers with dense polyoxyethylene comb graft. J Membr Sci. 535:239–247. doi: 10.1016/j.memsci.2017.04.046.

Tawalbeh M, Al-Ismaily M, Kruczek B, Tezel FH. 2021. Modeling the transport of CO_2, N_2, and their binary mixtures through highly permeable silicalite-1 membranes using Maxwell-Stefan equations. Chemosphere. 263:127935. doi: 10.1016/j.chemosphere.2020.127935.

Teramoto M, Nakai K, Ohnishi N, Huang Q, Watari T, Matsuyama H. 1996. Facilitated transport of carbon dioxide through supported liquid membranes of aqueous amine solutions. Ind Eng Chem Res. 35:538–545. doi: 10.1021/ie950112c.

Tiwari RR, Jin J, Freeman BD, Paul DR. 2017. Physical aging, CO_2 sorption and plasticization in thin films of polymer with intrinsic microporosity (PIM-1. J Membr Sci. 537:362–371. doi: 10.1016/j.memsci.2017.04.069.

Tiwari RR, Smith ZP, Lin H, Freeman BD, Paul DR. 2014. Gas permeation in thin films of "high free-volume" glassy perfluoropolymers: Part I. Physical aging. Polymer. 55:5788–5800. doi: 10.1016/j.polymer.2014.09.022.

Tocci E, De Lorenzo L, Bernardo P, Clarizia G, Bazzarelli F, Mckeown NB, Carta M, Malpass-Evans R, Friess K, Pilnacek K, et al. 2014. Molecular modeling and gas permeation properties of a polymer of intrinsic microporosity composed of ethanoanthracene and Troger's base units. Macromolecules. 47:7900–7916. doi: 10.1021/ma501469m.

Tome LC, Florindo C, Freire CSR, Rebelo LPN, Marrucho IM. 2014. Playing with ionic liquid mixtures to design engineered CO_2 separation membranes. Phys Chem Chem Phys. 16:17172–17182. doi: 10.1039/c4cp01434k.

Tomita T, Nakayama K, Sakai H. 2004. Gas separation characteristics of DDR type zeolite membrane. Microporous Mesoporous Mater. 68:71–75. doi: 10.1016/j.micromeso.2003.11.016.

Torres D, Perez-Rodriguez S, Cesari L, Castel C, Favre E, Fierro V, Celzard A. 2021. Review on the preparation of carbon membranes derived from phenolic resins for gas separation: from petrochemical precursors to bioresources. Carbon. 183:12–33. doi: 10.1016/j.carbon.2021.06.087.

Van Den Bergh J, Tihaya A, Kapteijn F. 2010. High temperature permeation and separation characteristics of an all-silica DDR zeolite membrane. Microporous Mesoporous Mater. 132:137–147. doi: 10.1016/j.micromeso.2010.02.011.

Van Den Bergh J, Zhu W, Gascon J, Moulijn JA, Kapteijn F. 2008. Separation and permeation characteristics of a DD3R zeolite membrane. J Membr Sci. 316:35–45. doi: 10.1016/j.memsci.2007.12.051.

Van Gestel T, Sebold D, Hauler F, Meulenberg WA, Buchkremer H-P. 2010. Potentialities of microporous membranes for H_2/CO_2 separation in future fossil fuel power plants: evaluation of SiO_2, ZrO_2. Y_2O_3-ZrO_2 and TiO_2-ZrO_2 sol-gel membranes. J Membr Sci. 359:64–79. doi: 10.1016/j.memsci.2010.04.002.

Wade JL, Lackner KS, West AC. 2007. Transport model for a high temperature, mixed conducting CO_2 separation membrane. Solid State Ionics. 178:1530–1540. doi: 10.1016/j.ssi.2007.09.007.

Wade JL, Lee C, West AC, Lackner KS. 2011. Composite electrolyte membranes for high temperature CO_2 separation. J Membr Sci. 369:20–29. doi: 10.1016/j.memsci.2010.10.053.

Walden P. 1914. Molecular weights and electrical conductivity of several fused salts. Bull. Acad. Imp. Sci. St-Petersbourg. 8:405–422.

Wang B, Ho WSW, Figueroa JD, Dutta PK. 2015. Bendable zeolite membranes: synthesis and improved gas separation performance. Langmuir. 31:6894–6901. doi: 10.1021/acs.langmuir.5b01306.

Wang H, Chung T-S, Paul DR. 2014a. Physical aging and plasticization of thick and thin films of the thermally rearranged ortho-functional polyimide 6FDA-HAB. J Membr Sci. 458:27–35. doi: 10.1016/j.memsci.2014.01.066.

Wang H, Chung T-S, Paul DR. 2014b. Thickness dependent thermal rearrangement of an ortho-functional polyimide. J Membr Sci. 450:308–312. doi: 10.1016/j.memsci.2013.09.006.

Wang H, Lin YS. 2011. Effects of synthesis conditions on MFI zeolite membrane quality and catalytic cracking deposition modification results. Microporous Mesoporous Mater. 142:481–488. doi: 10.1016/j.micromeso.2010.12.037.

Wang H, Lin YS. 2012. Synthesis and modification of ZSM-5/silicalite bilayer membrane with improved hydrogen separation performance. J Membr Sci. 396:128–137. doi: 10.1016/j.memsci.2012.01.008.

Wang S, Li X, Wu H, Tian Z, Xin Q, He G, Peng D, Chen S, Yin Y, Jiang Z, et al. 2016. Advances in high permeability polymer-based membrane materials for CO_2 separations. Energy Environ Sci. 9: 1863–1890. doi: 10.1039/C6EE00811A.

Way JD, Noble RD, Reed DL, Ginley GM, Jarr LA. 1987. Facilitated transport of CO_2 in ion exchange membranes. AIChE J. 33:480–487. doi: 10.1002/aic.690330313.

Weber J, Su Q, Antonietti M, Thomas A. 2007. Exploring polymers of intrinsic microporosity - microporous, soluble polyamide and polyimide. Macromol Rapid Commun. 28:1871–1876. doi: 10.1002/marc.200700346.

Wei Q, Wang F, Nie Z-R, Song C-L, Wang Y-L, Li Q-Y. 2008. Highly Hydrothermally Stable Microporous Silica Membranes for Hydrogen Separation. J Phys Chem B. 112:9354–9359. doi: 10.1021/jp711573f.

Weng X, Baez JE, Khiterer M, Hoe MY, Bao Z, Shea KJ. 2015. Chiral polymers of intrinsic microporosity: selective membrane permeation of enantiomers. Angew Chem Int Ed Engl. 54:11214–11218. doi: 10.1002/anie.201504934.

Williams R, Burt LA, Esposito E, Jansen JC, Tocci E, Rizzuto C, Lanc M, Carta M, Mckeown NB. 2018. A highly rigid and gas selective methanopentacene-based polymer of intrinsic microporosity derived from Troger's base polymerization. J Mater Chem A. 6:5661–5667. doi: 10.1039/C8TA00509E.

Wong KK, Jawad ZA. 2019. A review and future prospect of polymer blend mixed matrix membrane for CO_2 separation. J Polym Res. 26: 289. doi: 10.1007/s10965-019-1978-z.

Woo KT, Lee J, Dong G, Kim JS, Do YS, Jo HJ, Lee YM. 2016. Thermally rearranged poly(benzoxazole-co-imide) hollow fiber membranes for CO_2 capture. J Membr Sci. 498:125–134. doi: 10.1016/j.memsci.2015.10.015.

Wu W-H, Thomas P, Hume P, Jin J. 2018. Effective conversion of amide to carboxylic acid on polymers of intrinsic microporosity (PIM-1) with nitrous acid. Membranes. 8:20. doi: 10.3390/membranes8020020.

Xomeritakis G, Tsai C-Y, Brinker CJ. 2005. Microporous sol-gel derived aminosilicate membrane for enhanced carbon dioxide separation. Sep Purif Technol. 42:249–257. doi: 10.1016/j.seppur.2004.08.003.

Yamaguchi T, Boetje LM, Koval CA, Noble RD, Bowman CN. 1995. Transport properties of carbon dioxide through amine functionalized carrier membranes. Ind Eng Chem Res. 34:4071–4077. doi: 10.1021/ie00038a049.

Yamaguchi T, Niitsuma T, Nair BN, Nakagawa K. 2007. Lithium silicate based membranes for high temperature CO_2 separation. J Membr Sci. 294:16–21. doi: 10.1016/j.memsci.2007.01.028.

Yanaranop P, Santoso B, Etzion R, Jin J. 2016. Facile conversion of nitrile to amide on polymers of intrinsic microporosity (PIM-1). Polymer. 98:244–251. doi: 10.1016/j.polymer.2016.06.041.

Yang S, Chiang Y, Nair S. 2019. Scalable one-step gel conversion route to high-performance CHA zeolite hollow fiber membranes and modules for CO_2 separation. Energy Technol. 7:1900494. doi: 10.1002/ente.201900494.

Yang X, Du H, Lin Y, Song L, Zhang Y, Gao X, Kong C, Chen L. 2016. Hybrid organosilica membrane with high CO_2 permselectivity fabricated by a two-step hot coating method. J Membr Sci. 506:31–37. doi: 10.1016/j.memsci.2016.01.054.

Yasui T, Fujinami S, Hoshino T, Kamio E, Matsuyama H. 2020a. Energy dissipation via the internal fracture of the silica particle network in inorganic/organic double network ion gels. Soft Matter. 16: 2363–2370. doi: 10.1039/c9sm02174d.

Yasui T, Kamio E, Matsuyama H. 2018. Inorganic/organic double-network ion gels with partially developed silica-particle network. Langmuir. 34:10622–10633. doi: 10.1021/acs.langmuir.8b01930.

Yasui T, Kamio E, Matsuyama H. 2019. Tough and stretchable inorganic/organic double network ion gel containing gemini-type ionic liquid as a multiple hydrogen bond cross-linker. RSC Adv. 9:11870–11876. doi: 10.1039/c9ra01790a.

Yasui T, Kamio E, Matsuyama H. 2020b. Inorganic/organic nanocomposite ion gels with well dispersed secondary silica nanoparticles. RSC Adv. 10:14451–14457. doi: 10.1039/d0ra02478c.

Yave W, Car A, Funari SS, Nunes SP, Peinemann K-V. 2010. CO_2-philic polymer membrane with extremely high separation performance. Macromolecules. 43:326–333. doi: 10.1021/ma901950u.

Ye L, Wang L, Jie X, Yu C, Kang G, Cao Y. 2019. The evolution of free volume and gas transport properties for the thermal rearrangement of poly(hydroxyamide-co-amide)s membranes. J Membr Sci. 573:21–35. doi: 10.1016/j.memsci.2018.11.029.

Ye L, Wang L, Jie X, Yu C, Kang G, Cao Y. 2020. Effect of hexafluoroisopropylidene group contents and treatment temperature on the performance of thermally rearranged poly(hydroxyamide)s membranes. J Membr Sci. 595:117540. doi: 10.1016/j.memsci.2019.117540.

Yegani R, Hirozawa H, Teramoto M, Himei H, Okada O, Takigawa T, Ohmura N, Matsumiya N, Matsuyama H. 2007. Selective separation of CO_2 by using novel facilitated transport membrane at elevated temperatures and pressures. J Membr Sci. 291:157–164. doi: 10.1016/j.memsci.2007.01.011.

Yeo ZY, Chew TL, Zhu PW, Mohamed AR, Chai S-P. 2013. Synthesis and performance of microporous inorganic membranes for CO_2 separation: a review. J Porous Mater. 20:1457–1475. doi: 10.1007/s10934-013-9732-0.

Yeong YF, Wang H, Pallathadka Pramoda K, Chung T-S. 2012. Thermal induced structural rearrangement of cardo-copolybenzoxazole membranes for enhanced gas transport properties. J Membr Sci. 397-398:51–65. doi: 10.1016/j.memsci.2012.01.010.

Yoshimune M, Fujiwara I, Haraya K. 2007. Carbon molecular sieve membranes derived from trimethylsilyl substituted poly(phenylene oxide) for gas separation. Carbon. 45:553–560. doi: 10.1016/j.carbon.2006.10.017.

Yoshimune M, Fujiwara I, Suda H, Haraya K. 2005. Novel carbon molecular sieve membranes derived from poly(phenylene oxide) and its derivatives for gas separation. Chem Lett. 34:958–959. doi: 10.1246/cl.2005.958.

Yoshimune M, Fujiwara I, Suda H, Haraya K. 2006. Gas transport properties of carbon molecular sieve membranes derived from metal containing sulfonated poly(phenylene oxide). Desalination. 193:66–72. doi: 10.1016/j.desal.2005.04.138.

Yoshimune M, Haraya K. 2010. Flexible carbon hollow fiber membranes derived from sulfonated poly(phenylene oxide). Sep Purif Technol. 75:193–197. doi: 10.1016/j.seppur.2010.07.017.

Yoshimune M, Haraya K. 2013. CO_2/CH_4 mixed gas separation using carbon hollow fiber membranes. Energy Procedia. 37:1109–1116. doi: 10.1016/j.egypro.2013.05.208.

Yoshino M, Ito K, Kita H, Okamoto K-I. 2000. Effects of hard-segment polymers on CO_2/N_2 gas-separation properties of poly(ethylene oxide)-segmented copolymers. J Polym Sci B Polym Phys. 38:1707–1715. doi: 10.1002/1099-0488(20000701)38:13<1707::AID-POLB40>3.0.CO;2-W.

Yoshioka T, Maki T, Asaeda M, Tsuru T. 2007. Gas permeation characteristic of metal doped microporous silica membranes for CO_2 separation prepared by metal salt-added sol-gel processing. Maku. 32:45–53. doi: 10.5360/membrane.32.45.

Yoshioka T, Nakanishi E, Tsuru T, Asaeda M. 2001. Experimental studies of gas permeation through microporous silica membranes. AIChE J. 47:2052–2063. doi: 10.1002/aic.690470916.

Yoshioka T, Tsuru T, Asaeda M. 2004. Molecular dynamics study of gas permeation through amorphous silica network and inter-particle pores on microporous silica membranes. Mol. Phys. 102:191–202. doi: 10.1080/00268970310001649383.

Yu L, Kanezashi M, Nagasawa H, Guo M, Moriyama N, Ito K, Tsuru T. 2019. Tailoring ultramicroporosity to maximize CO_2 transport within pyrimidine-bridged organosilica membranes. ACS Appl Mater Interfaces. 11:7164–7173. doi: 10.1021/acsami.9b01462.

Yu L, Kanezashi M, Nagasawa H, Oshita J, Naka A, Tsuru T. 2017a. Pyrimidine-bridged organoalkoxysilane membrane for high-efficiency CO_2 transport via mild affinity. Sep Purif Technol. 178:232–241. doi: 10.1016/j.seppur.2017.01.039.

Yu L, Kanezashi M, Nagasawa H, Tsuru T. 2017b. Fabrication and CO_2 permeation properties of amine-silica membranes using a variety of amine types. J Membr Sci. 541:447–456. doi: 10.1016/j.memsci.2017.07.024.

Yu L, Kanezashi M, Nagasawa H, Tsuru T. 2018. Role of amine type in CO_2 separation performance within amine functionalized silica/organosilica membranes: a review. Appl. Sci. 8:1032. doi: 10.3390/app8071032.

Yu M, Funke HH, Noble RD, Falconer JL. 2011. H_2 separation using defect-free, inorganic composite membranes. J Am Chem Soc. 133: 1748–1750. doi: 10.1021/ja108681n.

Zhang H, Wei Y, Niu S, Qi H. 2021a. Fabrication of Pd-Nb bimetallic doped organosilica membranes by different metal doping routes for H_2/CO_2 separation. Chin J Chem Eng. 36:67–75. doi: 10.1016/j.cjche.2020.09.003.

Zhang H, Wei Y, Qi H. 2020. Palladium-niobium bimetallic doped organosilica membranes for H_2/CO_2 separation. Microporous Mesoporous Mater. 305:110279. doi: 10.1016/j.micromeso.2020.110279.

Zhang J, Kamio E, Kinoshita M, Matsuoka A, Nakagawa K, Yoshioka T, Matsuyama H. 2021b. Inorganic/organic micro-double-network ion gel-based composite membrane with enhanced mechanical strength and CO_2 permeance. Ind Eng Chem Res. 60:12698–12708. doi: 10.1021/acs.iecr.1c02228.

Zhang J, Kamio E, Matsuoka A, Nakagawa K, Yoshioka T, Matsuyama H. 2021c. Development of a micro-double-network ion gel-based CO_2 separation membrane from nonvolatile network precursors. Ind Eng Chem Res. 60:12640–12649. doi: 10.1021/acs.iecr.1c01529.

Zhang J, Kamio E, Matsuoka A, Nakagawa K, Yoshioka T, Matsuyama H. 2022a. Fundamental investigation on the development of composite membrane with a thin ion gel layer for CO_2 separation. J Membr Sci. 663:121032. doi: 10.1016/j.memsci.2022.121032.

Zhang J, Kamio E, Matsuoka A, Nakagawa K, Yoshioka T, Matsuyama H. 2022b. Novel tough ion-gel-based CO_2 separation membrane with interpenetrating polymer network composed of semicrystalline and cross-linkable polymers. Ind Eng Chem Res. 61:4648–4658. doi: 10.1021/acs.iecr.1c04800.

Zhang J, Kang H, Martin J, Zhang S, Thomas S, Merkel TC, Jin J. 2016. The enhancement of chain rigidity and gas transport performance of polymers of intrinsic microporosity via intramolecular locking of the spiro-carbon. Chem Commun. 52:6553–6556. doi: 10.1039/c6cc02308h.

Zhang Q, Chen G, Zhang S. 2007. Synthesis and properties of novel soluble polyimides having a spirobisindane-linked dianhydride unit. Polymer. 48:2250–2256. doi: 10.1016/j.polymer.2007.02.061.

Zhang X-L, Qiu L-F, Ding M-Z, Hu N, Zhang F, Zhou R-F, Chen X-S, Kita H. 2013. Preparation of zeolite T membranes by a two-step temperature process for CO_2 separation. Ind Eng Chem Res. 52: 16364–16374. doi: 10.1021/ie4025402.

Zhang X, Huo F, Liu Z, Wang W, Shi W, Maginn EJ. 2009. Absorption of CO_2 in the ionic liquid 1-n-Hexyl-3-methylimidazolium tris(pentafluoroethyl)trifluorophosphate ([hmim][FEP]): a molecular view by computer simulations. J Phys Chem B. 113:7591–7598. doi: 10.1021/jp900403q.

Zhang Y, Sun Q, Gu X. 2015. Pure H_2 production through hollow fiber hydrogen-selective MFI zeolite membranes using steam as sweep gas. AIChE J. 61:3459–3469. doi: 10.1002/aic.14924.

Zhang Y, Wang Z, Wang S. 2002. Novel fixed-carrier membranes for CO_2 separation. J Appl Polym Sci. 86:2222–2226. doi: 10.1002/app.11228.

Zhang Y, Wu Z, Hong Z, Gu X, Xu N. 2012. Hydrogen-selective zeolite membrane reactor for low temperature water gas shift reaction. Chem Eng J. 197:314–321. doi: 10.1016/j.cej.2012.05.064.

Zhao Y, Ho WSW. 2012. Steric hindrance effect on amine demonstrated in solid polymer membranes for CO_2 transport. J Membr Sci. 415-416:132–138. doi: 10.1016/j.memsci.2012.04.044.

Zhou J, Gao F, Sun K, Jin X, Zhang Y, Liu B, Zhou R. 2020. Green synthesis of highly CO_2-selective CHA zeolite membranes in all-silica and fluoride-free solution for CO_2/CH_4 separations. Energy Fuels. 34:11307–11314. doi: 10.1021/acs.energyfuels.0c01717.

Zhou J, Mok MM, Cowan MG, Mcdanel WM, Carlisle TK, Gin DL, Noble RD. 2014a. High-permeance room-temperature ionic-liquid-based membranes for CO_2/N_2 separation. Ind Eng Chem Res. 53: 20064–20067. doi: 10.1021/ie5040682.

Zhou M, Korelskiy D, Ye P, Grahn M, Hedlund J. 2014b. A uniformly oriented MFI membrane for improved CO_2 separation. Angew Chem Int Ed Engl. 53:3492–3495. doi: 10.1002/anie.201311324.

Zhu L, Huang L, Venna SR, Blevins AK, Ding Y, Hopkinson DP, Swihart MT, Lin H. 2021. Scalable polymeric few-nanometer organosilica membranes with hydrothermal stability for selective hydrogen separation. ACS Nano. 15:12119–12128. doi: 10.1021/acsnano.1c03492.

Zhu X, Wang H, Lin YS. 2010. Effect of the membrane quality on gas permeation and chemical vapor deposition modification of MFI-type zeolite membranes. Ind Eng Chem Res. 49:10026–10033. doi: 10.1021/ie101101z.

Zito PF, Brunetti A, Caravella A, Drioli E, Barbieri G. 2020a. Mutual influence in permeation of CO_2-containing mixtures through a SAPO-34 membrane. J Membr Sci. 595:117534. doi: 10.1016/j.memsci.2019.117534.

Zito PF, Brunetti A, Drioli E, Barbieri G. 2020b. CO_2 separation via a DDR membrane: mutual influence of mixed gas permeation. Ind Eng Chem Res. 59:7054–7060. doi: 10.1021/acs.iecr.9b03029.